INORGANIC CHEMISTRY
FRONTIERS

REVIEW

View Article Online
View Journal | View Issue

Cite this: *Inorg. Chem. Front.*, 2026, **13**, 2686

Understanding luminescence of metal-containing thermally activated delayed fluorescence (TADF) luminophores

Lubna Salah, [a,b] Paulina Marek-Urban, [a,b,c] Mieczysław Łapkowski, [a,b] Fernando B. Dias *[d] and Piotr Pander *[a,b]

Metal TADF (thermally activated delayed fluorescence) emitters, here understood as those containing a d-block metal, are an important and ever-growing group of luminophores. Although they often seem to belong more in the transition metal complex world, they are rightful contenders of not only phosphorescent transition metal compounds, but also conventional, metal-free TADF emitters. Their unique properties include extremely short TADF lifetimes, often in the range 0.1–10 μs, fast intersystem crossing (ISC) and reverse ISC (RISC), minimal prompt fluorescence or lack thereof, small Stokes shifts, and temperature-dependent behaviour, including dual TADF/phosphorescence emission – but not every metal TADF emitter displays all of them at once! In this review, we discuss the general photophysical properties of metal TADF emitters and the relevant photophysical approaches applicable to studies of them. We make a brief overview of the most recent examples of computational works on metal TADF luminophores that shed some light on the up-conversion mechanism. Finally, we review some recent examples of Cu(I), Ag(I), Au(I)/Au(III) as well as Zn(II) TADF emitters, and discuss possibly all relevant works on Pd(II), Pt(II), Ir(III), and Zr(IV) TADF complexes. We identify that metal TADF complexes form two principal groups: (I) those analogous to donor–acceptor or charge-transfer TADF emitters and (II) those analogous to multiresonance TADF emitters.

Received 30th October 2025,
Accepted 4th January 2026

DOI: 10.1039/d5qi02203g

rsc.li/frontiers-inorganic

1. Introduction

Thermally activated delayed fluorescence or TADF has clearly revolutionised the science of metal-containing luminophores, enabling not only strong but short-lived photoluminescence from otherwise weakly emissive systems. The developments in the realm of TADF in metal complexes – here referred to as metal TADF for short – have allowed expansion of the group of luminescent complexes used in organic light-emitting diodes (OLEDs) beyond the conventional luminophores like platinum(II) and iridium(III) compounds.[1] Here, the works of the groups of Yersin, Adachi, and Peters deserve mention as the first to introduce this concept into OLEDs.[2–5]

TADF itself has been described in detail decades ago by Parker and Hatchard in 1961,[6] while detailed descriptions of TADF in copper complexes date back to 1983.[7] We believe that the interest in metal TADF emitters really took off with the prospect of their use as emitters in OLEDs, making a promise of replacing the rather costly platinum and iridium metals. While Pt(II) and Ir(III) complexes may display strong phosphorescence and high radiative decay rates stemming solely from the strong heavy atom effect,[8] complexes of other, more abundant transition metals often do not display sufficient spin–orbit coupling (SOC). This results in low efficiency and long-lived phosphorescence. TADF opens a possibility for these metals to also contribute as central atoms of efficient luminophores, as it "borrows" the radiative decay rate from the emissive S_1 state of the complex (Fig. 1). Nowadays, the primary example of luminophores of this type are coinage metal complexes, like those of Cu(I), Ag(I), and Au(I) central atoms.[9] Complexes of central ions introducing strong spin–orbit coupling and hence often suitable phosphorescent properties, such as platinum(II) and iridium(III), show less obvious signs of the TADF mechanism, which might be one of the reasons why they are currently of lesser interest.

The general picture of metal TADF luminophores must involve three principle luminescent pathways: (1) fluorescence; (2) TADF; (3) phosphorescence. The influence of either of these three will depend on the magnitude of the heavy atom effect in each case (Fig. 1). The presence of moderate or strong heavy atom

[a]*Faculty of Chemistry, Silesian University of Technology, M. Strzody 9, 44-100 Gliwice, Poland. E-mail: piotr.pander@polsl.pl*
[b]*Centre for Organic and Nanohybrid Electronics, Silesian University of Technology, Konarskiego 22B, 44-100 Gliwice, Poland*
[c]*Faculty of Chemistry, Warsaw University of Technology, Noakowskiego 3, 00-664 Warsaw, Poland*
[d]*Department of Physics, Durham University, South Road, Durham, DH1 3LE, UK. E-mail: f.m.b.dias@durham.ac.uk*

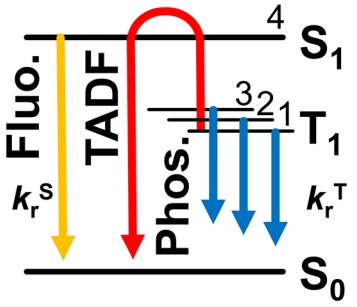

Fig. 1 General photophysical model of metal TADF luminophores including the lowest triplet state (T_1) splitting into three sublevels 1,2,3 and their respective decay pathways to the ground state (S_0) indicated with blue arrows. Fluorescence from the lowest singlet state (S_1, also denoted as 4) is depicted with a yellow arrow. TADF is depicted with a red arrow. k_r^S, k_r^T – radiative decay rate constants of singlet and triplet states.

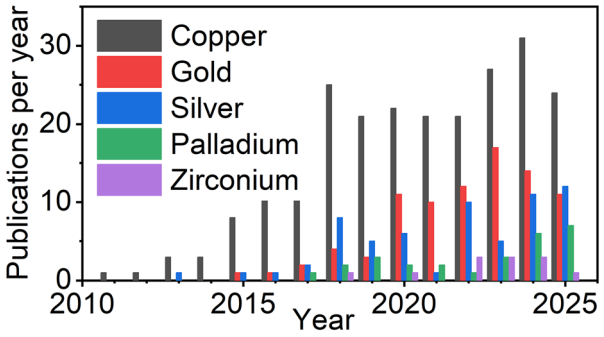

Fig. 2 Number of yearly publications according to the Scopus database featuring keywords "metal + TADF" for the metals indicated in the figure legend.

effect causes non-negligible splitting of the triplet states into three sublevels, also called zero-field splitting (ZFS). For this reason, considerations of TADF in transition metal complexes involve a minimum of four excited states: one singlet and three triplets,[1] unlike in metal-free TADF emitters, where a minimum of two excited states are required in the model.[10] Interestingly, oftentimes the presence of the metal makes the associated lowest singlet (S_1) and triplet (T_1) states sufficiently different to allow non-negligible SOC and hence direct interaction, without mediator states as often required in the metal-free TADF context.[11] In the simplest form of a four-state model of metal TADF, the states 1–3 represent the sublevels of the T_1 state, while the S_1 is represented by state 4. Therefore ZFS = ΔE_{1-3}, while the S_1–T_1 energy gap, relevant to TADF, can be defined as ΔE_{S-T} = ΔE_{1-4}, where 4 denotes the S_1 state.

TADF complexes form a subgroup among all metal complexes of varying luminescent nature. We hope we will convince the Readers that luminescent metal complexes exist on a continuous spectrum between TADF and phosphorescence at room temperature. With the stronger SOC (and hence faster radiative triplet decay) promoting phosphorescence, while weaker SOC (and slower triplet decay) facilitating TADF. We will delve into the details of this view further in this review.

Fig. 2 collects the yearly publication numbers for the keyword "TADF + metal name" for copper, silver, gold, palladium, and zirconium, showing an ever-increasing trend. We note that for metals like platinum and iridium the name of the element often appears together with the keyword TADF in a variety of different contexts unrelated to metal TADF and hence the data is skewed. On the other hand, these statistics do not represent the total number of publications representing each metal complex, but rather the popularity of the term used in publications.

It is immediately apparent that coinage metal complexes, like Cu(I), Au(I), or Au(III) are significantly more popular than those of other metals. It may on one side reflect their performance and desirability in practical applications, such as OLEDs. However, on the other hand it may also suggest that their properties are better understood than those of complexes of the other metals.

We believe that the lower interest in complexes other than the ones involving coinage metals might originate from various reasons. Some of them being synthetic chemistry and stability limitations, for example, other being limited understanding of the principles behind TADF in other groups of complexes. Some trends inevitably involve biases, such as negative bias against platinum and iridium complexes. In this minireview, we thought to collect not only the works that form the mainstream of research on metal-containing TADF emitters, but also wanted to point out other studies. We hope that we will be able to influence the mindset of the readers around the TADF emitters containing metals, and their distinctions and similarities with metalorganic phosphorescence emitters.

TADF and phosphorescent complexes can be used interchangeably in many applications, considering factors like the PL spectrum or radiative decay rate constants and often ignoring the mechanistic aspects of the origin of their luminescence. On the other hand, certain applications directly exploit the TADF mechanism itself, such as thermometry.[12] Therefore, it is relevant to look at some of the applications of luminescent transition metals more broadly, rather than focusing solely on those that are only applicable to TADF emitters.

2. Applications of metalorganic luminophores

Metalorganic luminophores have evolved as a versatile class of molecules with numerous applications in modern science and technology. Their structural design and adjustable photophysical properties are essential for diverse applications, including light-emitting diodes (OLEDs),[13] biological applications of labelling and sensing,[14,15] photodynamic therapy (PDT),[16] solar conversion,[17,18] photo-redox catalysis, and other various photonic applications. The benefits of metal complexes are high spin–orbit coupling (SOC) and high photoluminescence efficiency, providing a fantastic foundation for the development of next-generation materials with customised light-emitting properties. Luminescent metal complexes are traditionally associated with phosphorescence from triplet excited

states generated by heavy metal-induced intersystem crossing (ISC) and accelerated $T_1 \rightarrow S_0$ radiative decay rates thanks to singlet–triplet mixing and "borrowing" the radiative rate of singlets into triplet states. However, the past years witnessed an increase in reports on intriguing luminescent phenomena, like conventional fluorescence,[19] dual fluorescence/phosphorescence, TADF,[20] and dual phosphorescence. These findings indicate that in the world of luminescent metal complexes there may still exist areas unexplored and waiting to be discovered.

Organic light-emitting diodes

High-efficiency organic light-emitting diodes (OLEDs) have been a key research field in the last years, aiming to explore new materials that achieve red, green, and blue emission, but also near-infrared (NIR) and ultraviolet (UV), in OLED devices. However, achieving high efficiency and stability of blue OLEDs remains a significant challenge for researchers and the industry. In the past 30 years, this field has grown significantly. In particular, the display industry has recently shifted toward OLEDs due to their distinct advantages over conventional technologies like liquid crystal displays (LCDs). OLEDs do not require a backlight, unlike LCDs,[21,22] but instead OLED pixels generate light on their own. It is also easy to obtain true black as it simply requires the pixel to be turned off. Hence, black pixels in an OLED display do not consume power. Apart from creating true black colour, OLEDs make possible design of displays that are lighter, thinner, and bendable.[23] On the other hand, OLED displays improve the resolution, colour contrast, and provide a wide viewing angle, but also fast response times, and offer the potential for transparent screen designs.

Another interesting pathway is development of flexible OLED displays, which can be bent or rolled.[24] Examples include foldable smartphones like the Samsung Galaxy Fold, Huawei Mate X, and Royole FlexPai, as well as the Lenovo and Intel ThinkPad X1 Fold notebook.[25] However, OLED technology is still facing challenges with stability in blue and efficiency in NIR.

OLED technologies are often divided into four generations (Fig. 3). 1st generation are fluorescent OLEDs that reach up to 25% internal quantum efficiency due to spin statistics.[26–28] All the other generations allow for up to 100% internal quantum efficiency. 2nd generation are OLEDs based on phosphorescent transition metal luminophores, like Ir(III) and Pt(II) complexes.[29] 3rd generation are TADF emitters which bear important benefits over conventional transition metal emitters, such as shorter decay lifetimes, often independent of the magnitude of the heavy atom effect in those containing metal ions.[30] Hence our interest in TADF emitters that contain metals. The 4th generation of OLEDs involves hyperfluorescence[31] and hyperphosphorescence[32] – where TADF or phosphorescent molecules act as hosts for fluorescent terminal emitters. This approach has seen a great interest over the last years.[33,34] While TADF metal complexes can either display a majority TADF or phosphorescence emission, they can play a role in better understanding the differences and similarities between the two physical working principles in 4th generation OLEDs.

Metalorganic compounds are essential in the current state-of-the-art OLED technology.[35,36] In recent years, complexes of d^{10} metal ions like Cu(I) or Au(I) displaying TADF have gathered particular attention in this application.[37]

In 1999, Baldo and co-workers reported the first example of an electrophosphorescent OLED using the green-emissive *fac*-Ir(ppy)$_3$ complex.[38] This emitter remains a benchmark OLED material until today. In 2001, Thompson and co-workers demonstrated an OLED using the Ir(ppy)$_2$acac with an EQE of 12.3% at a wavelength of 525 nm.[39] Kim *et al.* in 2014 found that the choice of ancillary ligands in heteroleptic Ir(III) complexes affects the alignment of transition dipole moments. Using this effect, they achieved a green OLED with a very high EQE of 32.3%.[40] Williams and co-workers in 2008 designed a Pt(II) complex PtL^{2}Cl, the OLED device using this emitter exhibited an EQE of 14.5% and emission at 700 nm.[41] Li and coworkers reported another cyclometalated Pt(II) complex (PtN3N-ptb), and they achieved EQE of nearly 21.5%.[42] On the other hand, Tuong Ly *et al.* synthesised the homoleptic Pt(fprpz)$_2$ complex with emission at 740 nm, Φ_{PL} = 0.81 and EQE of 24%.[43]

To the best of our knowledge, the first use of a TADF metal complex in OLED was reported by Adachi and others in 2009, who used an Sn(IV) porphyrin complex.[2] The efficiency of such OLEDs was very low, however it was a proof-of-concept for the use of TADF in OLEDs. Nevertheless, Sn(IV) complexes have not become of particular interest over the following years. Shortly after this work other studies have emerged, like the work by Peters and others[5] from 2010 who reported an OLED using a TADF Cu(II) complex as the emitter and featuring 16.1% external quantum efficiency (EQE) – a truly impressive result at that time. Cu(I) and Au(I)/Au(III) complexes however, unlike the Sn(IV) counterparts, have become very popular as the main contenders to the Pt(II) and Ir(III) phosphorescent emitters.[44–46] The development of carbene metal amide (CMA) complexes of Cu(I) and Au(I) ions has provided a significant breakthrough in this field with highly efficient Au(I)-CMA emitters showing up to 27.5% EQE and luminance of up to 73 000 cd m^{-2}.[47] Although

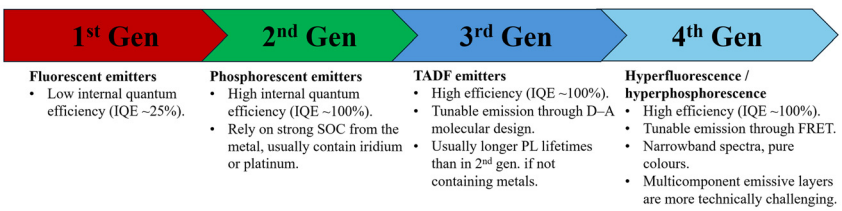

Fig. 3 Four generations of OLED emitters.

some progress has also been made with Ag(I)-CMA complexes they clearly gather much less interest than the other two coinage metal counterparts.[48] Research shows that metal TADF emitters like Au(I)-CMA complexes can be successfully used also in the 4th generation OLEDs.[49] The authors of the said work have achieved hyperfluorescent devices with 16.5% EQE. At this point, it is clear that short PL lifetimes are crucial for applications in OLED and some TADF complexes, like those featuring Zr(IV) ions are still far away from this application.[50] On the other hand, a significant progress has recently been made in Pt(II) and Pd(II) TADF complexes. Exemplar OLEDs featuring these metal ions and displaying efficiencies of above 20% and low efficiency roll-off have been described later in this review.[51,52] The above examples highlight the fundamental purpose and motivations for studying OLED emitters containing metals, whether they are phosphorescent, TADF, or both.

Bioimaging and photodynamic therapy

Luminescence bioimaging is a widely used technique for cell physiology and morphology investigations, real-life monitoring of biochemical processes at the subcellular level, as well as recognising and characterising pathologies in the clinical diagnostics field. Desired properties of suitable luminophores include high photostability enabling continuous exposure to irradiation *e.g.* in real-life imaging; as well as high luminescence quantum yield and possibly small overlap of absorption and emission which allows for avoiding self-quenching and thus reduced brightness, among others. Newly developed time-resolved and multiphoton imaging techniques brought a demand for probes with long emission decays and exhibiting multiple emissive states, both features being present in metal TADF complexes. Examples of such applications were depicted in a recent review.[53] However, it needs to be noted that, due to triplet states being quenched in oxygen-rich environments, the use of TADF-based probes for biological imaging, especially for TRLI (time-resolved luminescence imaging) remains a significant challenge. Removing oxygen or employing polymeric matrices to limit oxygen diffusion are possible strategies for improving the TADF luminescence signal.

An interesting application of a metal cation in TADF-exhibiting probes for imaging was proposed by Zhao, Yang *et al.*[54] They designed an organic D–A TADF luminophore, based on the PXZT exhibiting typical TADF features with emission maximum at 540 nm and delayed fluorescence lifetime τ = 939 ns. Titration with Zn^{2+} leads to the gradual formation of water-soluble **ZnPXZT1** complex showing both prompt and delayed fluorescence and enhanced ISC. This complex was then successfully introduced into HeLa and 3T3 cells, where subsequently added EDTA bound Zn^{2+} cations, leading to dissociation of the complex and hydrophobic aggregation of PXZT leading to enhanced fluorescence signal due to aggregation-induced delayed fluorescence. The approach led to the elimination of background signals giving a practical platform for time-resolved cell imaging (Fig. 4).

Photodynamic therapy (PDT) is considered to be a promising alternative for cancer treatment, as it relies on the local

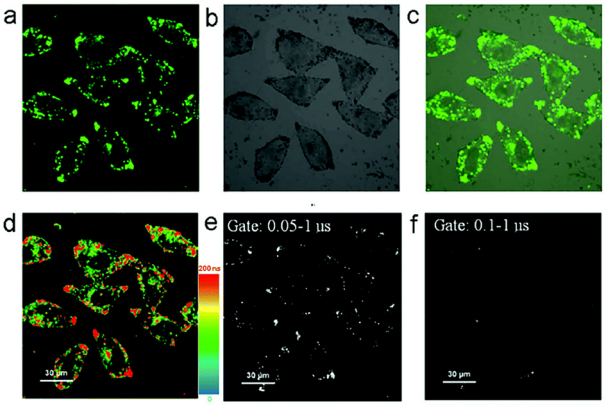

Fig. 4 Steady-state (a–c), luminescence lifetime (d) and time-gated (e and f) imaging of HeLa cells incubated with 10 μM **ZnPXZT1**. λ_{ex} = 405 nm, λ_{em} = 470–570 nm. (a) Darkfield; (b) bright field; (c) merging of (a) and (b). Reproduced from ref. 54.

cytotoxic effect of *in situ* generated reactive oxygen species (ROS) by means of a triplet photosensitizer. Photosensitizer is accumulated in the target lesional tissue, and after irradiation by, preferably long-wavelength light enabling deeper penetration, is excited, producing triplet states as a result. Henceforth, energy can be transferred to oxygen present in the cells, generating highly reactive singlet oxygen (type II ROS). Electron transfer may occur to surrounding tissue resulting in radicals such as hydroxyl ($OH^{\bullet}$), superoxide anions ($O_2^{\bullet-}$), and hydrogen peroxide (H_2O_2).

TADF emitters are considered to be superior to conventionally used photosensitizers due to enhanced triplet formation yield, which could translate into higher ROS generation yields. If a molecule exhibits rather large ΔE_{S-T} and thus longer triplet lifetimes, it provides enough opportunities to oxygen photosensitization to occur. This in turn allows for lowering the photosensitizer doses, possible longer irradiation intervals and overall lower dark cytotoxicity. Therefore, significant effort has been devoted to improve biocompatibility and subcellular localisation of the dyes, as well as shifting their absorption to the optical therapeutic window (700–1000 nm). This topic has been extensively explored in recent years, giving rise to TADF photosensitizers, predominantly based on organic dyes and nanoparticles.[55,56]

Among the most prominent applications of metal TADFs in PDT is Zr(IV) **Zr(^{Mes}PDP^{Ph})$_2$** complex first reported by Milsmann *et al.*[50] and further investigated as a PDT photosensitizer by Tang *et al.*[57] Nanoaggregates (nanoparticles, NPs) of the complex coassembled with 1,2-distearoyl-*sn*-glycero-3-phosphoethanolamine-*N*-[maleimide(polyethylene glycol)-2000] (DSPE-PEG$_{2000}$-MAL) and a cell penetrating peptide exhibited singlet oxygen generation quantum yield (Φ_Δ) of 0.56. Furthermore, NPs were observed to generate type-II ROS; superoxide anions and catalyse photoredox conversion of NADH to NAD^+, making **Zr(^{Mes}PDP^{Ph})$_2$** NPs a promising PDT agent in oxygen-poor, hypoxic tumours.

An interesting approach of combining photodynamic therapy using TADF systems with chemotherapy was proposed

by Song and colleagues,[58] resulting in excellent pharmaceutical outcomes following the idea of using supramolecular coordination complexes for enhanced PDT. Upon complexation detrimental photosensitizer aggregation is prevented, simultaneously providing the benefit of cytotoxic properties of the metal node. A self-assembling platinum(II) metallocene employed thiadiazole-based BTZPy TADF organic linker which on its own shows superior singlet oxygen generation yield – 0.95. The Φ_Δ was mostly retained in the resultant complex, with $^1O_2$ Φ_Δ for **BTZPy-Pt** determined at 0.86. More importantly, the half-maximal inhibitory concentration of the metallocene against HeLa cells was reduced by half in comparison to the non-coordinated organic photosensitizer, equalling 0.5 μg mL^{-1}. Therefore, outperforming BODIPY and porphyrin agents, highlighting the beneficial role of platinum nodes.

Somewhat metal TADF systems seem to be underrepresented in PDT applications. In our view, it may be due to the growing popularity of the heavy-atom-free trend leading towards the use of purely organic dyes.

Photocatalysis

Photocatalysis has been demonstrated as a powerful tool for a wide range of organic transformations, providing milder conditions and allowing to design green, cost-effective, and highly efficient synthetic strategies toward a variety of molecular designs. Due to the tunability of the absorption region of the dyes, variable and wide redox potential window of ground and excited states and long excited state lifetimes, TADF compounds emerged as an undeniably interesting class of photocatalysts. Quite uniquely in TADF photocatalysts, both S_1 and T_1 states are accessible for electron or energy transfer, broadening the scope of catalysed reaction types and starting molecules. Notably, the majority of efforts in this area are devoted to purely organic molecules and metal TADF materials remain in the minority. This topic has been extensively discussed elsewhere.[59–61] We note however, that substantial examples of metal TADF photocatalysts have already been reported.[62–64] Here we describe a few examples of metal TADF complexes used in these applications.

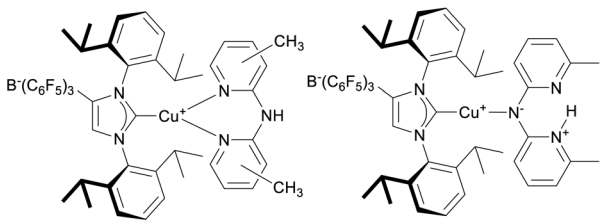

C2: Hdpa
C3: 3,3'Me$_2$Hdpa
C4: 4,4'Me$_2$Hdpa
C5: 5,5'Me$_2$Hdpa

C6: 6,6'Me2Hdpa

An example of using electron transfer from "long lived" singlet was presented by Lalevée *et al.*[65] in a comparative study of **[Cu(I)(POP)(dmbpy)][BF$_4$]** and **[Cu(I)(POP)(tmbpy)][BF$_4$]** (dmbpy = 4,4′-dimethyl-2,2′-bipyridyl; tmbpy = 4,4′,6,6′-tetramethyl-2,2′-bipyridyl; POP = bis[2-(diphenylphosphino)-phenyl]ether) copper cationic complexes, used as initiators for free radical and cationic polymerization. Introduction of two additional methyl groups in the bipyridine ligand of **[Cu(I)(POP)(tmbpy)][BF$_4$]** complex was sufficient to limit photoinduced flattening distortion of the molecule, reducing nonradiative deactivation to the ground state, hence improving Φ_{PL} from 0.09 to 0.55, and, most importantly, enabling TADF and "elongating" singlet excited state lifetime over 100-fold (from 0.02 μs to 2.5 μs).[66] Despite the lower molar absorption coefficient in **[Cu(I)(POP)(tmbpy)][BF$_4$]** and observed photolysis upon excitation, for both FRP and CP polimerizations of methacrylates and epoxy resins, respectively, the TADF exhibiting variant outperformed both of its counterparts and organic TADF photosensitizers, generating larger quantities of reactive species, radicals and cations, as an initiator of polymerization, leading to higher polymerization rates and giving higher monomer conversion.[67]

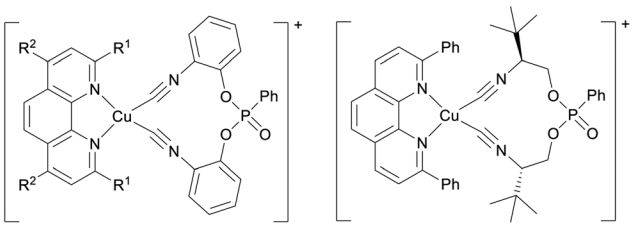

[Cu(dpp)(binc)]$^+$: R^1 = Ph, R^2 = H
[Cu(dmp)(binc)]$^+$: R^1 = Me, R^2 = H
[Cu(dpdmp)(binc)]$^+$: R^1 = Me, R^2 = Ph
[Cu(dap)(binc)]$^+$: R^1 = p-MeOPh, R^2 = H

[Cu(dpp)(binc*)]$^+$

Other Cu(I) complexes reported by Reiser *et al.*[68] were tested as ATRA (atom transfer radical addition) triplet photoredox photoinitiators. As evidenced by the proposed reaction mechanism, excited catalyst species transfer an electron to the ATRA reagent following an oxidative quenching cycle. Among tested systems, **[Cu(dpp)(binc)]BF$_4$** was shown to be the most active photocatalyst due to its increased triplet lifetime as well as higher reduction potential in the excited state in comparison to the reference [Cu(dap)$_2$]Cl complex. Moreover, the catalyst was tested in scarcely investigated allylation of organohalides with trimethylallylsilane yielding very good reaction yields (64–82%), depending on the starting material, with only 0.5 mol% catalyst loading and moderate reaction time (24 h).

Similarly, long-lived and highly populated triplet manifold of Zn(II) TADF dithiolate carbene complex enabled its use as a triplet photosensitizer in Dexter energy transfer photo-isomerisation of (*E*)-stilbene to (*Z*)-stilbene. Triplet energy requirement for the reaction to occur is 2.2 eV, hence **Z1** complex with triplet states energy ranging from 1.6 to 2.48 eV proved to be adequate, yielding 93% conversion rate after 4 h of irradiation (450 nm LED) and only 2 mol% loading. The complex outperformed the conventionally used [Ru(Bpy)$_3$](PF$_6$)$_2$ catalyst, both in the quantity of catalyst used (less) and reaction time. Further to that, the **Z1** complex also presents excellent photostability crucial in this application.[68]

Rapid intersystem crossing observed in TADF zirconium **Zr(^{Mes}PDP^{Ph})$_2$** complex, with intersystem crossing time τ_{IC} = 1.0 ps

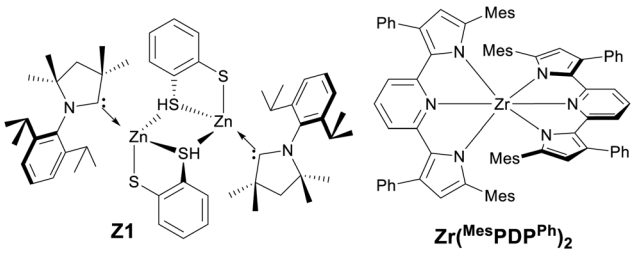

leads to a complete depopulation of S_1 upon excitation, and hence the absence of prompt fluorescence. Concomitant to that a long-living triplet excited state (τ = 1.04 ms) is formed. This in turn allows for use of this complex in photogeneration of singlet oxygen and a wide range of photoredox transformations, such as dehalogenation of aryl iodide, isomerisation of stilbene, atom transfer radical addition and trifluoromethylation of electron-rich arenes. Due to the introduced steric hindrance of mesityl groups in 2,6-bis(5-(2,4,6-trimethylphenyl)-3-phenyl-pyrrolid-2-yl) pyridine *NNN* pincer ligand. The complex exhibits excellent functional group tolerance in catalysed transformations in comparison to its methyl predecessor. Furthermore, the triplet excited state of **Zr(MesPDPPh)$_2$** can be involved in both oxidative as well as reductive quenching, along with energy transfer processes, which with high photo- and hydrolytic stability of the complex proves its high versatility as a photocatalyst.[50]

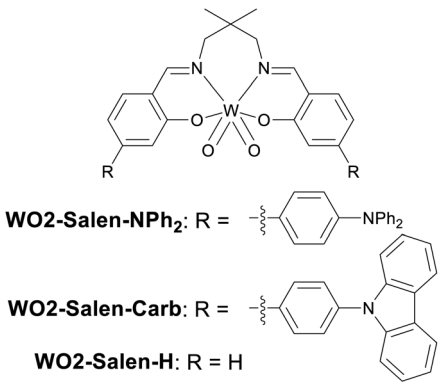

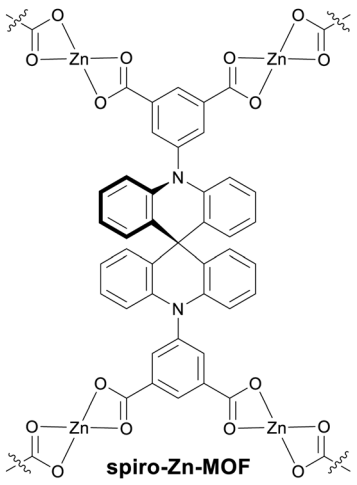

Furthermore, considering good photooxidating properties of **WO$_2$-Salen-NPh$_2$**, [E(W*/W$^-$)] and [E(W$^+$/W*)] potentials equal to +1.10 eV and −1.29 eV, respectively, complex was tested as photocatalyst in a wide range of visible-light-induced transformations, including borylation of aryl halides, C–C reductive coupling of benzylic halides and arylacyl bromides, decarboxylative coupling and cyanation of redox-active esters, dehalogenation of aryl halides and homocoupling of silyl enol ethers. Overall, obtained yields were good or very good, depending on the reaction.[69]

Photoreduction of CO_2 promises tackling serious environmental issues like global warming and climate change, simultaneously offering production of chemicals useful in synthesis as "byproducts". An extensive review on this topic using TADF compounds as photosensitizers has recently been presented elsewhere.[70] An interesting example are TADF-MOF photosensitizers proposed as a solution benefiting from well-tailored interplay between intrinsic porosity capable of CO_2 absorption and capture, and elongated excited state lifetimes to enhance its photoreductive properties. In example presented by Yang *et al.*[71] triplet harvesting is realised by an organic donor–acceptor spiral bi-acridine-based backbone, whereas zinc nodes provide an integrated photocatalyst, additionally ordering the structure and increasing crystallinity. Spiro-Zn-MOF exhibited delayed fluorescence inherent to its organic linker, retained in both air and CO_2 conditions. Finally, MOF catalyst was tested in CO_2 reduction experiments yielding a high photocatalytic efficiency of 50 μmol h^{-1} g^{-1}, while reference $Zn(NO_3)_2$, the linker as well as their physical mixture was inactive in the process of CO_2 photoreduction under the conditions tested.

Metal TADFs also gained recognition as photocatalysts in stereoselective transformations such as azetidine synthesis, [3 + 1] radical cascade cyclisation of cyclobutanols or intermolecular [2 + 2] homo-dimerization of chalcones, cinnamates and cinnamamides. Extensive mechanistic details and more examples including also the use of metal-free TADF emitters have been presented by Qiu *et al.*[62]

Thermometry and oxygen sensing

One way the TADF emitters differ from other main classes of luminophores is the presence of two emissive molecular energy levels which allow dual emissive properties. An advantage of metal TADF luminophores over metal-free TADF emitters in this respect is the possibility to eliminate prompt fluorescence from the picture. Fast intersystem crossing in most of metal TADF emitters results in a negligible intensity of prompt fluorescence – hence the non-temperature-dependent fluorescence does not interfere with the temperature reading. Prompt fluorescence originates directly from the lowest singlet (S_1) state and is not a part of the thermal equilibrium.

When the equilibrium between phosphorescence and TADF is just right at around room temperature both components will be present, allowing for a simple, optical, ratiometric temperature reading. With this approach, the optical sensor can be considered self-referenced.

Another way to detect temperature changes is by monitoring the TADF lifetime as a function of temperature, which applies to a wider variety of materials, but brings the challenges of interference or cross-talk from oxygen quenching. However, with the appropriate approach this issue can be turned into a feature allowing for simultaneous temperature and oxygen sensing.[72]

An earlier example of a ratiometric temperature sensor features benzoporphyrin Pd(II) complexes with $\Delta E_{S-T} \approx 0.3$ eV featuring red TADF emission and near-infrared (NIR) phosphorescence (Fig. 5).[12] In this example, the visible photoluminescence intensity of the sensor is temperature-dependent, thanks to the invisible NIR phosphorescence.

In a different example, especially engineered Pd(II) and Pt(II) complexes displaying dual phosphorescence + TADF emission at room temperature are used to produce a dual temperature and oxygen sensor.[73] This is achieved by a combination of self-referenced ratiometric temperature sensing and temperature-corrected time-resolved oxygen sensing. The Pd(II) complex displays a larger quantity of TADF *vs.* phosphorescence than its Pt(II) analogue, despite comparable $\Delta E_{S-T} \approx 0.25$ eV, due to the latter showing a faster radiative triplet decay.

Another examples of temperature sensors involve Zn(II) complexes emitting long-lived TADF with a lifetime of ~1 ms and with a $\Delta E_{S-T} \sim 0.2$–0.3 eV. Borisov and others have used either porphyrin Zn(II)[72] or Schiff-base[74] zinc complexes. Both of these groups of complexes display emission in the visible region comprised solely of fluorescence/TADF and without visible phosphorescence at RT. The combined temperature and oxygen sensing is done through time-resolved spectroscopy, by calibrating the dyes in a two-dimensional space defined by these two variables.

In order to eliminate the interference from oxygen Borisov and others have used a multi-layered structure in which the sensing film is protected first by an oxygen-scavenging layer produced with off-stoichiometry thiol–ene polymer (Fig. 6).[74] The excess unreacted thiol groups in this case act as an oxygen scavenger. This layer is coated with a film of poly(vinylidene chloride-*co*-acrylonitrile) acting as an oxygen barrier. The authors have achieved a sensitivity of 4.1% K^{-1} on change of TADF lifetime at 25 °C and a resolution of 0.03 °C or better.

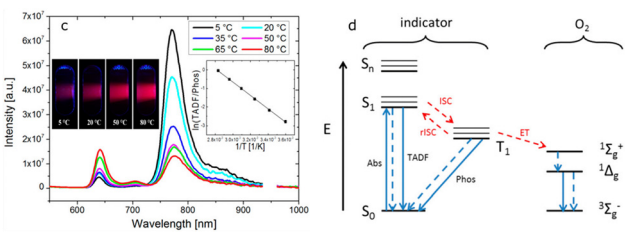

Fig. 5 Figure presenting an example photoluminescent behaviour of a Pd(II) benzoporphyrin TADF complex acting as a self-referenced temperature sensor. Left: photoluminescence spectra and photographs; right: schematic of the temperature activation and oxygen quenching pathways. Adapted with permission from ref. 12. Copyright 2017 American Chemical Society.

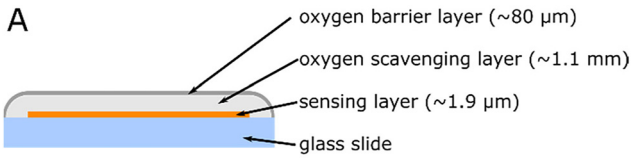

Fig. 6 A schematic representation of the encapsulation strategy for oxygen-insensitive temperature sensing. Adapted with permission from ref. 74. Copyright 2020 American Chemical Society.

What we note in all of these examples is the use of emitters with a relatively long-lived TADF decay and a rather large ΔE_{S-T}. It is in fact no surprise as a small ΔE_{S-T} would lead to dominance of TADF at RT (*i.e.* no dual emission for self-referenced sensing). Furthermore, larger ΔE_{S-T} actually acts beneficially as it increases the sensitivity of the TADF response to temperature, as per the Arrhenius equation.

Luminescent metal–organic frameworks (LMOFs)

Many researchers focus on luminescent metal–organic frameworks (LMOFs).[75] These materials retain the desirable emissive properties of molecular complexes while introducing structural features that enable new functionalities. LMOFs have created new opportunities in the fabrication of sophisticated photonic materials beyond traditional metal–organic luminophores.[75–78] They are crystalline, porous networks made up of metal nodes or clusters connected by organic ligands, which can exhibit tunable luminescence originating from the metal centre, the ligand, or charge-transfer states. On the other hand, their expanded framework design allows for additional functionalities like guest-responsive emission, multi-channel sensing, and energy transfer within the lattice.

LMOFs exhibit great potential in chemical sensing because of their high surface area and modular nature.[79] They display the ability to sense gases,[80,81] ions, or organic vapours with high selectivity through luminescence wavelength or PL intensity changes. Their porosity also makes them strong candidates for photocatalysis, drug delivery with real-time imaging, light harvesting, and environmental monitoring. Inclusion of TADF-active ligands or metal centres in the MOF framework has allowed for the investigation of delayed fluorescence in porous materials, merging structural complexity with improved photophysics.[80,82–84]

3. Photophysics

With the immense interest in the development of luminescent transition metal complexes, their TADF counterparts have emerged as luminophores that complement that larger group of emitters. They bring their own advantages, like shorter radiative decay times which benefit OLEDs or, temperature-dependent behaviour that finds its application in thermometry. But they also bear their own photophysical complexity.

In the context of typical transition metal complexes spin–orbit coupling (SOC) related effects must not be neglected and

shall be carefully considered (Fig. 1). One of the important consequences of the presence of the heavy atom is the splitting of the triplet excited state into three quasi-degenerate sublevels.[1] In this case, the energy splitting between the bottom (1st) and the top (3rd) sublevel of the T_1 is called the zero-field splitting (ZFS). Formally, this splitting occurs for all kinds of molecules, but can be neglected when no heavy atoms are present.

Usually in the luminescent transition metal field, and traditionally in photophysics more generally, energy gaps and spectral shifts are expressed in cm^{-1}. While this unit is useful for fundamental reasons it is not compatible with the current trends in expressing energy gaps in electronvolts (eV), as it is done in the TADF field. As metal TADF complexes form a subdivision to the broader metal complex field, some conventions traditionally used for the latter have been adopted when reporting data of metal TADF complexes. However, this hinders the mutual intelligibility of research outputs between metal-TADF complexes and metal-free TADF emitters. For example, parameters such as ΔE_{S-T} should be expressed in eV to be immediately comparable between emitters, while ZFS should be expressed in the same units as the ΔE_{S-T}.

Therefore, it is of paramount importance for those who prefer the convention of presenting energy in cm^{-1} to also use eV or meV alongside the traditional units

In many aspects, TADF and phosphorescent (also called RTP for room temperature phosphorescence) emitters are similar to each other and often the main factor differentiating them is the ΔE_{S-T}. Most metal-free TADF emitters are often designed with covalently linked electron donor and acceptor units to create charge transfer states.[10] The objective is to decrease the overlap integral between the frontier molecular orbitals, HOMO and LUMO. As the singlet–triplet energy gap, ΔE_{S-T}, is proportional to the overlap integral,[85] a small HOMO–LUMO overlap can result in small, sometimes negligible, ΔE_{S-T}, which is the crucial parameter for TADF to be observed.

However, while a small ΔE_{S-T} is key for TADF to be active, there is growing evidence that controlling the radiative and non-radiative processes, such as spin–orbit interactions and electronic–vibrational coupling, are also crucial for a successful TADF outcome. This is particularly evident in metal complexes, where the enhanced SOC interactions give little room for fluorescence to be observed. It is thus important to discuss how those metal complexes showing TADF emission can be distinguished from standard metal complexes showing RTP luminescence, based on experimental evidence.

Obviously, TADF and RTP properties can coexist. For example, TADF may manifest in organometallic complexes with heavy-transition metals, if the energy gap between the singlet and triplet states is small enough to allow the RISC rate to compete with the triplet decay rate. In this case, compounds may show only TADF – if the RISC rate is so fast that entirely outcompetes the triplet decay rate – or, most likely, show TADF and RTP emissions simultaneously. RTP can also be observed in metal-free emitters. In cases where the ISC rate is sufficiently fast to create a high triplet yield, and the non-radiative decay pathways have been sufficiently suppressed to allow the triplet radiative decay rate to compete, substantial RTP can be observed. Materials carrying n-donor atoms, such as halogens, oxygen, nitrogen, and sulphur, where n–π* transitions are present, can be good RTP emitters.

How to differentiate metal TADF emitters from phosphorescent luminophores?

In heavy-metal complexes where ΔE_{S-T} is large (Fig. 7), the fast ISC rate between S_1 and T_1 leads to almost 100% triplet formation.

The large ΔE_{S-T} makes the RISC rate unable to compete with the rate of triplet decay. Therefore, luminescence consists exclusively of RT phosphorescence. This luminescence is characterised by a single exponential decay in the μs to ms range, depending on the central ion present in the structure. In this case, the emission intensity tends to increase as temperature decreases, due to the progressive cancellation of non-radiative decay channels. Substantial apparent Stokes shift can also be observed as the emission appears exclusively from the low-energy triplet state and is hence often significantly shifted away from the stronger singlet absorptions. A good example of this class of emitters is the mononuclear Pt(II) complex with a tetradentate *ONCN*-coordinating ligand reported by Che *et al.*[86] As expected, this complex shows RTP lifetime of around 10 μs, and high Φ_{PL} = 0.79. Many other examples of heavy-metal RTP emitters with similar performances in different regions of the visible spectrum have been reported in the literature.[87] A clear example of a metal complex showing TADF is the cyclometallated di-Pt(II) complex of a bistetradentate ONCN–NCNO-coordinating ligand given in Fig. 28 as **Pt-1**.[88] **Pt-1** is analogous to the complex reported earlier by Che *et al.* and discussed above. Luminescence of this complex in methylcyclohexane is characterised by a very small Stokes shift, high Φ_{PL} = 0.83 – and relatively shorter decay lifetime, 2.1 μs, compared with its mononuclear analogue. The emission profile is also clearly more complex in the diplatinum complex than in its mononuclear analogue. The luminescence of the diplatinum complex shows overlapping blue-shifted and red-shifted emission bands, see

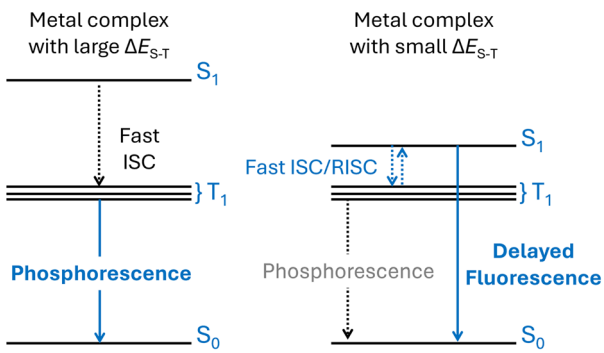

Fig. 7 Scheme showing how the small energy gap between singlet and triplet states can induce fast up and down ISC processes resulting in the observation of delayed fluorescence.

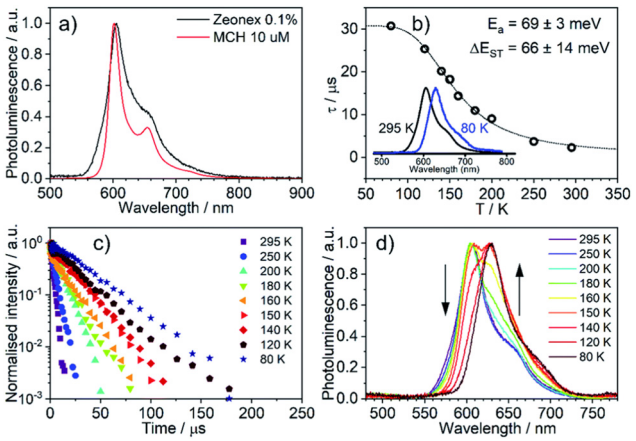

Fig. 8 Photoluminescence of **Pt-1** in Zeonex: (a) PL spectra in Zeonex and methylcyclohexane; (b) temperature dependence of decay lifetime; (c) photoluminescence decay traces as a function of temperature; (d) PL spectra as a function of temperature. Reproduced from ref. 88.

Fig. 8, attributed to dual TADF and RTP emissions. These emission bands show opposite temperature dependence. As temperature decreases, the intensity of the bluer emission band, attributed to TADF, decreases with temperature, while the intensity of the red-shifted emission band, assigned to RTP, increases relatively to TADF. This is due to both the RISC and non-radiative decay rates slowing down at lower temperatures. At room temperature, the TADF luminescence dominates the overall emission, whereas below 100 K, the emission is entirely attributed to phosphorescence. A similar pattern is expected in most metal TADF emitters.

Another important feature of metal TADF complexes is an often pronounced overlap between their absorption and PL spectra not otherwise observed in phosphorescent complexes (Fig. 9).

However, one must not be misled by the idealistic description where the TADF intensity is expected to increase with temperature in absolute terms. For emitters with lower Φ_{PL} or in cases where the TADF-driven emission and phosphorescence have similar quantum yields (or likewise is the phosphorescence quantum yield higher than the effective quantum yield of TADF), then this may not be observed. We stress here that the *increase of intensity with increasing temperature* cannot be used as evidence for TADF on its own. Likewise, the *drop in intensity with increasing temperature* shall not disqualify the TADF mechanism. What one should look for primarily is the existence of two emissive excited states and the thermal equilibrium between them that can be monitored *via* PL spectra. Other evidence, if present, is simply confirming this same scenario.

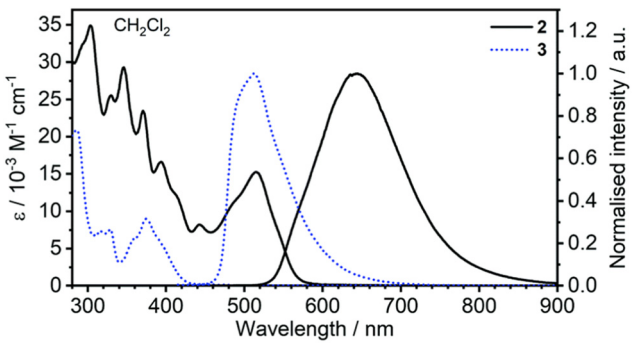

Fig. 9 Comparison of absorption and PL spectra of **Pt-2** (2) and its phosphorescent mono-Pt(II) analogue (3) in dichloromethane. Reproduced from ref. 89.

A common problem in studying TADF emitters with a large degree of conformational freedom is blue shifting of the PL spectrum at lower temperatures, caused by restricting molecular vibrations. The effect is more evident in a solution as at low temperatures the liquid freezes, changing the environment around the molecule completely. Hence, comparisons between RT PL in solution and frozen solvent in 77 K are not useful for characterising metal TADF emitters. Such blue shifts also sometimes occur in films and therefore cause significant complications in studying these luminophores and proving the nature of the luminescence mechanism.

TADF in organic and metalorganic emitters: similarities and differences

In clear contrast with metal TADF emitters, molecules without heavy-transition metals rarely show significant phosphorescence emission at RT. This happens due to a significantly lower ISC rate, allowing the radiative decay rate from S_1 to outcompete the ISC rate from S_1 to T_1. As a result, metal-free TADF emitters which share the same property tend to show prompt (PF) and delayed (DF) fluorescence emissions that are easily separated in time, giving origin to double exponential decays. The PF component appears directly from the radiative decay of the initially formed singlet states and often shows lifetimes in the order of tens of nanoseconds. The DF appears because of thermal triplet up-conversion to the singlet manifold caused by a small singlet–triplet energy gap, showing lifetimes in the order of 10 to 100 s of microseconds, equal to the triplet lifetime. Importantly, both PF and DF show the same spectrum as the emission always comes from the singlet excited state. Therefore, PF and DF are indistinguishable in steady-state conditions. However, if spectra are collected as a function of temperature, the DF component progressively becomes less intense as the temperature decreases. The DF lifetime also increases as the temperature decreases. This is caused by slower RISC process at lower temperatures.

This is in clear contrast with the luminescence decay in metal TADF emitters. In this case fast ISC/RISC rates mean the singlet and triplet states are in fast equilibrium. As a result, the DF and RTP bands decay with the same lifetime, and the prompt fluorescence is often not observed, due to the high ISC rate that outcompetes the radiative decay from the singlet state. In these cases the luminescence shows a single monoexponential decay.

Common to all TADF emitters is the effect of oxygen on the delayed fluorescence and phosphorescence. Since oxygen is a strong triplet quencher, and TADF and phosphorescence both originate from the triplet state, the presence of oxygen tends to quench the TADF and phosphorescence emissions.[11] This effect is frequently used to confirm and quantify, the contribution of DF to the overall emission. However, as oxygen tends to quench long-lived emissions in general, in some instances, especially in a solution, PF quenching also occurs.[90,91] Therefore, this experiment should be used with caution and only as a rough indicator, but not as a proof of triplet emission on its own. Methods based on time-resolved luminescence are thus preferable.

We have observed a growing significance of the Strickler-Berg approach for determining the radiative decay rate constant for the $S_1 \rightarrow S_0$ transition (k_r^S) in metal TADF emitters.[92] The final, practical equation used by Strickler and Berg in their work is presented below:

$$k_r = \frac{1}{\tau_0} = 2.880 \times 10^{-9} n^2 \left\langle \tilde{\nu}_f^{-3} \right\rangle_{Av} \frac{g_l}{g_u} \int \varepsilon \mathrm{d} \ln \tilde{\nu} \quad (1)$$

where: τ_0 – natural decay lifetime of emission; n – refractive index of the medium; $\tilde{\nu}_f$ – average wavenumber of the PL spectrum; g_l – multiplicity of the lower state, so $g_l = 1$ for S_0; g_u – multiplicity of the upper state, so $g_u = 1$ or 3 for S_1 and T_1 respectively; ε – extinction coefficient of absorption; $\tilde{\nu}$ – wavenumber representing points of the lowest absorption band in the spectrum.

In principle, this relationship was primarily designed for strong allowed transitions – the authors of the original work found it likely to be less accurate in the case of weak or forbidden transitions. However, experimental evidence suggests that this approach may still be applied for estimating the k_r even in those cases.[91,93] The benefit of this approach is the possibility of obtaining the k_r^S directly from the absorption spectrum and hence independently from the analysis of the photoluminescence spectra and lifetimes. Given that TADF is a complex process, in the simplest case involving the transition from the T_1 to the S_1 and subsequently from S_1 to S_0, the overall observable *apparent* radiative decay rate constant k_r will depend on the Boltzmann distribution between the S_1 and T_1 states. As a consequence the k_r in a metal TADF emitter may be significantly lower than the k_r^S obtained from eqn (1). However, the k_r^S obtained in this way is often found to match the value calculated from the kinetic analysis of the PL decay lifetime as a function of temperature.[94] On the other hand, the Strickler-Berg analysis performed for a phosphorescent emitter typically returns a comparable radiative decay rate constant to that obtained from the decay lifetime and Φ_{PL}.

Mathematical description of TADF in metal complexes

When the singlet–triplet energy difference ΔE_{S-T}, is small, and in the presence of a heavy-transition metal that enhances SOC interactions, the ISC process from S_1 to T_1 is very fast. Likewise, the reverse process from T_1 to S_1 (RISC) is equally fast. Herein, we assume the rates of ISC and RISC are related by eqn (2), where the factor of 1/3 accounts for the triplet degeneracy.

$$k_{RISC} = \frac{1}{3} k_{ISC} \exp\left(-\frac{\Delta E_{S-T}}{k_B T}\right) \quad (2)$$

were k_{ISC} and k_{RISC} are the ISC and RISC rates from S_1 to T_1 and from T_1 to S_1, respectively. k_B is the Boltzmann constant and T is the temperature. The singlet, n_S, and triplet, n_T, populations are described by eqn (3) and (4), where αI represents the rate of absorbed photons.

$$\frac{\mathrm{d}n_S}{\mathrm{d}t} = \alpha I - k_S n_S + k_{RISC} n_T \quad (3)$$

$$\frac{\mathrm{d}n_T}{\mathrm{d}t} = k_{ISC} n_S - k_T n_T \quad (4)$$

Herein:

$$k_S = k_r^S + k_{nr}^S + k_{ISC} \quad (5)$$

$$k_T = k_r^T + k_{nr}^T + k_{RISC} \quad (6)$$

Applying steady-state conditions to eqn (3) and (4), the singlet and triplet populations can be related to each other:

$$n_T = \frac{k_{ISC}}{k_T} n_S \quad (7)$$

$$n_S = \frac{\alpha I}{k_S - \frac{k_{RISC} k_{ISC}}{k_T}} \quad (8)$$

The total PL quantum yield can thus be defined as carrying the contributions from singlet and triplet states:

$$\Phi_{PL} = \frac{k_r^S n_S + k_r^T n_T}{\alpha I} = \frac{k_r^S k_T + k_r^T k_{ISC}}{k_S k_T - k_{RISC} k_{ISC}} = \frac{k_r^S (k_{T_0} + k_{RISC}) + k_r^T k_{ISC}}{k_{S_0} k_{T_0} + k_{S_0} k_{RISC} + k_{T_0} k_{ISC}} \quad (9)$$

where:

$$k_{S_0} = k_r^S + k_{nr}^S \quad (10)$$

$$k_{T_0} = k_r^T + k_{nr}^T \quad (11)$$

As the singlet and triplet are in a fast equilibrium, $k_{ISC} \gg k_{S_0}$ and $k_{RISC} \gg k_{T_0}$, eqn (9) can be simplified:

$$\Phi_{PL} \approx \frac{k_r^S k_{RISC} + k_r^T k_{ISC}}{k_{S_0} k_{RISC} + k_{T_0} k_{ISC}} \quad (12)$$

Now, using eqn (1),

$$\Phi_{PL} \approx \frac{\frac{1}{3} k_r^S \exp\left(-\frac{\Delta E_{S-T}}{k_B T}\right) + k_r^T}{\frac{1}{3} k_{S_0} \exp\left(-\frac{\Delta E_{S-T}}{k_B T}\right) + k_{T_0}} \quad (13)$$

Eqn (3) and (4) can also be solved without the pump term, αI, to obtain the luminescence decay components as a function of the rate constants in the system. The system involves

two different kinetic species, and therefore, the decay of singlet and triplet populations will be described by two exponential terms, with time constants λ_1, and λ_2.

$$\lambda_1 = \frac{1}{\tau_1} \approx k_{ISC} + k_{RISC} \tag{14}$$

$$\lambda_2 = \frac{1}{\tau_2} \approx k_{T_0} + \frac{1}{3}k_{S_0}\exp\left(-\frac{\Delta E_{S-T}}{k_B T}\right) \tag{15}$$

In metal TADF emitters $k_{ISC} + k_{RISC}$ is so high that in practice only one decay component, λ_2, is observed. Therefore, from eqn (13) and (15), the radiative rate can be obtained:

$$k_r = k_r^T + \frac{1}{3}k_r^S\exp\left(-\frac{\Delta E_{S-T}}{k_B T}\right) \tag{16}$$

The luminescence decay rate constant given in eqn (16) is strongly dependent on temperature, typically showing a sigmoidal dependence. At low temperatures, as both non-radiative decay pathways and RISC processes have been suppressed, the lifetime becomes constant, representing the phosphorescence contribution. However, as temperature increases and both the RISC processes and non-radiative decay pathways progressively become more active, the lifetime becomes faster. The abrupt decrease in lifetime observed as temperature increases reflects the increase of the S_1/T_1 population ratio. The temperature dependence of the average luminescence lifetime in metal-TADF emitters is usually described by eqn (17).

$$\tau(T) = \frac{3 + \exp\left(-\frac{\Delta E_{S-T}}{k_B T}\right)}{3k_r^T + k_r^S\exp\left(-\frac{\Delta E_{S-T}}{k_B T}\right)} \tag{17}$$

Eqn (17) assumes that the S_1 and T_1 states are in fast equilibrium, and that k_r^S and k_r^T are independent of temperature. By fitting the luminescence lifetime with eqn (17), the singlet–triplet energy difference, ΔE_{S-T}, k_r^S and k_r^T can be determined.

The discussion above, as well as eqn (17), presents a simplified approach where the k_r^T is treated as being independent of temperature. In reality, due to the triple degeneracy of the state, especially in the presence of ions like Pt(II) or Ir(III) the k_r^T displays a temperature-dependent behaviour due to the thermal equilibrium between the triplet sublevels 1–3:

$$k_r^T = \frac{k_r^1 + k_r^2 e^{-\frac{\Delta E_{1,2}}{k_B T}} + k_r^3 e^{-\frac{\Delta E_{1,3}}{k_B T}}}{1 + e^{-\frac{\Delta E_{1,2}}{k_B T}} + e^{-\frac{\Delta E_{1,3}}{k_B T}}} \tag{18}$$

where k_r^1, k_r^2, k_r^3 are the radiative rate constants of the sublevels 1–3; $\Delta E_{1,2}$, $\Delta E_{1,3}$ are the energy gaps between the sublevels 1–2 and 1–3.

Including the radiative rate constants of the quasi-degenerate triplet sublevels 1–3 gives eqn (19):

$$\tau(T) = \frac{1 + e^{-\frac{\Delta E_{1,2}}{k_B T}} + e^{-\frac{\Delta E_{1,3}}{k_B T}} + e^{-\frac{\Delta E_{S-T}}{k_B T}}}{k_r^1 + k_r^2 e^{-\frac{\Delta E_{1,2}}{k_B T}} + k_r^3 e^{-\frac{\Delta E_{1,3}}{k_B T}} + k_r^4 e^{-\frac{\Delta E_{S-T}}{k_B T}}} \tag{19}$$

where ΔE_{S-T} is calculated between the S_1 and the sublevel 1 of the T_1 state.

In cases where ZFS is relatively small as in Cu(I), Ag(I), Au(I) or Zr(IV) complexes, for example, and in the temperature range >77 K one may use eqn (17). In other cases eqn (19) is more appropriate.

The authors observe the use of k_{TADF} to describe the radiative decay rate constant of TADF. It is not a very fortunate notation given that this apparent constant describes a complex process. While the use of the experimental "as measured" radiative decay rate constant k_r defined as $k_r = \Phi_{PL}/\tau$ (where τ – measured PL decay lifetime) is justified being just a mathematical value describing what is being observed experimentally. However, often the observed emission displays a portion of TADF and a portion of RTP, which makes the meaning of k_{TADF} even more problematic. To sum up, we believe that the use of k_{TADF} notation is unjustified and unhelpful, and should be avoided.

Finally, in the context of a fast equilibrium between S_1 and T_1 in metal-TADF emitters the prompt fluorescence is in practice not observed. Therefore, it is legitimate to ask how can DF be observed? To answer this question, we first consider that the total fluorescence contribution to the overall luminescence, Φ_F, where $\Phi_F = \Phi_{PF} + \Phi_{DF}$, with Φ_{PF} and Φ_{DF} representing the yields of prompt and delayed fluorescence, respectively – appears as a result of singlet and triplet states being recycled through multiple consecutive ISC/RISC steps. Eqn (20), then relates the PF and DF contributions with the yields of triplet formation through ISC, Φ_{ISC}, and the yield of singlet states formed through RISC, Φ_{RISC}.

$$\Phi_F = \Phi_{PF} + \Phi_{DF} = \sum_{i=0}^{n}\Phi_{PF}(\Phi_{ISC}\Phi_{RISC})^i = \Phi_{PF}\frac{1}{1 - \Phi_{ISC}\Phi_{RISC}} \tag{20}$$

We then simulate the DF yield for hypothetical model systems with triplet formation yield Φ_{ISC}, ranging from 99.9% to 98%. To simplify, the effect of non-radiative decay is neglected. The prompt fluorescence yield is taken as $\Phi_{PF} = 1 - \Phi_{ISC}$. Fig. 10 shows the variation of the DF yield, Φ_{DF}, as a function of the RISC yield, Φ_{RISC}. It is immediately clear that in metal TADF emitters $\Phi_{ISC}\Phi_{RISC} \approx 1$ must hold, but Φ_{PF} must not be zero, for DF to be observed. Clearly, even for a very modest PF yield, ranging between 0.1% and 2%, the DF contribution can be substantial. However, Φ_{RISC} must also be high to maintain the system in fast equilibrium.

4. Computational studies

Current outlook

In this section we review selected works that are devoted to the computational arm of research on metal TADF luminophores. Due to the immense popularity of coinage metal complexes there is no surprise that Cu(I) complexes are of the main focus in those studies.

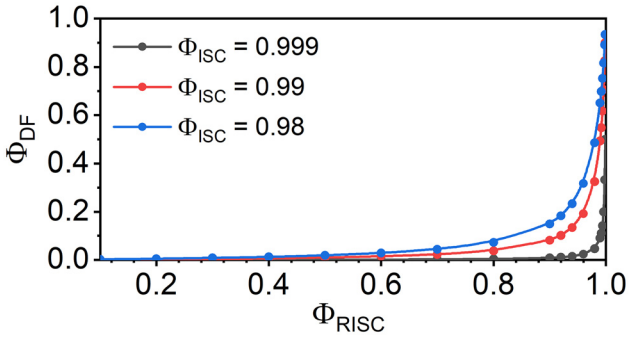

Fig. 10 DF contribution *vs.* RISC yield for different ISC yields.

Cu(I) complexes of the popular carbene–metal–amide (CMA) type, and likewise those of the Ag(I) and Au(I) ions, display a similar linear structure, which lends the two ligands binding from both ends of the complex a significant degree of rotational freedom. This behaviour complicates the photophysical description of this group of molecules, and current research in this topic aims to address the issue. This feature is somewhat similar to the behaviour of the donor–acceptor metal-free TADF molecules where rotation between the two moieties is usually unhindered.[95] Coinage metal complexes at the +1 oxidation state are somewhat unique in this respect, with complexes of many other metals generally displaying a donor–acceptor structure embedded within the coordination plane. The rigidity of these complexes and consequently narrow PL spectra and small Stokes shifts are reminiscent of multiple-resonance TADF emitters (MR-TADF).[96–98]

In 2022 Gao, Cui and colleagues studied the TADF mechanism in a CMA-type Cu(I) complex **CAAC-Cu-Cz**.[99] They proposed a TADF mechanism involving only the S_1 and T_1 excited states (Fig. 11). They calculated the radiative decay rates for the singlet and triplet states as well as the k_{ISC} and k_{RISC} constants, producing a full kinetic model of the emitter. Feeding these results into a kinetic model gave an estimate radiative decay lifetime similar to that obtained experimentally. The authors report SOC coupling constant $\langle T_1|\hat{H}_{SO}|S_1\rangle \approx 2$–$4$ cm^{-1} which aligns with the large k_{RISC} of $\sim 10^6$ s^{-1} obtained. Gao, Cui and colleagues carefully described the methodology they used for modelling and the work can without a doubt be recommended as a valuable tutorial for those interested in modelling radiative decay rates in luminescent metal complexes.

In 2024, Salman and colleagues systematically studied a group of Cu(I) CMA complexes with the *N*-carbazole unit decorated with zero, one or two CN groups at positions 3 and 6, as well as one or two carbonyl groups in the carbene ligand. Their results are in agreement with the experimental data reported for the studied complexes. Although they obtain $\langle T_1|\hat{H}_{SO}|S_1\rangle \approx 2$–$3$ cm^{-1} – similar to that obtained earlier by Gao, Cui and colleagues for other CMA complexes, the authors of the work conclude that these values are small and perhaps the T_2 state may be involved in RISC in some of the cases due to the $\langle T_2|\hat{H}_{SO}|S_1\rangle \approx 100$ cm^{-1}. The authors of this review note that SOC above 2 cm^{-1} is generally considered sufficient for efficient RISC in TADF emitters.[100]

In the same year, *de Silva* and others used the nuclear ensemble method to give a more in-depth insight into the behaviour of Cu(I) CMA complexes(Fig. 12).[101] They considered the coplanar and perpendicular arrangements of the *N*- and *C*-coordinating ligands along the N–Cu–C axis and created four ensembles: for S_1 and T_1 states of each of the conformers. This approach clearly benefits from a computational analysis that closer resembles that of an experimental system, where multiple conformations, rotations and vibrations are allowed. The authors find that the ISC mechanism clearly involves upper triplet states, while RISC effectively only involves the S_1 and T_1 states. Furthermore, they observe that RISC only occurs for the perpendicular conformation **CMA1**$^{\perp}$, whereas the parallel conformation **CMA1**$^{\parallel}$ displays phosphorescence.

Recently, in 2025, Romanov, Linnolahti and colleagues have performed a computational study in which they screened a wide variety of different *N*-coordinating ligands in Au(I) CMA emitters.[102] The authors use a somewhat standard computational approach using TD-DFT and involving SOC calculations. In their research they considered key parameters allow-

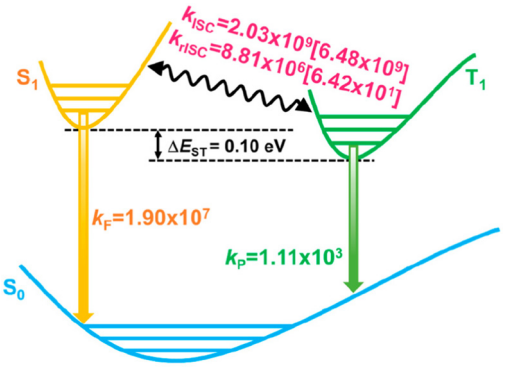

Fig. 11 Energy level diagram proposed by Gao, Cui and co-workers for CMA emitter **CAAC-Cu-Cz**. k_{ISC} and k_{RISC} are presented for T = 298 K and in square brackets for T = 77 K. Reproduced with permission from ref. 99. Copyright 2022 American Chemical Society.

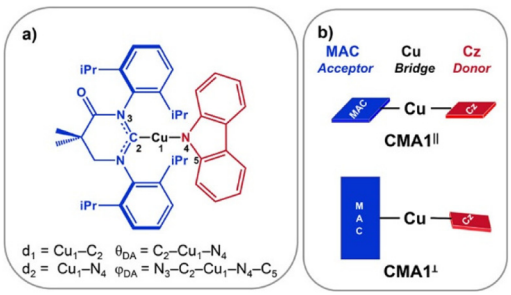

Fig. 12 (a) Structure of **CMA1** discussed in the work by *de Silva* and others. (b) Structural and conformational considerations undertaken in the study: (top) parallel configuration **CMA1**$^{\parallel}$ and (bottom) perpendicular configuration **CMA1**$^{\perp}$. Reproduced with permission from ref. 101. Copyright 2024 American Chemical Society.

ing selection of best Au(I) CMA emitters, like: % contribution of Au to HOMO and LUMO, HOMO/LUMO overlap integral, S_1 energy and oscillator strength f_{osc}, and ΔE_{ST}. They then selected the two most promising ones to be synthesised and studied experimentally.

Gao, Cui and co-workers have reported[103] a computational study of an Ir(III) complex which they describe as originally described in an earlier experimental work as displaying TADF (Fig. 13). However, the original work[104] actually claims a mechanism that is TADF-*like* – a similar thermally activated process, but without the involvement of the S_1 state and instead relying on a hypothetical upper triplet state with a singlet-like radiative decay rate. While the authors of this review do believe that the said paper indeed presents evidence for the conventional metal TADF it has nevertheless not been claimed by the authors of the experimental paper. Regardless of that, Gao, Cui and co-workers computationally demonstrate and model the metal TADF behaviour of the mono-Ir(III) complex using the time-dependent DFT (TD-DFT) and multi-state complete active space second-order perturbation theory (MS-CASPT2) methods. They use a two-state model involving S_1 and T_1 states in which the k_{RISC} from the T_1 is in the order of 10^9 s^{-1} at RT and hence sufficient to support the TADF mechanism. In this example the strong heavy atom effect of the Ir(III) ion sufficiently differentiates the S_1 and T_1 states such that efficient RISC can occur without the involvement of a third state.

A case computational study was reported by Cui, Gao and co-workers[105] based on the experimental work[88] by Pander, Williams, Kozhevnikov and others reporting on a first strongly fluorescent TADF Pt(II) complex. The authors point out that the $\langle T_1|\hat{H}_{SO}|S_1\rangle$ = 0.1 cm^{-1}, however $\langle T_2|\hat{H}_{SO}|S_1\rangle$ = 64 cm^{-1}, thus suggesting that the simple model for RISC involving solely S_1 and T_1 states is not feasible and hence proposing the involvement of the T_2 to be crucial. They subsequently calculated the k_{RISC} rates for both state pairs T_1–S_1 and T_2–S_1, pointing out that the latter is larger by a factor of 10^4. This work demonstrates that the heavy atom effect in some metal TADF luminophores can be minimal even in certain Pt(II) complexes, leading to the necessary involvement of states other than S_1 and T_1 in the overall TADF mechanism, as it occurs for metal-free TADF emitters.[106]

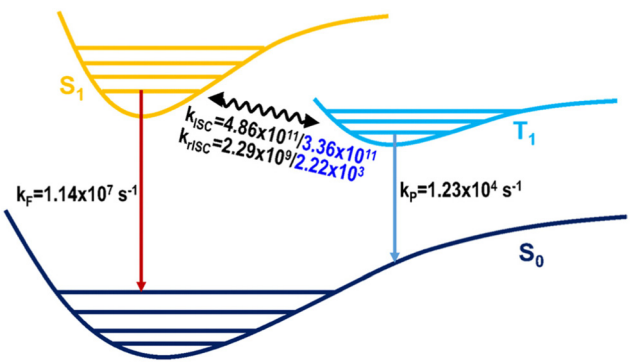

Fig. 13 Energy level diagram proposed by Gao, Cui and co-workers for the TADF Ir(III) complex. Values in black are obtained for T = 300 K, while those in blue for T = 77 K. Reproduced from ref. 103.

Modelling the luminescence kinetics and SOC of metal TADF luminophores

The popular DFT/TD-DFT approach often used to both metal-free and metal TADF luminophores is usually insufficient in describing the latter group of molecules. At this level of theory the triplet excited states are strictly non-emissive. In order to properly model triplet excited states in metal-containing molecules one should use computational methods that include SOC and relativistic effects, such as zeroth-order regular approximation (ZORA).

For example, if using popular ORCA software[107–109] then the calculation outputs contain the list of excited states including state compositions and energies, as well as the respective oscillator strength f_{osc} for both singlet and triplet states. The outputs also include an SOC matrix.

The spin–orbit coupling matrix element (SOCME) $\langle T_n|\hat{H}_{SO}|S_m\rangle$ for the T_n and S_m states can be calculated from the respective x, y and z components according to the equation below:[99]

$$\langle T_n|\hat{H}_{SO}|S_m\rangle = \sqrt[2]{\left(\langle T_n|H_x^{S0}|S_m\rangle\right)^2+\left(\left\langle T_n\middle|H_y^{S0}\middle|S_m\right\rangle\right)^2+\left(\langle T_n|H_z^{S0}|S_m\rangle\right)^2} \quad (21)$$

where T_n and S_m are the respective triplet and singlet wavefunctions; H_x^{S0}, H_y^{S0} and H_z^{S0} are the spin–orbit operators of the x, y and z components.

Intersystem crossing rate between two states S_m and T_n can be calculated using the following expression:[99,110–112]

$$k_{ISC} = \frac{1}{Z}\langle T_n|\hat{H}_{SO}|S_m\rangle^2\int_{-\infty}^{\infty} C(t)e^{it\Delta E_{mn}}dt \quad (22)$$

where $C(t)$ is the time-correlation function described in detail in ref. 99, while ΔE_{mn} is the adiabatic S–T energy gap. Z is partition function based on Boltzmann distribution:

$$Z = \sum_j e^{\frac{E_j}{k_B T}}$$

analogous to that presented in eqn (19), for example.

Oscillator strength f_{osc} can be used to calculate radiative decay rates of singlet and triplet states from equation:[99,113]

$$k_r = \frac{2\pi\nu^2 e^2}{\varepsilon_0 mc^3} f_{osc} \quad (23)$$

where ν is the emission wavenumber; e is the elemental charge; ε_0 is the vacuum permittivity; m is the mass of the electron; c is the speed of light.

Or a similar equation to 3, but in a different form and including the medium refractive index n:[114,115]

$$k_r = \frac{n^2\nu^2}{1.5} f_{osc} \quad (24)$$

where both eqn (23) and (24) originate from the Strickler-Berg equation.[92] Both 23 and 24 are applicable to either singlet or triplet states.

The thus obtained k_r can be fed into eqn (19) to obtain the combined radiative rate of the metal TADF emitter as a function of temperature.

Singlet and triplet states in metal TADF complexes

We understand anecdotally that there is a common notion among some inorganic chemists and photophysicists that singlet and triplet states in transition metal complexes are indistinguishable. This simplistic view is basically incorrect as shown by theory and computations. Spin–orbit coupling (SOC) induced by the presence of transition metal ions indeed causes a splitting of the triplet levels into three sublevels, but also mixing of the singlet and triplet states with each other.[8,115–117] The use of theory levels that include spin–orbit coupling and relativistic effects for correctly modelling heavy atoms allows to visualise this effect computationally.[114] Hence, it is true that in those cases pure states no longer exist. However, often the dominating nature of the state is evident in the computational picture, hence the attribution of S_n and T_n labels is justified.[118] Such calculations can easily be performed using ORCA, for example.[119]

Nevertheless, often these heavy atom effects can be neglected or simplified models can be used for complexes with relatively modest SOC, like those of Cu(I), Ag(I), Au(I), Zr(IV) or Zn(II) central ions. In the case of Pt(II) or Ir(III) central ions these effects may be more significant and hence must be carefully assessed. However, state multiplicity, singlet or triplet, can often be quantified even in this case.[118,120] On the other hand, certain heavy metal complexes can display surprisingly weak SOC. As demonstrated earlier, the $\langle T_1|\hat{H}_{SO}|S_1\rangle$ in certain Pt(II) complexes can be comparable to that in metal-free systems,[88,105] indicating a relatively insignificant state mixing in this case.

In conclusion, metal complexes exist on a continuum where the strength of the heavy atom effect (HAE) defines the magnitude of the state mixing. Weak or moderate HAE therefore often allows for either neglecting the state mixing altogether or at least for clearly identifying dominating excited state character.

5. Overview of metal complexes

In this section of the review, we describe examples of the most important metal TADF emitters, aiming to give similar attention to each of the various metal ions, rather than considering publication volumes. In this way we want to highlight the importance of the metal centre and its effect on the properties of each of the metal TADF emitters. Each section opens with a more general overview of the subject pertaining to each of the metal complexes, followed by a discussion of selected, recent works. In some cases where there are not too many examples of strong TADF, like in Pt(II), Pd(II), Zr(IV) or Ir(III) complexes, all of them or nearly all of them have been cited in this review – in other cases we have made a selection of works that could be interesting to the readership of the journal. We have introduced our own numbering of luminophores which consists of the chemical symbol of the metal involved followed by a hyphen and a consecutive number.

Principal types of metal emitters: MR-like and CT-like TADF

While preparing this review we have encountered a plethora of different structural design patterns that generally follow the typical coordination geometry of the central ions. While this is definitely a way to systematically arrange emitters in groups, it does not seem to be particularly helpful. However, metal TADF complexes can be divided into two main categories based on their photophysical and structural parameters (Fig. 14).

Complexes with relatively narrowband, structured PL are often rigid and contain flat chelating ligands – they display a form of CT states that *reside* within the coordination plane/sphere of the central ion. They often display excited states with a mixed intraligand CT and metal-to-ligand (or ligand-to-metal) CT character. These complexes can be characterised as MR-type TADF and the most prominent examples are certain Pt(II), Pd(II), Zr(IV) or Ir(III) complexes. The behaviour and structure of these complexes are reminiscent of metal-free MR-TADF emitters.[121] At the other end of the spectrum are CT-type TADF complexes with a pronounced metal-perturbed interligand CT that acts similarly to the metal-free donor–acceptor CT TADF molecules.[95] They often have more conformational freedom than their rigid counterparts. The prime example of these are the CMA-type complexes. We find that many metal TADF complexes are at either end of the spectrum, but some also occupy the fuzzy area between them.

Copper(I) complexes

Copper(I) complexes are probably the largest and the most investigated group of metalorganic luminophores displaying TADF, perhaps next to gold(I) complexes. The main premise for the use of copper(I) complexes is the low cost and abundance of the metal itself. However, they often prove challenging for introduction into optoelectronic or other applications due to low stability. We understand that some of these com-

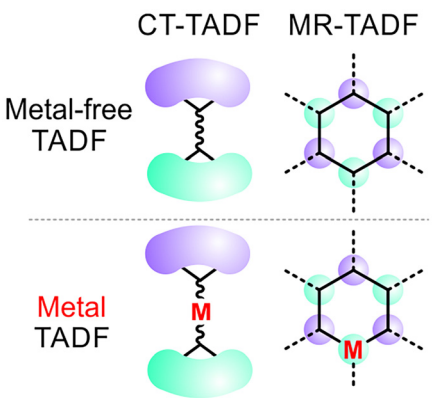

Fig. 14 Schematic representation of frontier molecular orbitals in MR-type and CT-type TADF emitters. Cyan – HOMO, magenta – LUMO; M – coordinated metal ion.

plexes are not air-stable, not to mention their stability in OLED devices. Cu(I) complexes were used as OLED luminophores already back in 1999.[122,123] Yersin and colleagues in 2011 identified TADF in one of their Cu(I) complexes.[124] In their work they named it as singlet harvesting, but the term triplet harvesting used in the context of TADF is more common nowadays (as triplets are the targets of the TADF mechanism). Since then, many Cu(I)-based TADF emitters have been developed. The relatively more recent discovery of two-coordinate carbene–metal–amide (CMA) emitters (like **Cu-1**), which employ bulky *N*-heterocyclic carbene (NHC) ligands can be considered an important development in this topic.[47,125,126] As these complexes are so popular, we decided to pinpoint only a few examples of recent works that appear interesting (Fig. 15).

Lam, Cheng, Che *et al.*[127] in 2022 presented a series of thermally and air-stable CMA Cu(I) emitters featuring bulky pyrazine- and pyridine-fused NHC ligands. Complexes **Cu-2** to **Cu-6** show high Φ_{PL} of up to 0.89 in solid film and 0.74 in toluene, and k_r in the order of 10^6 s^{-1} and as high as 2.2×10^6 s^{-1}. The complexes display a relatively narrowband and vibronically resolved PL in low polarity solvents, while their emission broadens and loses its vibronic resolution in more polar media. They emit in the range from 502 nm to 660 nm in toluene and from 470 nm to 600 nm in solid films, with the highest Φ_{PL} in toluene, at 0.74 reported for **Cu-6** and the lowest, at 0.11 reported for **Cu-4**. Complexes **Cu-2** to **Cu-6** display submicrosecond TADF lifetimes in the range of 0.11–0.55 μs in toluene and 0.36–0.47 μs in solid films. The authors of this work report highly efficient OLEDs obtained with EQE exceeding 20%, for example, for **Cu-2** they reported 21.2%, while for **Cu-6** 23.6%. They also reported a relatively long operational lifetime of the **Cu-4** based OLED (LT_{90} at 1000 cd m^{-2}) at 1300 hours, while the **Cu-6** based device gave 11.6 hours in the same test, which was the shortest lifetime recorded.

Traskovskis *et al.*[128] in 2022 reported CMA Cu(I) complexes **Cu-7** to **Cu-10** featuring phenylsulphonyl groups in the carbene ligand. The authors observe through-space charge transfer between the carbazole donor and the phenylsulfonyl acceptor. These complexes display Φ_{PL} of up to 0.90, but relatively low k_r in comparison with other CMA complexes, in the order of 10^5 s^{-1}. Complexes **Cu-7** to **Cu-10** display weak prompt fluorescence with τ = 6–18 ns and rather long TADF lifetimes in the millisecond range. OLED devices featuring these complexes display EQE of below 1%.

Pflaum, Steffen *et al.*[129] in 2023 reported chiral BINAP Cu(I) TADF complexes **Cu-11** and **Cu-12**. Both complexes display circularly polarised luminescence (CPL) behaviour, while **Cu-12** additionally displays mechanoresponsive luminescent behaviour (Fig. 16). The PL spectra are typical of other Cu(I) TADF complexes – broad and featureless. The ΔE_{S-T} is estimated at 0.06 eV in **Cu-11** and 0.08 eV in **Cu-12**. Φ_{PL} of these complexes is in the range 0.5–0.8 and above 0.7 in the solid state. TADF lifetimes are in the microsecond range, τ = 1.5 to 5.5 μs. The emission dissymmetry factor g_{lum} characterising the CPL was measured at 0.02. The authors used **Cu-11** in a proof-of-concept OLED, demonstrating circularly polarised electroluminescence.

Li, Artiem'ev *et al.*[130] in 2023 introduced a structurally unique class of charge-neutral Cu(I) TADF emitters **Cu-13** to **Cu-15** with a zwitterionic structure, containing both positively and negatively charged coordinated Cu(I) centres. The cationic centres are formed by Cu^+ ions coordinated with tris(2-pyridyl) phosphine (Py_3P) nitrogen atoms, while the anionic centres form $[Cu_xI_y]^{z-}$ ions. The luminescent study was conducted for various solvates of the presented complexes, involving molecules of acetonitrile, dichloromethane, benzonitrile, or acetone being embedded in the crystal lattice. They display green PL at 508–526 nm as solvates and a more red-shifted PL is observed in the non-solvated form of **Cu-13** and **Cu-14**, which emit at 540 nm. Various forms of complexes **Cu-13** to

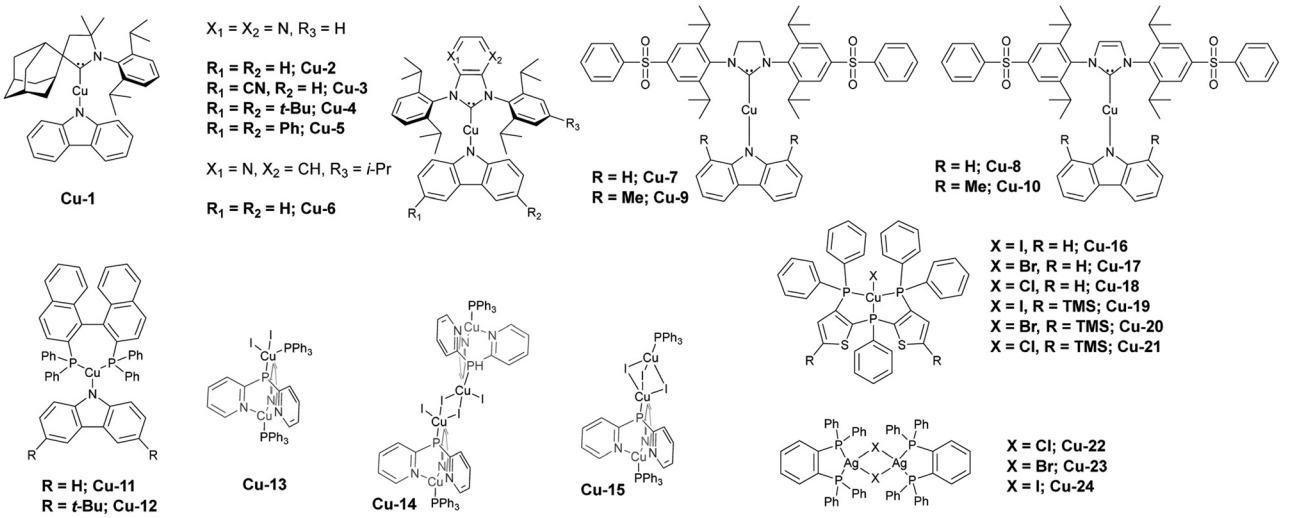

Fig. 15 Examples of metal TADF complexes containing Cu(I) ions.

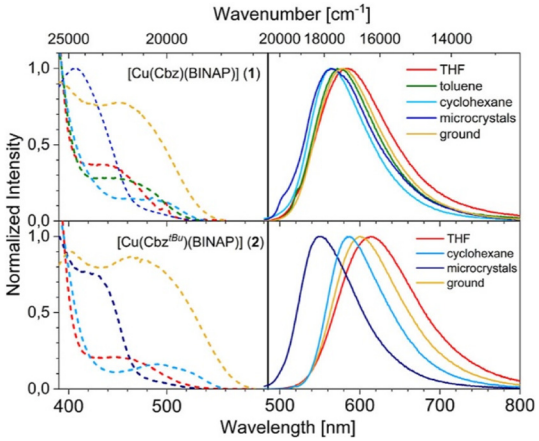

Fig. 16 Excitation spectra (left) and photoluminescence spectra (right) of **Cu-11** (1) and **Cu-12** (2). Reproduced with permission from ref. 129. Copyright 2023 American Chemical Society.

Cu-15 show similar TADF lifetimes, in the range 1.5–4 μs. The investigated solvates display high Φ_{PL} in the 0.8–1.0 range, while non-solvates are significantly less efficient, with Φ_{PL} = 0.10 for **Cu-13** and Φ_{PL} = 0.15 for **Cu-14**. As calculations suggest, in complex **Cu-13** the HOMO is primarily localised on the $[CuI_2]^-$ unit, while the LUMO is on the Py_3P ligand. The recorded ΔE_{S-T} of the solvates is in the range 50–90 meV. The authors find that grinding the solvate of complex **Cu-13** with MeCN leads to release of the lattice solvent molecules, resulting in a PL redshift, which can be reversed upon exposure to the same solvent (Fig. 17). Finally, the authors demonstrated radioluminescent properties of the solids which were comparatively luminous to the BGO ($Bi_4Ge_4O_{12}$) reference material.

Fa-Bao Li, Guijiang Zhou *et al.*[131] in 2024 reported two rigid triphosphine ligands and their corresponding Cu(I) halide complexes. The ligands L1 and L2 differ by the latter containing an electron-donating TMS group. The ligands are tridentate and the coordination sphere of the central ion is completed with a halide ion: Cl, Br, I, giving six complexes in total: **Cu-16** to **Cu-21**. The complexes were studied in form of powders and they display PL at 553–581 nm (**Cu-16** to **Cu-18**) and 565–589 nm (**Cu-19** to **Cu-21**). Φ_{PL} is generally larger in the TMS-decorated series, 0.19–0.29 for **Cu-16** to **Cu-18** and 0.36–0.61 for **Cu-19** to **Cu-21**, with the TADF lifetimes being similar in both groups: τ = 3.8–9.4 μs and τ = 2.2–7.6 μs on average. However, **Cu-16** and **Cu-19** significantly differ as the former displays τ = 8.0 μs, while the latter τ = 2.2 μs. The ΔE_{S-T} is below 0.1 eV in all complexes, in the range 64–78 meV in **Cu-16** to **Cu-18** and slightly larger in **Cu-19** to **Cu-21**, at 79–99 meV. Calculations suggest that the HOMO in those complexes is localised on the Cu–X axis and on the coordinating P atoms, while LUMO is mainly on the thiophene rings. The TMS groups stabilise the LUMO, explaining the average slight PL red shift of complexes **Cu-19** to **Cu-21** in respect to **Cu-16** to **Cu-18**. The effect of the TMS group is explained by the authors with a σ–π hyperconjugation. Complex **Cu-19** was selected for OLED fabrication giving a yellow electroluminescence at 584 nm (Fig. 18). The best device gave 14.6% EQE, but a limited luminance, below 1000 cd m^{-2}.

Lin, Chen *et al.*[132] reported in 2024 three di-Cu(I) complexes **Cu-22**, **Cu-23**, and **Cu-24** featuring a 1,2-bis(diphenylphosphino)-benzene (dppb) ligand and bridged with halogenide ligands: chloride, bromide, and iodide, respectively. These complexes display typical broadband and featureless PL, characteristic to the CT emissive states. The emission slightly blue shifts with the increasing atomic number of the halogen, from 535 nm in **Cu-22** to 500 nm in **Cu-24**. Φ_{PL} increases in the same order, with 0.37 in **Cu-22**, 0.44 in **Cu-23**, and 0.61 in **Cu-24**. Similarly, the smallest ΔE_{S-T} is observed for the **Cu-24** complex featuring bridging iodide ligands: 0.18 eV for **Cu-22**, 0.12 eV for **Cu-23**, and 0.07 eV for **Cu-24**. The radiative decay rate constant k_r in those complexes is in the order of 10^5 s^{-1}. These complexes were studied as X-ray scintillators and although effective, their properties were inferior to those of the analogous Ag(I) complexes featured in the next section of this review.

Silver(I) complexes

Ag(I) TADF complexes have generally been very popular in recent years, although not as much as luminophores featuring the other two coinage metal ions. Attractiveness of Ag(I) com-

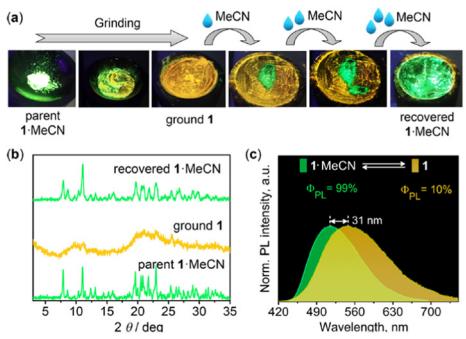

Fig. 17 Solvatochromism of **Cu-13**: (a) the effect of grinding and subsequent addition of MeCN. (b) PXRD patterns of the solvate and non-solvate forms. (c) PL spectra of the solvate and non-solvate forms. Reproduced from ref. 130.

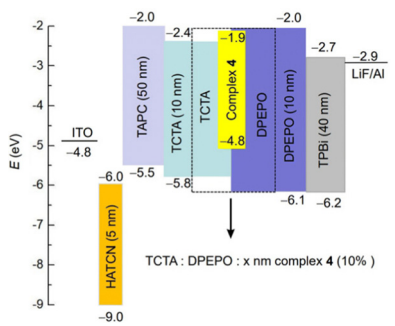

Fig. 18 OLED structure used for the complex **Cu-19** (denoted as **4** in the original work). Reproduced from ref. 131.

plexes stems out from the relative abundance and low price of silver in respect to gold, however Ag(I) luminophores are generally considered the least stable from the three coinage metal emitters. Ag(I) ions with d^{10} configuration allows TADF emitters with high Φ_{PL} through appropriate design of ligands.[133–137] By adjusting the energy levels of the ligands it is possible to design complexes that emit light across the entire visible spectrum.[138,139] Below we list some examples where Ag(I) TADF complexes were used in OLEDs. There have also been attempts to use them in light-emitting electrochemical cells (LEECs).[140] A selection of Ag(I) TADF emitters is presented in Fig. 19.

Romanov, Credgington, Bochmann *et al.*[141] reported in 2018 two Ag(I) CMA complexes **Ag-1** and **Ag-2**, featuring carbazole and *t*-butyl carbazole units. They display green PL with Φ_{PL} 0.74 and 0.55, respectively, in deaerated toluene. The PL lifetimes were recorded at $\tau \sim 300$–500 ns and k_r in the order of 10^6 s^{-1}, indicating extremely fast TADF emission. Although originally the authors report monoexponential PL, upon a closer investigation in the solid film they find that the decay of their complexes is biexponential – featuring both prompt fluorescence with a $\tau \sim 4$ ns and the aforementioned TADF component. Using the temperature dependence of TADF they identify ΔE_{S-T} = 108 meV for **Ag-1** and ΔE_{S-T} = 84 meV for **Ag-2**, in a polymer film. Considering the PL decay in function of temperature the authors discuss three regimes: (I) prompt fluorescence, (II) TADF, and (III) a third regime visible only <150 K which they attribute to ^{3}LE phosphorescence. Given that in a TADF mechanism the TADF and phosphorescence emissions should be in an equilibrium, *i.e.* decaying with identical decay rates, the presence of a ^{3}LE phosphorescence as a separate and longer-lived component puts the role of this state in the TADF mechanism in question.

In their proposed excited state model the ^{3}LE state resides above the ^{1}CT/^{3}CT manifold, while the RISC/ISC operate between the aforementioned pair of singlet and triplet CT states. The authors have produced vacuum-deposited as well as solution-processed OLEDs using both **Ag-1** and **Ag-2** and despite their similar molecular structure they obtained very different outcomes. They achieved EQE of 4.6% and 13.7% with vacuum-deposited OLEDs and 3.8% and 11% with solution-processed OLEDs, respectively for **Ag-1** and **Ag-2**.

Thompson *et al.*[142] presented in 2019 a study of two Ag(I) complexes **Ag-3** and **Ag-4** alongside analogous Cu(I) and Au(I) complexes coordinated with *N*-carbazolyl as amide and two different carbene ligands: CAAC = (5*R*,6*S*)-2-(2,6-diisopropyl phenyl)-6-isopropyl-3,3,9-trimethyl-2-azaspiro[4.5]decan-2-ylidene and MAC = 1,3-bis(2,6-diisopropylphenyl)-5,5-dimethyl-4-keto-tetrahydropyridylidene. **Ag-3** (τ = 0.37 μs; Φ_{PL} = 0.71) displays overall better PL performance in 2-methyltetrahydrofuran (2-MeTHF) than its counterpart **Ag-4** (τ = 0.04 μs; Φ_{PL} = 0.06). Their performance in polystyrene film is more alike: **Ag-3** shows τ = 0.50 μs; Φ_{PL} = 1.00, while **Ag-3** shows τ = 0.33 μs; Φ_{PL} = 0.79 (Fig. 20). Hence, the k_r exceeds 10^6 s^{-1}. X-ray crystallographic study reveals that the molecules form a configuration with the coplanar carbene and amide ligands – one of the two considered theoretically as relevant to the TADF mechanism, as described in the computational section of this review. **Ag-3** and **Ag-4** display ΔE_{S-T} in the order of 10–30 meV, depending on the model used. The authors observe that their complexes display a very structured PL spectra in frozen 2-MeTHF at 77 K – completely different from those at RT or recorded in polystyrene matrix. They rationalise it with rigidification of the solvent matrix that restricts the relaxation of the structure of the complex, destabilises the emitting ^{1}CT state, pushing it above the ^{3}LE energy of carbazole. Authors

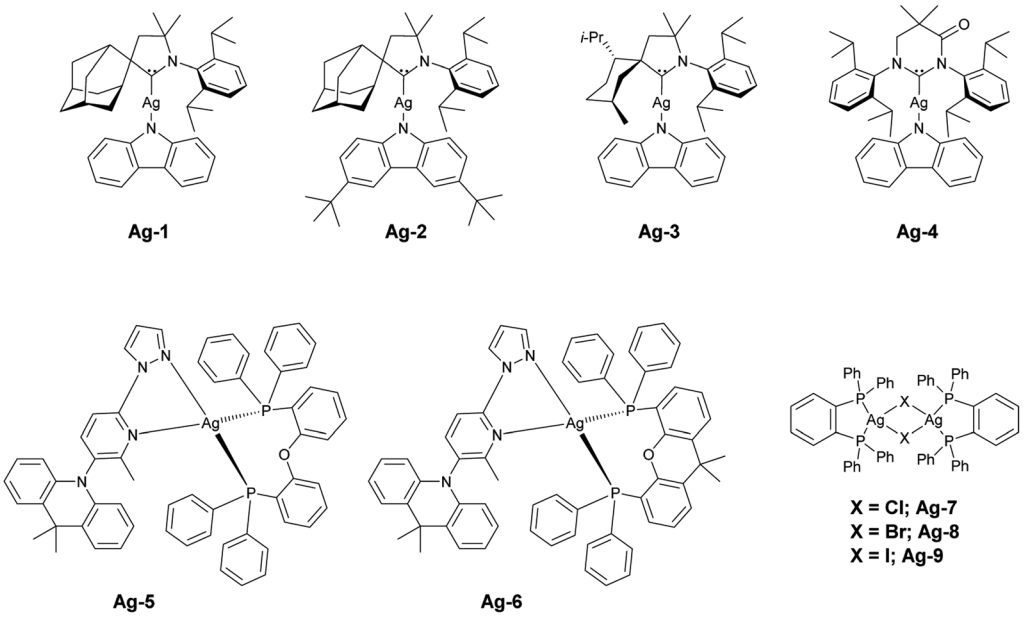

Fig. 19 Examples of metal TADF complexes containing Ag(I) ions.

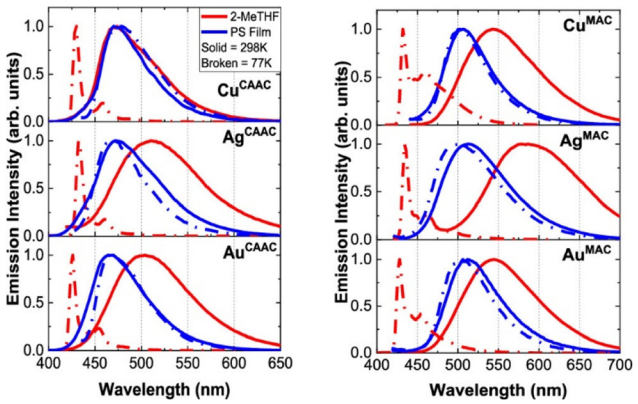

Fig. 20 PL spectra of **Ag-3** (Ag^{CAAC}) and **Ag-4** (Ag^{MAC}) alongside those of their Cu(I) and Au(I) analogues presented in the same work. Colour coding is shown in the figure legend. Reproduced with permission from ref. 142. Copyright 2019 American Chemical Society.

report no OLEDs were fabricated due to the issues with sublimation.

Can-Zhong Lu *et al.*[143] reported in 2020 two Ag(I) TADF complexes based on a donor–acceptor ligand: **Ag-5** and **Ag-6**. The idea for the work was that the donor–acceptor ligand does not show TADF, but displays room temperature phosphorescence behaviour. Upon coordination of the ligand with an Ag(I) ion and supporting diphosphine ligands the resultant complex does display TADF. The excited state landscape of the donor–acceptor ligand and the Ag(I) complex are shown in Fig. 21. The complexes display PL at 471–472 nm and near unity Φ_{PL} in PMMA films. They show both prompt fluorescence and TADF components: 4.1 ns and 6.3 μs for **Ag-5**, and 5.8 ns and 6.5 μs for **Ag-6** and consequently $k_r^S \sim 10^7$ s^{-1}. The ΔE_{S-T} = 0.17 eV for **Ag-5**, while ΔE_{S-T} = 0.15 eV for **Ag-6**.

While the specific principle presented in this work is novel, in a wider context it actually is a common notion in the field – most ligands coordinating transition metal complexes are non-TADF and often low-luminescent. The metal ion introduces its own set of orbitals, giving rise to a new set of excited states of a fundamentally different character. This is in opposition to a somewhat similar concept presented in Zn(II) complexes and described later in this review. In this latter case the Zn(II) ion does indeed lower the ΔE_{S-T} but its effect can mainly be attributed to simply escalating the strength of the acceptor. In the case of the Ag(I) ions the coordination fundamentally changes the orbital landscape, creating an essentially new luminophore upon coordination.

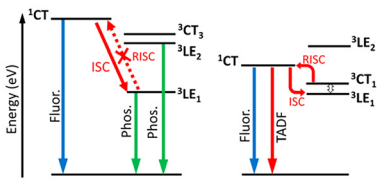

Fig. 21 Excited state landscape of the donor–acceptor ligand (left) and Ag(I) complexes **Ag-5** and **Ag-6**. Reproduced with permission from ref. 143. Copyright 2020 American Chemical Society.

Lin, Chen *et al.*[132] reported in 2024 a series of halogen(X)-bridged di-Ag(I) complexes displaying TADF: **Ag-7**, **Ag-8**, **Ag-9** where X = Cl, Br, I, respectively (Fig. 19), featuring 1,2-bis (diphenylphosphino)-benzene (dppb) ligands. These complexes were studied in powders. The bridging halogenide ligand has a profound effect on the PL behaviour of these complexes, giving a visible gradual change in the PL maximum from 487 nm in **Ag-7** to 450 nm in **Ag-9**. Furthermore, the Φ_{PL} decreases with the weight of the halogenide bridge: from 0.76 for **Ag-7**, 0.10 for **Ag-8** and 0.03 for **Ag-9**. These complexes display PL features typical of metal TADF, like a strong dependence of the PL lifetime upon temperature. The authors report ΔE_{S-T} of 0.13 eV in **Ag-7**, 0.17 in **Ag-8** and 0.20 in **Ag-9** and relatively low k_r at RT in the order of 10^4 s^{-1}. The complexes display strong radioluminescence and have been demonstrated to work as efficient X-ray scintillators. These materials work so well the authors have even produced scintillator screens used for X-ray radiographic imaging of selected objects.

Gold(I) complexes

Au(I) TADF materials have recently gained attention as efficient emitters for organic light-emitting diodes due to their promising electroluminescence performance.[144–146] These emitters display long operating lifetimes, low efficiency roll-off at high current densities, and high external quantum efficiencies (EQEs). Au(I) complexes are direct competitors to conventional phosphorescent and purely organic TADF emitters due to their favourable electronic and photophysical characteristics.[147–149] These play a significant role in efficient reverse intersystem crossing (RISC) or fast radiative decay rates. Linnolahti, Bochman, Credgington and coworkers demonstrated efficient TADF from a ligand-to-ligand charge transfer (LLCT) excited state in a carbene–metal–amide (CMA) Au(I) complex **Au-1** and highly efficient OLEDs incorporating this emitter (Fig. 22).[47] Since then, significant structural changes have been investigated, both on the electron-donating amide units and the electron-accepting carbene ligands. These modifications have produced a vast family of CMA complexes. These CMA systems are currently among the most common designs for Au(I) TADF complexes.[150–153]

Kai Li, Chuluo Yang *et al.*[154] reported in 2023 a metal-containing multiresonant TADF (MR-TADF) emitter **Au-2**. MR-TADF emitters are known for a rigid structure leading to narrowband photoluminescence, but suffer from long TADF lifetimes and thus require special emissive layer compositions to achieve high efficiency and low roll-off.[121,155] The authors used a MR-TADF emitter known as DtBuCzB and modified it with an Au(I)-carbene fragment. The thus obtained **Au-2** complex shares the properties of both Au(I) TADF complexes and MR-TADF emitters. The TADF properties of the **Au-2** are significantly better than those of the parent MR-TADF emitter recorded in mCP film, with TADF lifetime τ = 4.3 μs significantly shorter than that of DtBuCzB, at τ = 71.4 μs. In this case the prompt fluorescence lifetime of the Au(I) derivative is simi-

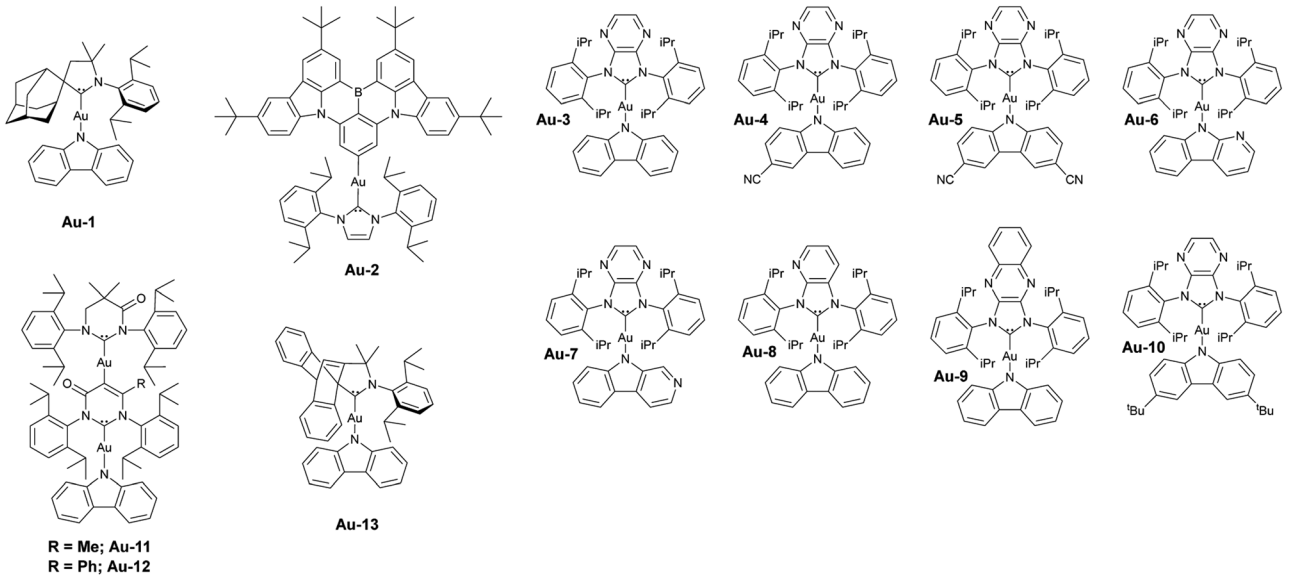

Fig. 22 Examples of metal TADF complexes containing Au(I) ions.

larly shorter, at τ = 1.6 ns compared to τ = 7.4 ns in the MR-TADF parent, thanks to the faster ISC rate in **Au-2**. The ΔE_{S-T} is smaller than in the parent emitter, at 90 meV *vs.* 110 meV. Complex **Au-2** emits at 508 nm with a Φ_{PL} = 0.95 in mCP. Orbitals of the Au(I) centre participate in both the S_1 and T_1 states, giving an improved S_1–T_1 SOC matrix element at 0.21 cm^{-1} in comparison with the reference emitter, where the said value is 0.024 cm^{-1}. The authors have used **Au-2** in both vacuum-deposited and solution-processed OLEDs. Usually, MR-TADF emitters require an emissive layer composed of a host and an assistant TADF host to work efficiently, but the authors used **Au-2** in a conventional host DMIC-TRZ to demonstrate its effectiveness without the need for assistant TADF emitter.[156] The OLED featuring **Au-2** emits at 510 nm with a high luminance 135 000 cd m^{-2} and negligible efficiency roll-off with maximum EQE at 35.8% and similarly high value of 35.7% at 1000 cd m^{-2} and 32.3% recorded at 10 000 cd m^{-2}. The reference device with the parent MR-TADF emitter displays a maximum EQE of 31.4%, but a significantly lower value at 1000/10 000 cd m^{-2} at 16.1% and 7.5%, respectively. The solution-processed OLED displays a lower efficiency of 25.7%, but still displays a better efficiency roll-off than the vacuum-deposited reference device. The example of **Au-2** demonstrates the key necessity for and benefits of connecting the two worlds: metal-free TADF and transition metal complexes.

Lam, Cheng, Che *et al.*[157] studied eight Au(I)-TADF complexes **Au-3** to **Au-10** of the CMA type featuring sterically bulky N-heterocyclic carbene ligands. These complexes emit in a broad range in toluene, from sky blue to near infrared with the PL maxima in the range 485–768 nm with Φ_{PL} = 0.02–0.76. In mCP or mCBP film the emission maxima span from 466 to 666 nm and the Φ_{PL} is larger, in the range 0.63–0.99. The TADF lifetime in toluene is shorter τ < 0.5 μs, but in films τ = 0.21–1.1 μs with the k_r in both media at ~10^6 s^{-1}. The authors report key TADF parameters for complexes **Au-3** and **Au-7** to **Au-10**, which are comparable among all. The $k_{RISC} \sim 10^9$ s^{-1}, $k_{ISC} \sim 10^{10}$ s^{-1}, ΔE_{S-T} = 40–80 meV. These complexes display significant solvatochromism visible in their PL and absorption spectra. For example, complex **Au-3** displays PL at ~550 nm in hexane and 730 nm in acetonitrile. The authors produced vacuum-deposited OLEDs featuring emitters **Au-3** to **Au-10** and studied their operational stability. They achieved very high maximum EQE in the range 21.3–26.9 for complexes **Au-3** to **Au-7** with electroluminescence in the 502–566 nm range. A bluer **Au-8** gave 15.1% at 487 nm, while red/near infrared emissive **Au-9** and **Au-10** gave maximum efficiency of 17.4% at 632 nm and 10.0% at 705 nm, respectively. The operational lifetime of OLEDs is highly varied among emitters with the largest LT_{95} value recorded for **Au-3** based OLED at 2082 h at luminance 1000 cd m^{-2}.

Tian-Yi Li *et al.*[158] reported two bimetallic Au(I) complexes with a tandem carbene structure (NHC-Au(I)–NHC-Au(I)-carbazolyl): **Au-11** and **Au-12** (Fig. 23). This structure is interesting as it features both twisted and coplanar configurations of the ligands. The complexes overall do not present any spectacular behaviour that would be exceptional among all the other Au(I)-CMA complexes discussed in this review. However, the dinuclear tandem structure deserves a note. The authors of the work report a likely phosphorescence-only behaviour of complex **Au-11** and a dual TADF and phosphorescent behaviour of complex **Au-12**. The authors use the term thermally stimulated delayed phosphorescence or TSDP to describe the behaviour of their system. The term TSDP on its own is rather confusing from the photophysics perspective as to the meaning of the phrase delayed phosphorescence, while we believe that the behaviour of the complex **Au-12** requires some more in-depth analysis to be fully understood. The authors identify two exponential components in the luminescence of **Au-12** PL in polystyrene film at

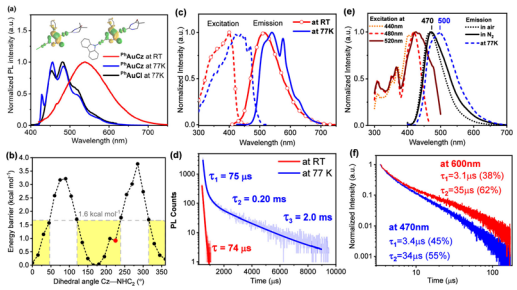

Fig. 23 Photoluminescent behaviour of **Au-11** (^{Me}AuCz) and **Au-12** (^{Ph}AuCz). Reproduced with permission from ref. 158. Copyright 2024 American Chemical Society.

RT with τ_1 = 3.4 μs attributed to TADF and τ_2 = 34 μs attributed to phosphorescence. Both components display temperature-dependent behaviour and the lifetime of both increases at lower temperatures. This feature *per se* is common to both TADF and phosphorescence in certain cases and hence not particularly unique. The lifetime of τ_2 = 34 μs is rather short for a phosphorescent Au(I) complex, but long if it were TADF. We recommend the readers to make their own conclusions about the work.

Linnolahti, Romanov *et al.*[159] in 2025 explored a version of Au(I)-CMA complexes[126,160] using the cyclic(amino)(barrelene) carbene (CABC) ligand: complex **Au-13**. The CABC ligand is thought as a modification of the cyclic alkyl amino carbene (CAAC) ligand, like one present in **Au-1**. **Au-13** emits at 660 nm in toluene and at 565 nm in polystyrene (the emission is red-shifted in respect to **Au-1**, where the PL maximum is at 505 nm). The Φ_{PL} = 0.66, τ = 0.92 μ and k_r = 7.2 × 10^5 s^{-1} in polystyrene. The complex displays a very pronounced PL blue shift at 77 K in solution to 520 nm – the same is not observed in polystyrene. Photophysics of **Au-13** overall is very similar to that of **Au-1**, but the former is structurally interesting due to the use of the barrelene motif as a sterically bulky fragment of the carbene ligand.

Gold(III) complexes

Au(III) is an attractive candidate for development of luminescent materials because of the high SOC, efficient triplet harvesting and strong bond between gold and ligand.[161] Au(III) is a tetracoordinated ion with a planar configuration similar to that of the isoelectronic Pt(II) ions of the same d^8 electron configuration. Hence, it forms structurally rigid complexes often with CNC diphenylpyridine or analogous ligands. Gold is also more abundant and accessible than some other noble metals, like iridium. The past few years saw a significant development in the usage of Au(III) complexes in OLEDs and efficiencies exceeding 25% have already been achieved.[162] The use of chelating tetradentate ligands gives rigid scaffolds that provide improved operational stability in OLED, preventing excited-state structural deformation and giving enhanced thermal stability of metal complexes.[163,164] Au(III) thanks to its d^8 configuration can be used in such rigid complexes.[165,166] Examples of Au(III) TADF complexes discussed in this review are shown in Fig. 24.

Cheng, Tong, Che *et al.*[167] in 2020 designed and investigated three pincer Au(III) complexes **Au(III)-2** to **Au(III)-4**, modifications of the previous structure **Au(III)-1**.[162] The structural changes in the new complexes involve replacing the OEt moiety in the *CNC* ligand with a more electron-donating NMe_2 group in **Au(III)-2** and **Au(III)-3** and addition of fluorine atoms *para* to the nitrogen in the donor, in **Au(III)-3**. Complex **Au(III)-4** does not have the OEt nor the NMe_2 group attached to the pyrimidine unit. **Au(III)-2** and **Au(III)-3** emit at 495 nm and 483 nm, respectively, while **Au(III)-4** emits at 566 nm. **Au(III)-2** to **Au(III)-4** emit TADF with a submicrosecond lifetime, at τ = 0.68 μs, τ = 0.67 μs, and τ = 0.84 μs, respectively and high Φ_{PL} in the 0.60–0.93 range. The k_r of these complexes is in the order of ~10^6 s^{-1}. Complexes **Au(III)-2** to **Au(III)-4** were used in solution-processed OLEDs. The bluer-emitting complexes **Au(III)-2** and **Au(III)-3** gave sky blue electroluminescence at 473 and 465 nm, respectively, with efficiencies of 15.3% for **Au(III)-2** and 6.8% for **Au(III)-3**. **Au(III)-4** was more efficient, at 24.3% but with green electroluminescence at 534 nm.

Che *et al.*[161] reported in 2020 novel, highly emissive, charge-neutral tetradentate *CCNC* Au(III) complexes synthesised using microwave-assisted C–H bond activation. Thanks to their rigid structure they present exceptional stability and high Φ_{PL}. These complexes can be subdivided into two groups – those with their PL dominated by phosphorescence (**Au(III)-5**, **Au(III)-6**, **Au(III)-7**, **Au(III)-9**, **Au(III)-10**, **Au(III)-13**) and the others with PL dominated by TADF (**Au(III)-8**, **Au(III)-11**, **Au(III)-12**). The former group is characterised by low k_r ~ 10^3 s^{-1} and long PL lifetimes of 77–225 μs, but also relatively high Φ_{PL} in the range 0.26–0.77, except for **Au(III)-13** with a very low Φ_{PL} = 0.003 and τ = 1.0 μs. The latter group displays high k_r ~ 10^5–10^6 s^{-1}, τ = 0.62–1.61 μs and Φ_{PL} 0.47–0.94 demonstrating the importance of the TADF mechanism. Both of the aforementioned characteristics apply to toluene solutions. Complexes **Au(III)-7**, **Au(III)-8**, **Au(III)-11**, and **Au(III)-12** display broad featureless spectra, while the other complexes show vibronically-resolved, structured PL. This is a consequence of the donor–acceptor structure of complexes **Au(III)-7**, **Au(III)-8**, **Au(III)-11**, and **Au(III)-12**, where the diphenylamine or phenothiazine acts as a donor. The authors also perform femtosecond transient absorption studies, revealing ISC rates k_{ISC} of the studied complexes at 10^{11}–10^{12} s^{-1}. Calculations suggest that indeed the Au(III) centre acts as an acceptor against the appended diphenylamine or phenoxazine donors. TADF complexes **Au(III)-8**, **Au(III)-11**, **Au(III)-12** were used as emitters in vacuum-deposited OLEDs achieving impressive external quantum efficiencies exceeding 20%. Complex **Au(III)-8** gave the best performance at 25.0% and low roll-off with 22.0% efficiency recorded at 1000 cd m^{-2}. This OLED also showed a promising operational lifetime LT_{95} with 105 h at 1000 cd m^{-2} and 5280 h at 100 cd m^{-2}.

Chan, Yam *et al.*[168] in 2021 investigated a series of cyclometalated alkynylgold(III) complexes (**Au(III)-14** to **Au(III)-19**) featuring *CNC*-coordinating diphenylthienopyridine ligands. The

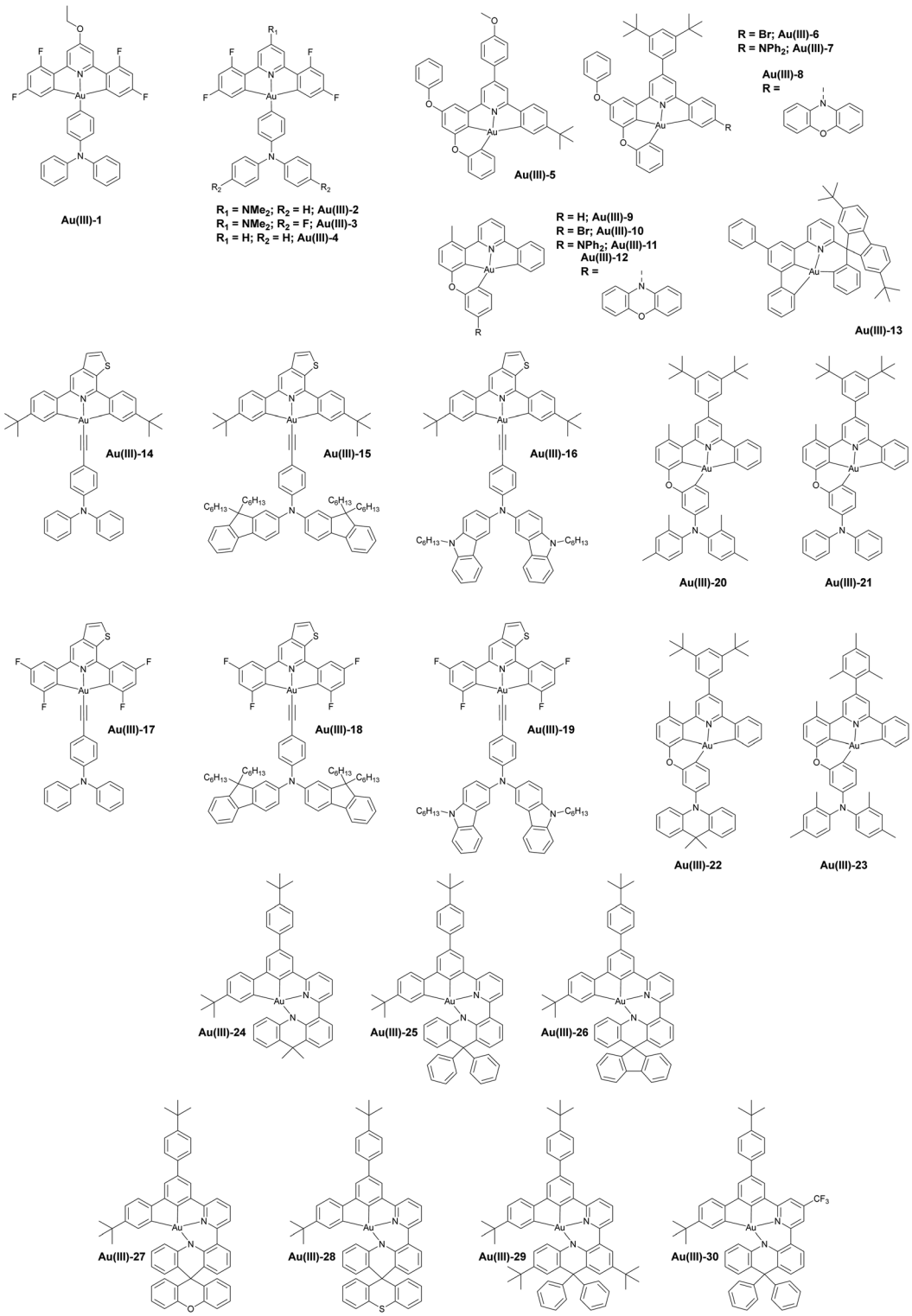

Fig. 24 Examples of metal TADF complexes containing Au(III) ions.

design of these complexes features an acceptor centre of the Au(III)-*CNC* coordinated unit and the triarylamine donor attached *via* the alkynyl linker, creating a donor–acceptor system. This design promotes small ΔE_{S-T} and red-shifted PL. As the calculations show, for example, in **Au(III)-16**, the HOMO is localised on the triarylamine unit, while the LUMO on the Au(III)-*CNC* unit, giving a small orbital overlap between the MOs (Fig. 25). PL of complexes (**Au(III)-14** to **Au(III)-19**) can

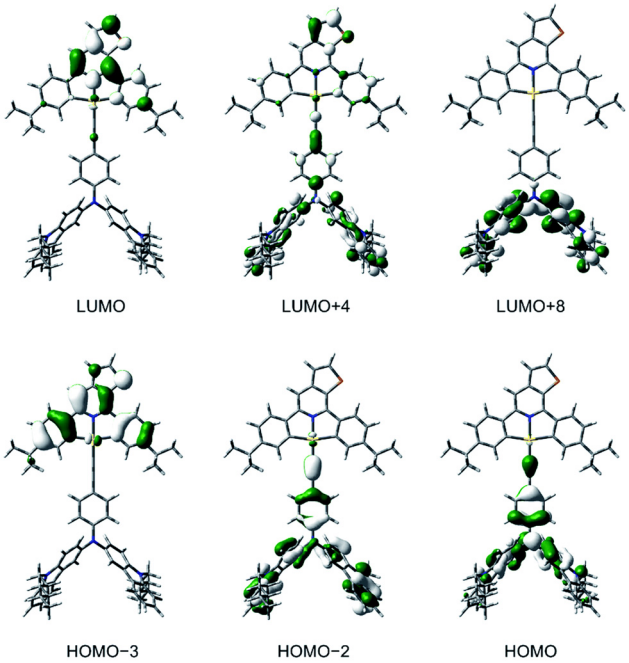

Fig. 25 Calculated molecular orbital isosurfaces for **Au(III)-16**. Reproduced from ref. 168.

either be attributed to ^{3}IL (intraligand) with some CT character, like in **Au(III)-14**, so mainly to phosphorescence or to ^{1}LLCT (ligand-to-ligand CT or interligand CT), like in **Au(III)-16** and **Au(III)-19**, so to TADF. The distinction is immediately apparent as **Au(III)-14** emits at 524 nm in toluene with a resolved PL spectrum and displays $k_r \sim 10^3$ s^{-1}. Comparatively low $k_r \sim 10^4$ s^{-1} in toluene is displayed also by **Au(III)-15**, **Au(III)-18** and **Au(III)-19**, while other emitters display various contributions of TADF as their reported k_r is larger, at ~10^5 s^{-1}. **Au(III)-15**, like **Au(III)-14**, displays green PL at 525 nm, but all the other complexes emit in the 600–750 nm range. The Φ_{PL} of these complexes is generally low (<0.1) in toluene, but in the range 0.40–0.83 in mCP at low concentration. ΔE_{S-T} for **Au(III)-16** and **Au(III)-18** was estimated at 30 meV. The authors report solution-processed OLEDs using emitters **Au(III)-14** to **Au(III)-18** with the best efficiencies for each complex in the range 5–10% with the highest reported for **Au(III)-14** at 10% emitting at 528 nm (despite it not displaying TADF according to the authors!). The authors point out that at the time of publication the device featuring complex **Au(III)-18** with 5.3% efficiency and electroluminescence at 616 nm was the first example of such red-shifted emission from a device featuring an Au(III) complex.

Tong, Cheng, Che *et al.*[169] reported in 2022 tetradentate *CCNC*-coordinated Au(III) complexes featuring the donor–acceptor structure known from previously discussed works, featuring arylamine units as donors. Complexes **Au(III)-20** to **Au(III)-23** display broadband PL spectra, characteristic of emissive CT states, and a pronounced solvatochromism. Complexes **Au(III)-20** to **Au(III)-23** emit in the green region in toluene (547–532 nm), with Φ_{PL} = 0.77–0.88 and τ = 0.56–0.69 μs. **Au(III)-20**, **Au(III)-21**, and **Au(III)-23** show $k_r \sim 10^6$ s^{-1}, while **Au(III)-22** with the weakest dimethylacridine donor shows $k_r \sim 10^5$ s^{-1}. The estimated ΔE_{S-T} values for **Au(III)-20** to **Au(III)-23** in PMMA films are 83 meV, 97 meV, 76 meV, and 109 meV, respectively. Interestingly, complex **Au(III)-22** contains the weakest acceptor among all and clearly shows the lowest k_r, suggestive of lesser TADF contribution, yet the reported ΔE_{S-T} for this complex is the smallest among all. The authors performed femtosecond transient absorption experiments which reveal $k_{ISC} \sim 10^{11}$ s^{-1} – in line with that reported for other Au(III) complexes. Vacuum-deposited devices using complexes **Au(III)-20**, **Au(III)-21**, and **Au(III)-23** as emitters achieved maximum EQE values of 24.5% to 27.3% and minimal efficiency roll-off. Their electroluminescence was at 520–540 nm.

Vivian Wing-Wah Yam *et al.*[170] reported in 2023 tetradentate *CCNN*-coordinated Au(III) complexes featuring a donor–acceptor structure with the Au(III) centre and the phenylpyridine part of the *CCN*-cooordinating fragment acting as an acceptor and the *N*-coordinating acridine fragment acting as a donor (Fig. 26). Complexes **Au(III)-24** to **Au(III)-29** display red PL in toluene, at 615–650 nm, whereas **Au(III)-30** near-infrared emission at 714 nm. The PL in these complexes is assigned to intraligand CT. The PL of complexes **Au(III)-24** to **Au(III)-30** is red-shifted in respect to that in analogous carbazole-based *CCNN*-Au(III) complexes (their PL being at 528–554 nm).[171] This demonstrates the tuneability of this class of molecules. These complexes display k_r at 10^4 to 10^5 s^{-1} in toluene and in films. Temperature-dependent studies of molecule **Au(III)-25** gave a ΔE_{S-T} = 0.13 eV and S_1 lifetime of 3 ns. Subsequent transient absorption studies revealed a time constant for RISC at 7 ps. Complexes **Au(III)-24**, **Au(III)-25**, **Au(III)-26**, and **Au(III)-29** were selected for fabrication of solution-processed OLED

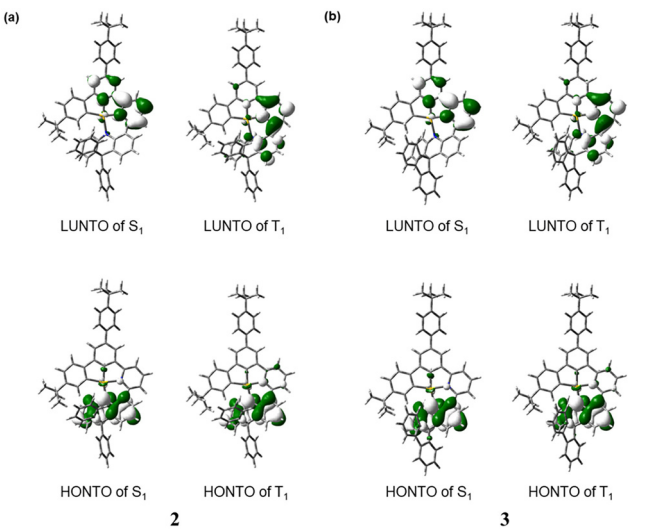

Fig. 26 Calculated natural transition orbital isosurfaces for **Au(III)-25** and **Au(III)-26**. Reproduced with permission from ref. 170. Copyright 2023 American Chemical Society.

devices, while **Au(III)-24** to **Au(III)-29** were also used in vacuum-deposited devices. Solution-processed device using **Au(III)-25** displayed 12.2% EQE emitting in the red and is said to be the most efficient solution-processed Au(III)-based OLED reported at the time of the original publication. A vacuum-deposited OLED with the same emitter achieved 12.7% EQE. Operational lifetime of vacuum-deposited OLEDs was characterised using the liberal LT_{70} and LT_{50} metric, rather than a more rigorous LT_{90} or LT_{95}. The LT_{70} at 100 cd m^{-2} spans from 157 h for the **Au(III)-26** based OLED to 6245 h for the OLED using **Au(III)-24**.

Palladium(II) complexes

Pd(II) complexes facilitate the formation of new carbon–carbon or carbon–nitrogen bonds, these complexes are commonly utilised in catalysis, particularly in cross-coupling reactions, such as Heck, Stille, and Suzuki reactions. Pd(II) complexes are definitely less common in optoelectronic and optical applications than they are in synthetic chemistry applications. Pd(II) complexes exhibit moderate SOC and they are rarely used in OLEDs unlike the closely related Pt(II) or Ir(III) complexes. It is primarily due to their usually low PL efficiency. Nonetheless, some luminescent examples are being explored in sensing and as photosensitizers.

The earliest accounts of Pd(II) complexes displaying efficient TADF can be attributed to Jian Li and others who presented a series of works on the topic several years ago.[20,172,173] Examples of these emitters are presented in Fig. 27: **Pd-1** and **Pd-2**. The authors of the original works presented the TADF phenomenon in Pd(II) complexes as different from the usual mechanism, naming it metal-assisted delayed fluorescence or MADF. However, there is in fact no difference between TADF and MADF. Hence, we use the term TADF to describe delayed fluorescence phenomena in Pd(II) complexes. Jian Li and others have presented efficient OLED devices featuring the said complexes with 20% external quantum efficiency, and a clear rationale for the advantages of TADF in blue Pd(II) emitters. One of them being provision of additional, blue-shifted PL component that can shift the colour coordinate of the emission more towards blue. On the other side, as TADF accelerates the overall PL decay (TADF + phosphorescence), it allows to outcompete the non-radiative decay in these complexes.

Kai Li *et al.*[52] presented two Pd(II) TADF complexes, **Pd-3** and **Pd-4**, which do not repeat the structural pattern of the previous examples **Pd-1** and **Pd-2**, but instead borrow their structural motif from metal-free donor–acceptor TADF molecules. In their design the Pd(II) centre is coordinated with a *CCC* chelating 1,3-bis(3′-butylimidazol-2′-ylidene)benzene ligand, while the coordination is completed with a monodentate carbazolyl

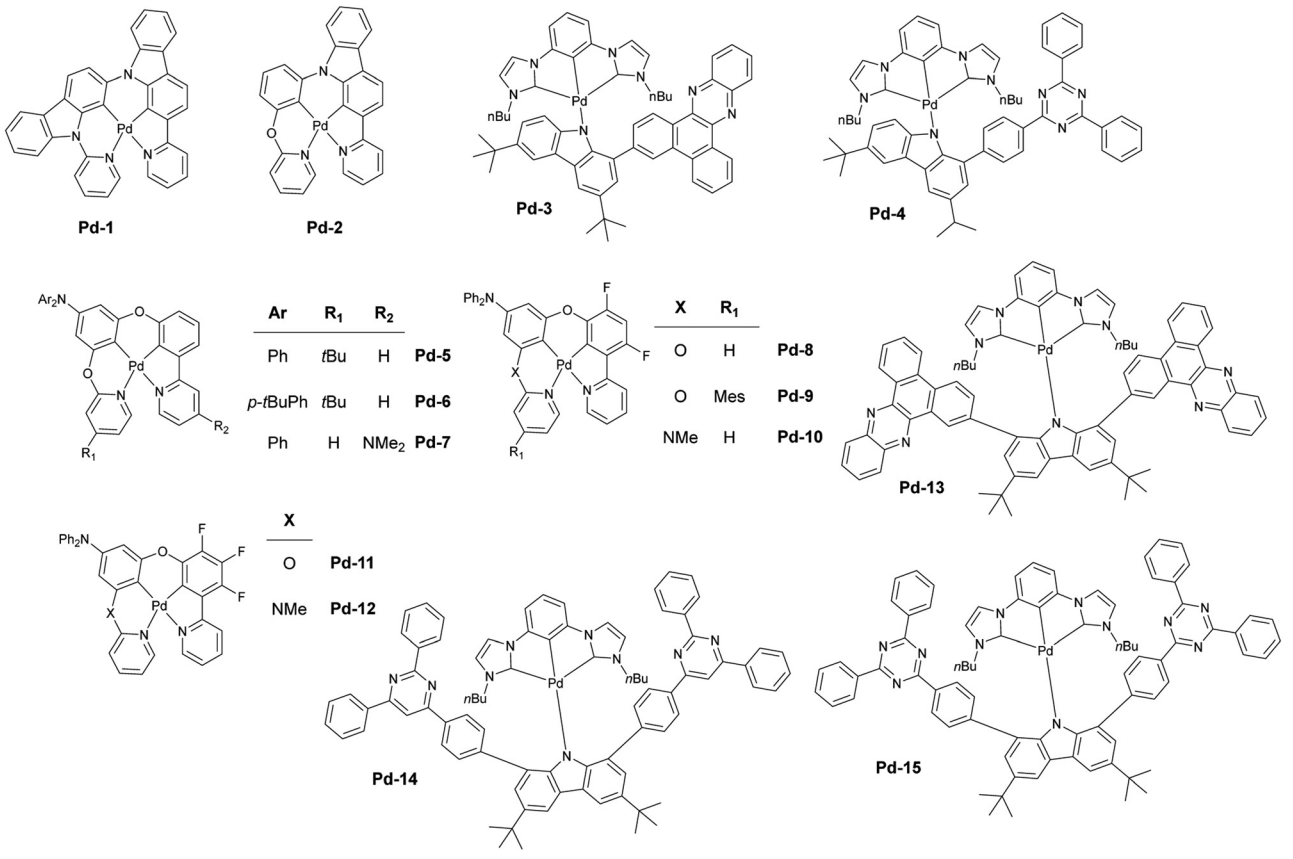

Fig. 27 Metal TADF complexes containing Pd(II) ions.

ligand with a pendant acceptor unit (Fig. 27). Analogous design has also been used in Pt(II) TADF complexes **Pt-4** and **Pt-5** presented later in this review. Such a molecular structure facilitates formation of intramolecular metal-perturbed CT states, which allow for low ΔE_{S-T} of 90 meV in **Pd-4**. In this design the Pd(II) ion acts as a donor, contributing to the HOMO, while the pendant acceptor contributes to the LUMO. Crucially, both complexes display a dominant TADF PL nature (>95%), unlike the previous Pd(II) complexes, where TADF was only a PL shoulder. This is thanks to the more efficient funnelling of triplet excitons through the S_1 manifold. They thus display short PL decay lifetimes τ = 0.97 μs and τ = 2.19 μs, and high radiative decay rates $k_r = 9.2 \times 10^5$ s^{-1} and $k_r = 3.7 \times 10^5$ s^{-1}, respectively for **Pd-3** and **Pd-4**. k_r values of nearly 10^6 s^{-1} are more akin to phosphorescent Ir(III) complexes or Pt(II) TADF emitters, but have been so far unachievable in Pd(II) complexes. This shows the powerful significance of the TADF mechanism in this case. In addition to the basic photophysical characterisation the authors have also studied ultrafast photoinduced absorption of **Pd-3** in toluene and obtained ISC time constant of 50 ps. These orange and red-emitting Pd(II) complexes show PL at 665 nm and 582 nm in toluene (637 nm and 598 nm in PMMA), and high Φ_{PL} of 0.89 and 0.82, respectively for **Pd-3** and **Pd-4**. The authors have used **Pd-3** in thermally-deposited OLEDs and achieved up to 30.1% EQE and exceptionally low roll-off, with 29.8% EQE recorded at 1000 cd m^{-2} – this thanks to the short PL lifetimes due to TADF.

Lam, Cheng, Che *et al.*[174] reported a series of Pd(II) complexes **Pd-5** to **Pd-12** using a more conventional coordination pattern, with tetradentate *NCCN*-chelating ligands of somewhat similar structure to those present in **Pd-1** and **Pd-2**. The authors however managed to obtain very small ΔE_{S-T} and thus efficient TADF, unlike in the structurally related predecessors. These complexes emit in the sky-blue to green region, with emission maxima ranging from 478–509 nm and Φ_{PL} = 0.27–0.84. The PL lifetimes τ range from 0.9 μs to 42 μs in solution and k_r values are in the range 10^4–10^6 s^{-1}. Complexes such as **Pd-5** and **Pd-7** display larger τ of 31 μs and 42 μs, respectively, and structured PL spectra, attributed mainly to a ligand-centred T_1 state. Complexes with a more Gaussian-like PL profile, **Pd-8** to **Pd-12** display shorter PL lifetimes, 3.2–12.0 μs. In this case the emission originates from metal-perturbed intraligand CT states. The authors have undertaken a more in-depth photophysical study of complexes **Pd-8** and **Pd-11** and determined the ΔE_{S-T} in dichloromethane at 25 meV and 27 meV, respectively. They have also conducted femtosecond time-resolved fluorescence measurements and identified the weak prompt fluorescence as well as the ISC time constant at 30–40 ps. Finally, they used **Pd-8** and **Pd-11** as emitters in OLEDs, achieving efficiencies of 23.2% and 24.8%, respectively.

Kai Li *et al.*[175] have developed another group of Pd(II) complexes based on their earlier designs **Pd-3** and **Pd-4**: **Pd-13** to **Pd-15** (Fig. 27). In this work they took the idea of non-covalent interactions in their molecules further. They find that these interactions, such as π–π stacking or hydrogen bonding improve not only photophysical properties of their complexes, but also benefit OLED stability and operational lifetime. These complexes display large contributions of TADF in their PL, up to 97%, like in the case of **Pd-3** and **Pd-4**. Complexes **Pd-13** to **Pd-15** emit bright yellow to red PL (549–644 nm) in PMMA films, where they show high Φ_{PL} = 0.87–0.94. Their emission lifetimes rangs from 0.52 to 8.08 μs at RT. The singlet–triplet energy gaps ΔE_{S-T} are 57 meV, 83 meV, and 74 meV for **Pd-13**, **Pd-14**, and **Pd-15**, respectively. In their work they achieved up to 31.5% EQE with minimal efficiency roll-off and an efficiency of 29.9% at 1000 cd m^{-2} for **Pd-15**. They have also observed a promising operational lifetime of the **Pd-15** based OLED, at 1615 hours at 3000 cd m^{-2}, although using the very liberal LT_{50} measure (rather than LT_{90} or LT_{95} for example), meaning a 50% drop in efficiency after the stated number of hours. This is nevertheless impressive in a non-industrial laboratory setting.

Platinum(II) complexes

Platinum(II) complexes have various applications such as photodynamic therapy,[176] bioimaging,[177] photocatalysis,[178–180] and organic light-emitting diodes (OLEDs).[181,182] Combining TADF and heavy metal emitters, such as Pt(II) complexes introduces a unique property due to a combination of fast decay from the S_1 state and rapid ISC and RISC due to the heavy atom effect. This enhancement of the SOC between S_1 to T_1, often allows fast and direct ISC/RISC process between these two states and exceptionally short luminescence lifetimes.[183] On the structural side, the planarity of Pt(II) complexes gives relatively narrowband and structured spectra, resulting in improved colour purity in OLEDs. They can be considered analogous to the metal-free MR-TADF emitters.[97] Pt(II) complexes are promising especially for their prospective use in near-infrared OLEDs.[44,184]

Pt(II) complexes are the ones with sufficient oxidative stability to be used in practical applications, and hence the only ones discussed in this review. However, to the best of our knowledge, the earliest example of a platinum complex displaying TADF can be ascribed to the unequivocally less stable oxidation state in a Pt(0)(*P^P*-binap)$_2$ complex.[185]

Pander, Williams, Kozhevnikov *et al.*[186] in 2021 presented the first example of a strongly TADF Pt(II) complex and its in-depth investigation. The complex **Pt-1** features a ditopic cyclometallating bis-*NCNO* chelating ligand (Fig. 28). It displays notable luminescent properties, with bright red luminescence and Φ_{PL} = 0.83 in deoxygenated methylcyclohexane at RT. The complex displays a very high $k_r = 4 \times 10^5$ s^{-1}, and a decay lifetime τ in the order of 1 μs, comparable to phosphorescent Ir(III) complexes, but much higher than related Pt(II) complexes. The complex displays very intense low energy absorption bands at ~600 nm with $\varepsilon \sim 20\,000$ M^{-1} cm^{-1} and crucially an unusually small Stokes shift of 7 nm or 200 cm^{-1} which were the first clues for its PL originating from TADF and not phosphorescence. The emission of the complex is particularly narrowband, thanks to its rigid structure. The authors obtained ΔE_{S-T} for **Pt-1** of 69 ± 3 meV by studying the temperature

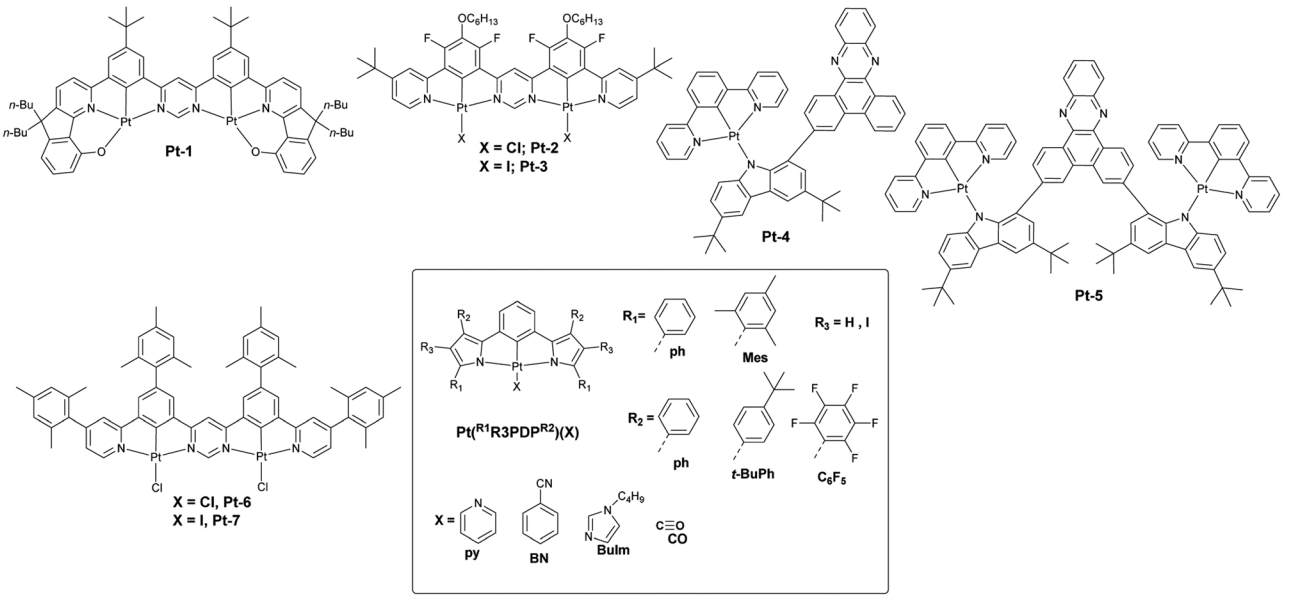

Fig. 28 Metal TADF complexes containing Pt(II) ions.

dependence of its PL decay in Zeonex. A value determined from PL spectra was ΔE_{S-T} = 66 ± 14 meV (Fig. 8). A kinetic study allowed to also determine the singlet radiative decay rate constant $k_r^S = 1.5 \times 10^7$ s^{-1}. The authors reported OLEDs with modest efficiency, at 7.4% and maximum luminance at 11 000 cd m^{-2}.

Pander, Williams, Kozhevnikov *et al.*[187] synthesised and studied a second example of a TADF dinuclear Pt(II) complex **Pt-2**, this time featuring a bis-*NCN* chelating ligand (Fig. 28). Unlike the previous example, this complex demonstrates dual luminescent behaviour, emitting both TADF and phosphorescence. The complex emits at 640 nm which is its principal phosphorescent component, and with a shoulder at 570–580 nm marking its TADF component. The dual TADF + phosphorescence properties and the domination of the latter stem out of a relatively large ΔE_{S-T} in the order of 0.16–0.2 eV. It also displays a relatively long PL lifetime at RT in the order of τ = 5 μs and singlet radiative decay rate k_r^S of 9 × 10^7 s^{-1}. While the luminescent properties of the complex **Pt-2** are not particularly remarkable and it displays pronounced aggregation in solid state leading to relatively modest Φ_{PL} in film. Nevertheless, it poses as an example of a new family of luminescent Pt(II) complexes displaying TADF, where the Pt–Cl moiety acts as a donor. A comparison of complex **Pt-2** with its closest mononuclear analogue provides a basis for explaining why dinuclear structure of Pt(II) complexes is more likely to promote TADF, pointing at stronger ligand-centred and singlet-like nature of the energetically lowest absorption bands, lower ΔE_{S-T} and slower phosphorescence being promoted by the dinuclear design. Complex **Pt-2** is an excellent example of how absorption and PL spectra in phosphorescent and TADF Pt(II) complexes differ: the latter show the typical absorption and PL overlap not usually observed in phosphorescent complexes (Fig. 9). The authors have presented proof-of-concept solution-processed OLEDs featuring **Pt-2** displaying up to 2.64% efficiency, emitting at 637 nm. They have also presented dimer-based OLEDs emitting at 805 nm with an efficiency of 0.51%.

Pander, Williams, Kozhevnikov *et al.*[188] presented a follow-up to the previous study of molecule **Pt-2**. This new study demonstrates the potential of modifying ancillary ligands to systematically enhance TADF properties. The new complex **Pt-3** explores the impact of halogen ligand substitution in a dinuclear Pt(II) TADF complex. Metathesis of the Pt–X ancillary ligand from X = Cl to X = I was found to provide significant improvements in photophysical performance. With the iodo-substituted complex achieving a threefold increase in the k_r to 3–4 × 10^5 s^{-1} in respect to the X = Cl complex **Pt-2**, matching the performance of phosphorescent Ir(III) complexes and the TADF Pt(II) complex **Pt-1**. These improved luminescent characteristics are attributed to the lower ΔE_{S-T} = 60 meV resulting from smaller HOMO–LUMO overlap integral. Hence, the complex is not showing a dual emission behaviour and its PL is dominated by TADF (Fig. 29). **Pt-3** emits at 630 nm. This study confirms that the Pt–X moiety in Pt(II) TADF complexes is crucial for modulating the magnitude of the ΔE_{S-T} and hence TADF. The authors have produced solution-processed OLEDs using **Pt-3** and achieving efficiencies up to 3.11% with emission at 612 nm.

Li, Li *et al.*[189] in 2024 synthesised two Pt(II)-based TADF complexes, **Pt-4** and **Pt-5**. These complexes feature a dipyridylphenyl *NCN* cyclometallating ligand with a monodentate donor–acceptor type ligand that creates metal-perturbed intraligand charge-transfer (MPICT) excited states. These complexes display small ΔE_{S-T} of 86 and 89 meV, respectively, for **Pt-4** and **Pt-5** and moderately large S_1–T_1 spin–orbit coupling

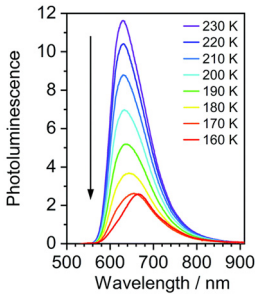

Fig. 29 Photoluminescence spectra of **Pt-3** in a dilute toluene solution at temperatures indicated in figure legend. Reproduced from ref. 188.

matrix element of ~10 cm^{-1}. Most crucially, these two complexes feature a fundamentally different architecture from that of the earlier reported complexes **Pt-1** to **Pt-3**, with the auxiliary monodentate ligand featuring a strong acceptor moiety, thus creating twisted intramolecular CT states more alike with those observed in metal-free donor–acceptor TADF molecules, or in certain coinage metal complexes. This appears to be a different and promising way to produce TADF complexes of this metal, but at the same time the PL spectra are broad and featureless.

Pt-4 and **Pt-5** display broad and featureless PL spectra around 645 nm in degassed toluene. In films, these complexes emit at 630 nm, with high Φ_{PL} = 0.82 in **Pt-4** and Φ_{PL} = 0.92 in **Pt-5**. They display PL lifetimes τ = 1.51 μs and τ = 1.63 μs as well as $k_r = 6.1 \times 10^5$ s^{-1} and $k_r = 5.0 \times 10^5$ s^{-1} for **Pt-4** and **Pt-5**, respectively. The authors find that TADF constitutes 97% of the total PL at RT (Fig. 30). On top of the usual PL characterisation of TADF emitters the authors have additionally performed ultrafast transient absorption experiments. They identified formation of the intraligand CT state (0–0.7 ps), intersystem crossing from S_1 to T_1 (1.77–574 ps), and T_1 decay that follows. The authors selected **Pt-4** for the use as the luminescent dopant in OLEDs due to its smaller molecular weight. **Pt-5** could not be used for this purpose. This highlights the necessity to seek Pt(II) TADF complexes with one metal centre as those with two metal ions tend to have excessive molecular weights, rendering them insublimable. The authors obtained the best OLED performance using 1% doping concentration of **Pt-4**, with EQE of 35.6% and exceptionally high maximum luminance of 136 800 cd m^{-2}. The OLED was also reported to have an exceptionally small efficiency roll-off, demonstrating the advantages of short PL lifetimes facilitated by TADF.

Pander, Williams *et al.*[190] in 2024 have made a further follow-up to their study on **Pt-2** and **Pt-3** which has focused on improving the cyclometallating bis-*NCN* ligand. They have used mesityl groups to limit aggregation and removed fluorine atoms which led to a visibly lower ΔE_{S-T} value. The new complexes **Pt-6** and **Pt-7** present a visible improvement over the parent complexes **Pt-2** and **Pt-3**. Both new complexes show overlap between their PL and absorption spectra – in line with the typical behaviour of TADF metal complexes of this type. **Pt-7** has a PL maximum of 627 nm, similar to the parent complex **Pt-3**. In contrast, complex **Pt-6** has a shorter PL wavelength at 576 nm, different than its analogue **Pt-2** ~ 620 nm. The difference in the PL wavelength arises from the smaller ΔE_{S-T} in **Pt-6**, giving dominance of TADF (singlet emission – higher energy) at RT, rather than phosphorescence, as in the parent molecule. **Pt-6** shows ΔE_{S-T} = 94 meV, while **Pt-7** ΔE_{S-T} = 66 meV in polystyrene, while their $k_r^S \sim 10^7$ s^{-1} (Fig. 31). **Pt-6** emits at 576 nm in toluene with Φ_{PL} = 0.11, τ = 0.34 μs, and $k_r = 3.3 \times 10^5$ s^{-1}, due to aggregation, and at the same wavelength in chlorobenzene with Φ_{PL} = 0.45, τ = 2.1 μs, and $k_r = 2.1 \times 10^5$ s^{-1}. **Pt-7** displays a Φ_{PL} = 0.23, τ = 0.4 μs, and $k_r = 5.7 \times 10^5$ s^{-1} in toluene. While both complexes are shown to display TADF, **Pt-6** shows visible aggregation, even in solutions, and therefore, the more promising **Pt-7** was studied more thoroughly. The authors have used **Pt-7** as emitter in solution-processed OLEDs, observing a significant improvement of the EQE from ~3% using **Pt-3** to 10% using **Pt-7**. This has been attributed to the beneficial effect of the mesityl groups in preventing aggregation of the emitter in the solid state.

Borisov *et al.*[191] recently reported a new group of Pt(II) complexes emitting from green to orange, showing Φ_{PL} in toluene between 0.13 to 0.86 and decay lifetime τ from 8.5 to 97 μs. The authors have used the pyridinedipyrrolide (PDP) ligand

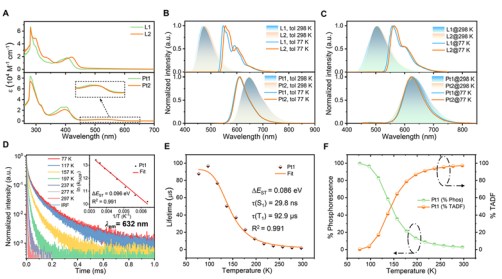

Fig. 30 Photoluminescent properties of **Pt-4** (Pt1) and **Pt-5** (Pt2) and their respective ligands L1 and L2: (a) absorption spectra in toluene; (b) PL spectra in degassed toluene; (c) PL spectra in PMMA; (d) PL decay at variable temperatures for **Pt-4**; (e) PL lifetimes in **Pt-4** and a Boltzmann-like fit; (f) contributions of TADF and phosphorescence in **Pt-4** in function of temperature. Reproduced from ref. 189.

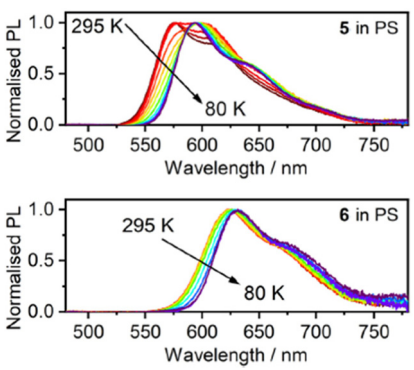

Fig. 31 PL spectra of **Pt-6** and **Pt-7** in polystyrene film over the temperature range from 80 to 295 K. Reproduced from ref. 190.

scaffold which is the same used in Zr(IV) complexes displaying TADF that are discussed later in this review.[192–195] The authors note that Pt(II) complexes of similar structure have previously been synthesised, but either their photophysical characteristics were not examined or they only produced phosphorescence.[196–198] Among the reported complexes only **Pt(PhPDPPh)(CO)** acts as an outlier with a very low Φ_{PL} of 0.01.

HOMO and LUMO reveal an interesting nature of the excited state with the HOMO localised on the PDP chelating ligand and the LUMO localised on the Pt(II) centre and either the auxiliary monodentate ligand alone, both the auxiliary and the PDP ligand, or solely on the PDP ligand (Fig. 32). The authors find that the larger degree of interligand charge-transfer (ILCT) the smaller the ΔE_{S-T}, hence more TADF and less phosphorescence. In this group of complexes, the cyclometallating PDP acts as a moderate donor, rather than a strong/moderate acceptor, hence, the central atom acts more like an acceptor than a donor.

The ΔE_{S-T} generally changes in a narrow range in polystyrene, from 0.14 eV for **Pt(MesIPDPC6F5)(BN)**, with the shortest decay lifetime at RT of τ = 9.5 μs, to **Pt(PhPDPPh)(BN)**, **Pt(PhPDPPh)(Py)**, and **Pt(PhPDPPh)(BuIm)** with ΔE_{S-T} = 0.24 eV and the longest decay lifetime $\tau \sim$ 120–130 μs. It is notable that these complexes display exceptionally long PL lifetimes as for TADF Pt(II) complexes and even longer than those typically observed in phosphorescent Pt(II) complexes. These complexes are an example of mono-Pt(II) TADF emitters and it is apparent that the TADF properties are promoted by exceptionally long phosphorescence lifetimes rather than small ΔE_{S-T} values.

The authors have used **Pt(PhPDPPh)(BN)**, **Pt(PhPDPPh)(Py)**, **Pt(PhPDPPh)(BuIm)**, and **Pt(MesPDPPh)(BN)** as optical temperature sensors (Fig. 33) in form of foils by doping the complexes into polyacrylonitrile (PAN), which displays low oxygen permeability. The authors have selected the **Pt(PhPDPPh)(Py)** as one with the most prominent ratiometric response to use in an encapsulated form in a biocompatible RL-100 polymer. The thus formed nanoparticles were used for nanoscale monitoring of temperature in the tumour microenvironment.

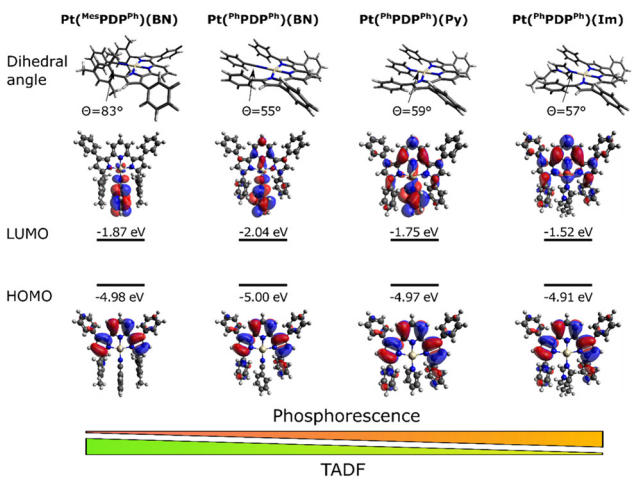

Fig. 32 HOMO and LUMO isosurfaces of selected Pt(II) complexes from the study by Borisov *et al.* The graphic shows the trend in the proportion between phosphorescence and TADF among the four complexes showing varying contributions of interligand CT (from left) to ligand-centred excitation (right). Reproduced from ref. 191 under the CC-BY 4.0 license.

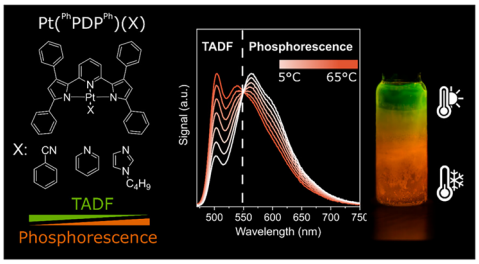

Fig. 33 Photoluminescence spectra in function of temperature and visualisation of temperature-dependent PL colours in the work by Borisov *et al.* Reproduced from ref. 191 under the CC-BY 4.0 license.

Iridium(III) complexes

The photophysical and photochemical properties of iridium(III) complexes as well as their application into OLEDs, have been intensely investigated in the past decades.[199,200] The low turn-on voltage of OLEDs and three-dimensional spatial structure of Ir(III) complexes make them particularly interesting.[201,202]

Ir(III) complexes could be tuned to display emission in the red, green, and blue colours. Many of these complexes have shown red and green electroluminescence with long-term stability but not for blue.[35,203–205] This can be explained by the high blue emission excitation energy, which may significantly reduce their stability and emission efficiency. Particularly, the longer radiative lifetime of blue phosphors, resulting from the reduced spin–orbit coupling and diminished metal-to-ligand charge transfer (MLCT) contribution in the excited state, has resulted in significant efficiency roll-off in OLEDs, exciton–exciton, and exciton–polaron annihilation. These problems are less significant in the typical red and green phosphors with relatively shorter radiative lifetimes.[206–208]

The subject of TADF in the context of Ir(III) complexes is very little known, however it presents an opportunity to understand these luminophores even further than before. While it may not be immediately apparent why TADF would be beneficial to a strongly phosphorescent system, it turns out that the delayed fluorescence contributions allow for accelerating their luminescent decay beyond the limits set out by phosphorescence. While it may appear that TADF is new to Ir(III) complexes it may have been present all along but left unnoticed.[120] The authors of this review hope that conscious use of TADF may one day resolve the outstanding problems of Ir(III) complexes, like lower efficiency or stability of complexes emitting in the blue and near-infrared regions.

Pander, Williams, Dias, Kozhevnikov, and colleagues[209] in 2023 designed a novel dinuclear iridium(III) complex **Ir-1** (Fig. 34). The complex features two Ir(*NC*-Meppy)$_2$ units bridged by a ligand derived from 4,6-bis(2-hydroxyphenyl)pyrimidine. The

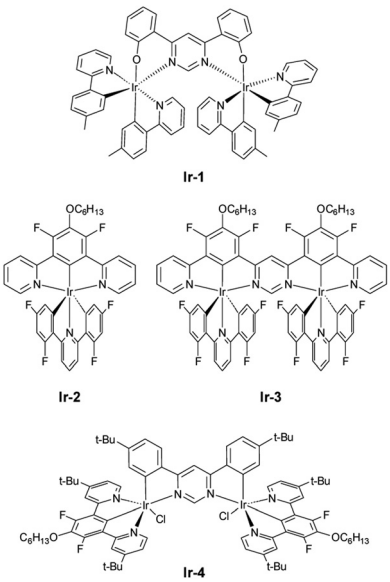

Fig. 34 Metal TADF complexes containing Ir(III) ions.

complex exhibits red PL, producing a broad, featureless spectrum in solution at room temperature, λ_{em} = 655 nm with Φ_{PL} = 0.3 in toluene. The PL of complex **Ir-1** decays monoexponentially with lifetimes τ ranging from 0.47 to 0.85 μs at room temperature, depending on the solvent. The temperature dependence of τ follows a model typical for metal TADF complexes with ΔE_{S-T} of 47 ± 7 meV and a k_r^S of (1.2 ± 0.2) × 10^7 s^{-1}, corresponding to a natural radiative lifetime for the singlet state of about 83 ns. Photoluminescence spectra of the complex display the typical change with temperature, where the two luminescent components associated with TADF and phosphorescence can be noted (Fig. 35). The authors undertake an in-depth computational analysis, confirming the S_1/T_1 nature of the emissive states involved in the TADF mechanism. This work presents a first example of an Ir(III) complex for which the TADF mechanism has been demonstrated.

Before the publication of the work by Pander, Williams, Dias, Kozhevnikov *et al.* featuring the TADF complex **Ir-1** Shafikov, Kozhevnikov and others[210] have presented two complexes: monometallic **Ir-2** and bimetallic **Ir-3** for which they

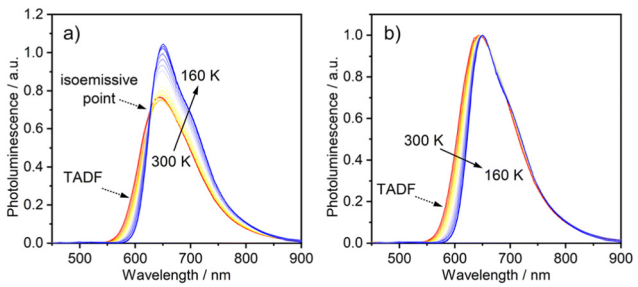

Fig. 35 Photoluminescence spectra of **Ir-1** recorded in dilute toluene solution at temperatures from 160 to 300 K: (a) spectra as recorded, (b) normalised spectra. Adopted from ref. 209.

reported a "TADF-like" behaviour. The structure of these complexes comprises an *NCN* cyclometallating ligand (**Ir-2**) or an *NCN–NCN* ditopic ligand (**Ir-3**) with the coordination sphere of the complex being completed with *CNC*-type ligands, forming a symmetrical and hence non-stereogenic structure. The claimed "TADF-like" mechanism involves the upper triplet T_2 state acting instead of the S_1 state normally involved in the TADF mechanism. Outside of these mechanistic discussions these two complexes display a behaviour observed in structurally related Pt(II) TADF complexes described earlier in this work. Gao, Cui and co-workers have subsequently demonstrated computationally[211] that **Ir-2** displays TADF, while recently Pander and others have claimed the same for **Ir-3**.[120] Considering the above evidence, the authors of this review believe that indeed **Ir-2** and **Ir-3** may have been the first examples of metal TADF emitters containing Ir(III) centres although not claimed by the authors of the original work. Shafikov, Kozhevnikov and others report ΔE_{IV-I} values of 0.21 eV and 0.12 eV for **Ir-2** and **Ir-3**, respectively, which can be interpreted as ΔE_{S-T} in the context of the TADF mechanism. They also report k_r^S values (although not attributed to singlet decay in the original work) in the range 10^8–10^9 s^{-1} – well within a range expected for decay from the S_1 state.

During the preparation of this review Pander and others[120] have presented another example of TADF among iridium(III) complexes, molecule **Ir-4**, originally featured in a work by Williams, Kozhevnikov and others[212] where it was presented as phosphorescent. Pander and others have demonstrated that the profound luminescence properties of this complex originate in part from the TADF mechanism. **Ir-4** shows ΔE_{S-T} = 28 ± 5 meV emitting at 551 nm in polystyrene. An OLED device featuring **Ir-4** has achieved nearly 10% EQE and maximum luminance of 18 000 cd m^{-2}.

Zirconium(IV) complexes

Zirconium is the fourth most earth-abundant metal on our planet. It is interesting because of its easily adjustable and inexpensive photoluminescent compounds. The challenge in using the Zr(IV) complexes is their excited state characterised by fundamentally distinct electronic structure, which can entail unfavourable photophysical and (photo)chemical properties and requires different strategies in respect with other transition metals.[213] Another problem of Zr(IV) complexes is the sensitivity of zirconium sources to moisture due to the strong susceptibility to the formation of Zr–O bonds. Hence, the synthesis of these complexes requires exceptional care and expertise in chemistry with the process requiring inert conditions.[214]

On the other hand, transition metal ions with electron configuration d^0 require reverse the "normal" charge transfer direction, as they prefer ligand-to-metal charge transfer (LMCT) rather than metal-to-ligand charge transfer. This can be achieved by merging the electron-deficient metal ion with specifically designed electron-rich ligands. Hence, the metal ion in this case plays a role of the acceptor, unlike in the case of some other transition metal ions, like Pt(II) or Ir(III), which act as donors.[215,216]

Milsmann and colleagues have presented a Zr(IV) complex **Zr(^{Mes}PDP^{Ph})$_2$**,[195] where $H_2{}^{Mes}PDP^{Ph}$ = 2,6-bis(5-(2,4,6-trimethylphenyl)-3-phenyl-1*H*-pyrrol-2-yl)pyridine. The highly stable luminophore and photosensitiser displays PL at 581 nm and PL lifetime at τ = 350 μs and relatively high photoluminescence efficiency Φ_{PL} = 0.45. It features TADF and facilitates photoredox catalytic processes. It displays ΔE_{S-T} = 0.205 eV and absorption maximum at 525 nm (ε = 21 570 M^{-1} cm^{-1}). The emission of this complex is attributed to the ligand-to-metal charge transfer (LMCT). Optical spectroscopy studies reveal fast intersystem crossing (ISC) from S_1 to T_1. The authors present temperature-dependent studies, demonstrating dominance of phosphorescence at lower temperatures and TADF at higher temperatures, including room temperature. Structural rigidification due to mesityl substituents improves stability, reduces vibrations, and suppresses decomposition – this is crucial especially for the originally designed role of the Zr(IV) complex as a triplet sensitiser.

Interestingly, Milsmann and colleagues,[194] prior to the above work, have reported an analogous Zr(IV) complex **Zr(^{Me}PDP^{Ph})$_2$** which displays overall similar PL behaviour to that of **Zr(^{Mes}PDP^{Ph})$_2$**, but with lower Φ_{PL} = 0.08 and PL at 595 nm. In this work, the authors also present a Ti(IV) analogue of the Zr(IV) complex that is non-emissive. We hypothesise whether it would be of interest to consider an analogous Hf(IV) complex Hf(^{Mes}PDP^{Ph})$_2$ or Hf(^{Me}PDP^{Ph})$_2$ as feasible and would it too display strong PL and TADF. However, in the case of **Zr(^{Me}PDP^{Ph})$_2$** no time-resolved nor temperature-dependent study was conducted and the nature of the emission could not be identified. Nevertheless, due to the structural similarity of both Zr(IV) complexes and the similar PL behaviour (they crucially both display a very evident overlap between the PL spectrum and the strong $S_0 \rightarrow S_1$ absorption band) it is very likely that **Zr(^{Me}PDP^{Ph})$_2$** also displays TADF properties. This example exposes the fundamental problem of metal complexes for which TADF properties are not known or widely recognised, which is also the case for Ir(III) complexes.

Borisov *et al.*,[192] have introduced a new class of Zr(IV) pyridinedipyrrolide complexes, analogous to those presented earlier by Milsmann and others. They display TADF which the authors employ for temperature sensing and imaging applications. These complexes display orange-red PL with monoexponential decay featuring solely TADF and no prompt fluorescence. The $\Phi_{PL} \sim 0.5$ in solution and $\Phi_{PL} \sim 1$ in polystyrene matrix. They display high stability, similarly to the parent complex reported by Milsmann and others. In addition to their PL and TADF properties the complexes are suitable for two-photon excitation, applicable in biological imaging. Despite producing a plethora of various derivatives (Fig. 36) the authors found their influence on the overall PL properties to be rather minimal due to the changes in both HOMO and LUMO energy balancing out. However, the substituents were found to alter the decay lifetimes of the PL.

Shortly after their 2020 paper, in the same year, Milsmann and others[217] have presented another work, this time examining the derivatives of their original TADF Zr(IV) complex **Zr(**^{Mes}**PDP**^{Ph}**)$_2$**. TADF properties were assumed for these complexes, however, no experimental data was presented to support this hypothesis. While the authors of this review have no doubt that these materials share the same TADF characteristics of the parent complex **Zr(**^{Mes}**PDP**^{Ph}**)$_2$** there is essentially no evidence left for any interpretation.

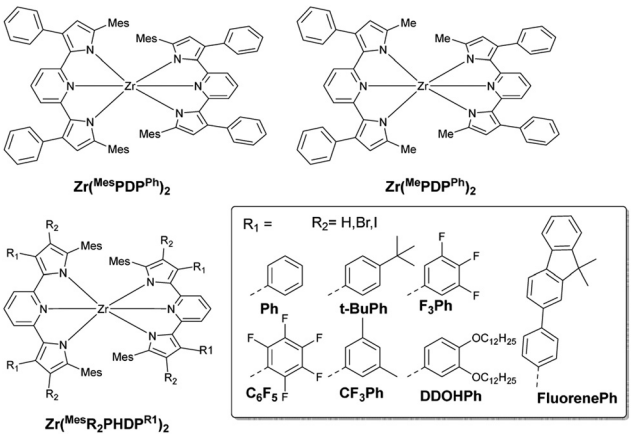

Fig. 36 Examples of Zr(IV) complexes displaying TADF.

Zhang *et al.*,[218] developed Cs_2ZrCl_6 perovskite nanograins that display high Φ_{PL} = 0.7 and efficient TADF. This is perhaps not an ideal fit for this review as the nanograins are very different from all the other luminophores featured in here, but nevertheless we thought it would be of interest to the readers. The nanograins display ΔE_{S-T} = 0.07 eV and photoluminescence at 447 nm. They were presented as efficient X-ray scintillators when combined with PDMS in form of films, allowing a clear visualisation of static and dynamic objects.

Zinc(II) complexes

Zinc(II) is a somewhat similar case to the Zr(IV) because of its d^{10} electron configuration in the ionic form. It introduces no significant spin–orbit coupling and acts rather as an acceptor/auxiliary acceptor in donor–acceptor TADF emitters (Fig. 37). Crucially, because of these properties of the Zn(II) ion, its complexes display a photophysical picture usually attributed to metal-free TADF emitters, with separate prompt and delayed fluorescence components. Appropriate design of a TADF/pro-TADF ligand allows the Zn(II) ion to bind and participate in emissive charge-transfer (CT) states, reducing the ΔE_{S-T} and thus enhancing or enabling TADF. The typical Zn(II) ligands in this case are tripyridyls that produce ionic complexes, and salen-type ligands, yielding neutral complexes.

Borisov *et al.*[219] synthesised in 2020 a new class of TADF emitters: Zn(II) Schiff base complexes, which they used for optical thermometry applications. **Zn-1** and **Zn-2**, emitting at 542 nm and 547 nm, display a significant temperature sensitivity of their decay lifetimes, thanks to the large ΔE_{S-T} of 0.34 eV and 0.30 eV from temperature-dependent decays, and 0.31 eV and 0.28 eV from fluorescence and phosphorescence spectra (Fig. 38). They display TADF lifetimes at RT of 435 μs and >2 ms for **Zn-1** and **Zn-2**, respectively.

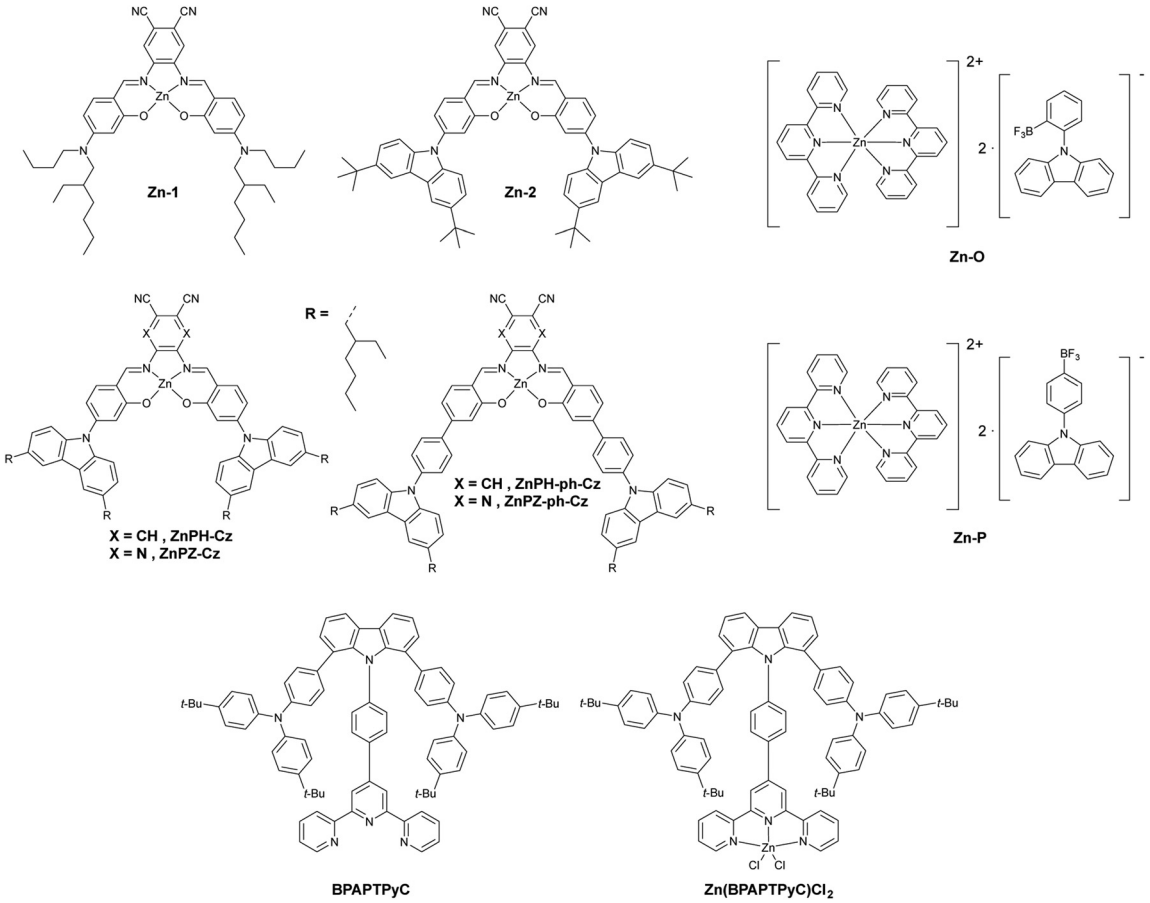

Fig. 37 Examples of Zn(II) complexes displaying TADF.

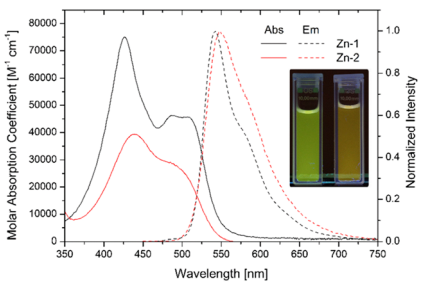

Fig. 38 Absorption and PL spectra of **Zn-1** and **Zn-2** in toluene and photographs of the two toluene solutions under UV light. Reproduced from ref. 219 under the CC-BY license.

The authors have also been able to estimate the proportion of TADF contributing to the total emission at 5% in **Zn-1** and 30% in **Zn-2**. This result highlights the difference between Zn(II)-based TADF emitters and other examples presented in this review. These temperature-sensing luminophores display severe oxygen quenching and an oxygen-blocking encapsulation had to be employed in order for a successful application in thermometric measurements. This approach has been is described earlier in this review.

Borisov *et al.*[220] in 2022 presented a follow-up study aimed at obtaining emitters with red-shifted luminescence to those reported in their work in 2020. The main structural novelty of their study is the introduction a pyrazine (or 2,3-pyrazinedicarbonitrile to be exact) acceptor unit that allowed shifting the PL of their complexes into red. They have also used branched 2-ethylhexyl chains for improved solubility. The complexes **ZnPH-Cz**, **ZnPZ-Cz**, **ZnPH-ph-Cz**, **ZnPZ-ph-Cz** (Fig. 37) have been studied in two forms – with and without an addition of pyrimidine (Py), acting as an axial ligand. The authors have found that the Py axial ligand improves the solubility of the complexes, but also alters their photoluminescent properties. By binding to the axial positions of the Zn(II) complexes (and probably replacing an unidentified weakly-bound ligand), reducing their susceptibility to π–π interactions.

The use of the 2,3-pyrazinedicarbonitrile acceptor in **ZnPZ-Cz** and **ZnPZ-ph-Cz** gave a red-shift to λ = 626 nm and λ = 611 nm, respectively, from λ = 554 nm and λ = 555 nm in **ZnPH-Cz** and **ZnPH-ph-Cz**, in polystyrene. This structural change also entails a drop in Φ_{PL} from 0.1–0.3 in **ZnPH-Cz** and **ZnPH-ph-Cz** to <0.06 in **ZnPZ-Cz** and **ZnPZ-ph-Cz**. The emitters display TADF lifetimes in the range 0.1–1 μs for **ZnPZ-Cz** and **ZnPZ-ph-Cz** and 1–4 ms for **ZnPH-Cz** and **ZnPH-ph-Cz**. The addition of pyridine alters the photo-

luminescence, but the effect is inconsistent: in **ZnPH-Cz** and **ZnPH-Ph-Cz** the authors have observed a shortening, while for **ZnPZ-Cz** and **ZnPZ-Ph-Cz** elongation of the TADF lifetime upon addition of pyridine. For example, for **ZnPH-Cz** the addition of pyridine (**ZnPZ-Cz/Py**) does not alter the TADF lifetime $\tau \sim 1.2$ ms, but the total Φ_{PL} increases from 0.32 in the former to 0.68 in the latter and likewise does so the Φ_{TADF} (part of Φ_{PL} attributed to TADF) as it rises from 0.16 to 0.47 without altering the emission wavelength of the complex.

Finally, the authors used the most promising emitter **ZnPZ-Cz/Py** as a temperature sensor both in form of a foil and nanoparticles, using the TADF lifetime calibrated against temperature. This approach required oxygen-free conditions for the proper performance of the sensor.

He *et al.*[221] in 2023 synthesised cationic Zn(II) complexes with terpyridyl ligands, **Zn-p** and **Zn-o**, featuring BF_3-Ar^- counterions featuring *N*-carbazolyls in *para* (**Zn-p**) and *ortho* (**Zn-o**) position to the $-BF_3$ group. These ionic pairs emit in the UV-A range when in solution (358 nm for **Zn-p** and 354 nm for **Zn-o**) with the emission originating from the isolated $[Zn(tpy)_2]^{2+}$ cations and carbazole-bearing anions. **Zn-p** and **Zn-o** in films form exciplexes between the cation and the anion of the ionic pair, which can be explained with a significantly lesser mobility of ions and significantly reduced solvation effects, leading to the formation of tightly bound ionic pairs in films and crystals. For example, in PMMA they display green-yellow PL at 528 nm (Φ_{PL} = 0.27) and 539 nm (Φ_{PL} = 0.29) for **Zn-p** and **Zn-o**, respectively. They both display TADF in PMMA films with ΔE_{S-T} of 0.05 and 0.02 eV, respectively, for **Zn-p** and **Zn-o**. Their properties differ in the crystalline state as they not only display different PL behaviour, but also mechanochromic luminescent behaviour (Fig. 39). The crystalline powders, as prepared, display blue or green-blue PL at 468 nm and 508 nm for **Zn-p** and **Zn-o**, while their ΔE_{S-T} are 0.33 eV and 0.06 eV, respectively. **Zn-p** does not display TADF in this form, in line with its large ΔE_{S-T}. After grinding both of the powders display a red-shift of their PL spectrum to 554 nm and 578 nm for **Zn-p** and **Zn-o**, respectively, with both now displaying TADF.

Deng *et al.*[222] in 2024 presented a blue-emitting weak TADF emitter **BPAPTPyC** featuring di(4-*tert*-butylphenyl) amino donors and a terpyridyl acceptor linked *via* a *p*-phenylene group. The terpyridyl was used as a cyclometallating ligand to bind Zn(II) ions, giving **Zn(BPAPTPyC)Cl$_2$**. The resultant Zn(II) complex displays stronger CT character and red-shifted emission at 585 nm (*vs.* 470 nm for the ligand). ΔE_{S-T} of the complex is significantly smaller, at 0.02 eV than that of the ligand, at 0.41 eV. The Zn(II) complex has a shorter TADF lifetime τ (2.7 *vs.* 10 μs), higher Φ_{PL} (0.72 *vs.* 0.22) and higher solution-processed OLED EQE (17.9% *vs.* 2.7%) than the ligand alone, respectively for the complex and ligand (Fig. 40). These characteristics are also reflected in the $k_{RISC} = 8.3 \times 10^5$ s^{-1} in **Zn(BPAPTPyC)Cl$_2$** and $k_{RISC} = 2.3 \times 10^3$ s^{-1} for **BPAPTPyC**. It remains however an open question whether the observed delayed fluorescence of **BPAPTPyC** can truly be attributed to TADF given the excessive ΔE_{S-T} = 0.41 eV. A more in-depth analysis is probably required in this case.

To conclude, the Zn(II) ion clearly not only increases the CT character of the excited state of the molecule through introduction of an electron-deficient centre, but also rigidifies the structure of the terpyridyl fragment, reducing molecular vibrations.

What could be discovered next?

Given the popularity of luminescent metal complexes and the overall notion that all of them, except perhaps for the examples discussed above, are phosphorescent has limited the studies of their potential TADF behaviour. A good example are Pt(II)[88] or Ir(III)[118] complexes, which only recently have been shown to be able to display TADF. The authors of this review point out that a pronounced spectral overlap between absorption and PL spectra in metal complexes should be considered suspicious and invite further investigation. A recent work demonstrates just that in the case of iridium(III) complexes.[120]

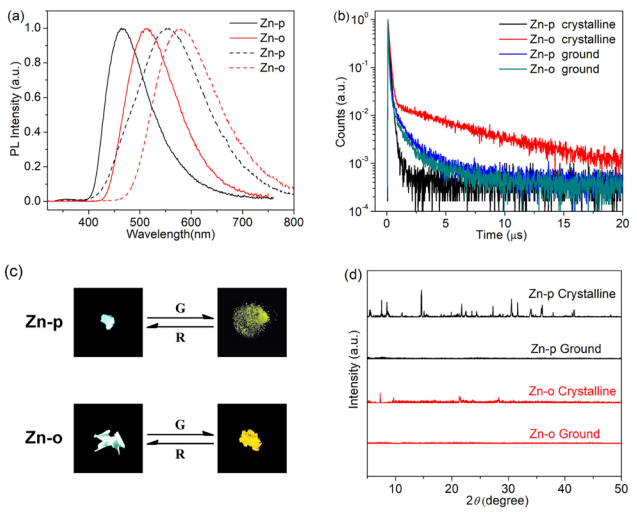

Fig. 39 Luminescent properties of **Zn-p** and **Zn-o** in form of crystalline and ground samples: (a) PL spectra; (b) luminescent decay traces; (c) photographs of different forms of powders under UV light; (d) PXRD diffractograms of crystalline and ground samples. Reproduced with permission from ref. 221. Copyright 2022 American Chemical Society.

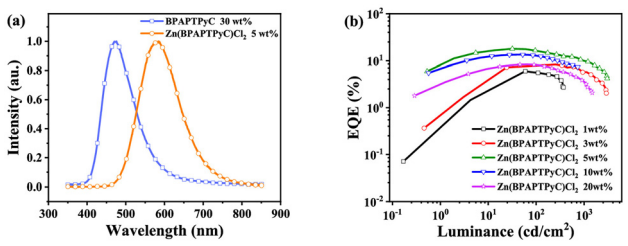

Fig. 40 (a) EL spectra of OLEDs featuring both **Zn(BPAPTPyC)Cl$_2$** and **BPAPTPyC**; (b) external quantum efficiency (EQE) of the OLED devices featuring complex **Zn(BPAPTPyC)Cl$_2$** at various concentrations in the emissive layer. Reproduced with permission from ref. 222. Copyright 2022 American Chemical Society.

Perhaps the best example of a group of complexes that displays some signs of potentially having TADF are certain Os(II) complexes with their clearly pronounced absorption and PL overlap.[223–226] We recommend the readers having an in-depth consideration of this group of luminophores, as new exciting discoveries may be hiding in plain sight!

6. Conclusions and perspectives

In this review we have discussed the most popular and yet hopefully the most interesting metal TADF emitters. In our discussions we considered the parity of metal centres rather than being guided by the popular interest and the number of publications in the subject. The topics pertaining to metals like platinum or iridium are relatively new, while there is a relatively slow development among some other categories, like Pd (II) or Zr(IV) emitters.

Undoubtedly and undeniably the main research focus is on developing Cu(I) and Au(I)/Au(III) TADF complexes. However, while Cu(I) emitters are interesting as those featuring one of the more earth-abundant metals, they are inferior to the related Au(I) complexes. There is an unequivocal advantage of Au(I)/Au(III) over Cu(I) complexes in terms of their air stability and operational stability in OLEDs. Zn(II) ions do not really seem to provide the same heavy-atom related advantages as most of the other discussed metals do and the behaviour of Zn (II) TADF complexes is alike those of the metal-free emitters. Zr (IV) complexes although they appear to behave similarly to some Pd(II) TADF emitters, they currently display relatively long TADF lifetimes, making them unsuitable for OLEDs, but clearly suitable as triplet sensitisers or optical temperature indicators.

A relatively new, but clearly relevant idea is combining TADF with narrowband photoluminescence in the form of MR-TADF emitters. This review hopefully clearly demonstrates that this approach can either be realised by perturbing the metal-free MR-TADF emitters with a metal centre, or that the metal TADFs can be MR emitters themselves. This concept is clearly of interest as the presence of the metal facilitates fast RISC rates which are very low in most typical metal-free MR-TADF emitters.

While OLEDs clearly are not the only application of metal TADF luminophores, they definitely remain one of the main driving forces in this area of research. Having considered the advantages and flaws of coinage metal complexes, the Au(I)/Au (III) compounds are probably the main contenders to the Ir(III) phosphorescent complex-dominated OLED industry. On the other end are Pt(II), Ir(III) and even Pd(II) TADF complexes, which are emerging as potentially interesting contenders to the current densely coinage-metal-dominated area of research. However, what is clear is that neither of these abovementioned metals are abundant or low-cost. A pertinent question emerges on whether the scientific development in this area of research moves more towards actually replacing iridium(III) emitters with something else, or instead whether the well-understood electroluminescent properties of platinum(II) and iridium(III) complexes will encourage developments that lead to further improving these luminophores.

From a purely scientific perspective, we believe that development in the metal TADF field brings a further understanding of the electronic levels in transition metal complexes. We wish for further development in this area of research and identification of examples of luminescent complexes of other metals, not featured in this review, that display TADF.

Conflicts of interest

There are no conflicts to declare.

Data availability

Our supporting research data is available from Zenodo: **https://zenodo.org/doi/10.5281/zenodo.18119045**.

Acknowledgements

P. P. acknowledges the National Science Centre, Poland for funding, grant no. 2022/45/B/ST4/02689 and Silesian University of Technology for Rector's pro-quality grant no. 04/040/RGJ26/0329.

References

1 H. Yersin, A. F. Rausch, R. Czerwieniec, T. Hofbeck and T. Fischer, The triplet state of organo-transition metal compounds. Triplet harvesting and singlet harvesting for efficient OLEDs, *Coord. Chem. Rev.*, 2011, **255**, 2622–2652.
2 A. Endo, M. Ogasawara, A. Takahashi, D. Yokoyama, Y. Kato and C. Adachi, Thermally Activated Delayed Fluorescence from Sn^{4+}-Porphyrin Complexes and Their Application to Organic Light Emitting Diodes – A Novel Mechanism for Electroluminescence, *Adv. Mater.*, 2009, **21**, 4802–4806.
3 R. Czerwieniec, J. Yu and H. Yersin, Blue-Light Emission of Cu(I) Complexes and Singlet Harvesting, *Inorg. Chem.*, 2011, **50**, 8293–8301.
4 S. B. Harkins and J. C. Peters, A Highly Emissive Cu_2N_2 Diamond Core Complex Supported by a [PNP]- Ligand, *J. Am. Chem. Soc.*, 2005, **127**, 2030–2031.
5 J. C. Deaton, S. C. Switalski, D. Y. Kondakov, R. H. Young, T. D. Pawlik, D. J. Giesen, S. B. Harkins, A. J. M. Miller, S. F. Mickenberg and J. C. Peters, E-Type Delayed Fluorescence of a Phosphine-Supported $Cu_2(\mu\text{-}NAr_2)_2$ Diamond Core: Harvesting Singlet and Triplet Excitons in OLEDs, *J. Am. Chem. Soc.*, 2010, **132**, 9499–9508.
6 C. A. Parker and C. G. Hatchard, Triplet-singlet emission in fluid solutions. Phosphorescence of eosin, *Trans. Faraday Soc.*, 1961, **57**, 1894.

7 J. R. Kirchhoff, R. E. Gamache, M. W. Blaskie, A. A. Del Paggio, R. K. Lengel and D. R. McMillin, Temperature dependence of luminescence from $Cu(NN)^{2+}$ systems in fluid solution. Evidence for the participation of two excited states, *Inorg. Chem.*, 1983, **22**, 2380–2384.
8 H. Yersin, *Highly Efficient OLEDs with Phosphorescent Materials*, Wiley, 2008.
9 A. Farokhi, S. Lipinski, L. M. Cavinato, H. Shahroosvand, B. Pashaei, S. Karimi, S. Bellani, F. Bonaccorso and R. D. Costa, Metal complex-based TADF: design, characterization, and lighting devices, *Chem. Soc. Rev.*, 2025, **54**, 266–340.
10 H. Uoyama, K. Goushi, K. Shizu, H. Nomura and C. Adachi, Highly efficient organic light-emitting diodes from delayed fluorescence, *Nature*, 2012, **492**, 234–238.
11 F. B. Dias, J. Santos, D. R. Graves, P. Data, R. S. Nobuyasu, M. A. Fox, A. S. Batsanov, T. Palmeira, M. N. Berberan-Santos, M. R. Bryce and A. P. Monkman, The Role of Local Triplet Excited States and D-A Relative Orientation in Thermally Activated Delayed Fluorescence: Photophysics and Devices, *Adv. Sci.*, 2016, **3**, 1600080.
12 P. W. Zach, S. A. Freunberger, I. Klimant and S. M. Borisov, Electron-Deficient Near-Infrared Pt(II) and Pd(II) Benzoporphyrins with Dual Phosphorescence and Unusually Efficient Thermally Activated Delayed Fluorescence: First Demonstration of Simultaneous Oxygen and Temperature Sensing with a Single Emitter, *ACS Appl. Mater. Interfaces*, 2017, **9**, 38008–38023.
13 X. Li, Y. Xie and Z. Li, Diversity of Luminescent Metal Complexes in OLEDs: Beyond Traditional Precious Metals, *Chem. – Asian J.*, 2021, **16**, 2817–2829.
14 A. S. Manna, S. Ghosh, T. Ghosh, N. Karchaudhuri, S. Das, A. Roy and D. K. Maiti, Smart Luminescent Materials for Emerging Sensors: Fundamentals and Advances, *Chem. – Asian J.*, 2025, **20**, e202401328.
15 V. Sathish, A. Ramdass, M. Velayudham, K.-L. Lu, P. Thanasekaran and S. Rajagopal, Development of luminescent sensors based on transition metal complexes for the detection of nitroexplosives, *Dalton Trans.*, 2017, **46**, 16738–16769.
16 Q. Zheng, X. Liu, Y. Zheng, K. W. K. Yeung, Z. Cui, Y. Liang, Z. Li, S. Zhu, X. Wang and S. Wu, The recent progress on metal–organic frameworks for phototherapy, *Chem. Soc. Rev.*, 2021, **50**, 5086–5125.
17 C. Förster and K. Heinze, Photophysics and photochemistry with Earth-abundant metals – fundamentals and concepts, *Chem. Soc. Rev.*, 2020, **49**, 1057–1070.
18 C. E. Housecroft and E. C. Constable, Solar energy conversion using first row d-block metal coordination compound sensitizers and redox mediators, *Chem. Sci.*, 2022, **13**, 1225–1262.
19 D. N. Kozhevnikov, V. N. Kozhevnikov, M. Z. Shafikov, A. M. Prokhorov, D. W. Bruce and J. A. G. Williams, Phosphorescence vs Fluorescence in Cyclometalated Platinum(II) and Iridium(III) Complexes of (Oligo)thienylpyridines, *Inorg. Chem.*, 2011, **50**, 3804–3815.
20 Z. Q. Zhu, C. D. Park, K. Klimes and J. Li, Highly Efficient Blue OLEDs Based on Metal-Assisted Delayed Fluorescence Pd(II) Complexes, *Adv. Opt. Mater.*, 2019, **7**, 1801518.
21 A. Arjona-Esteban and D. Volz, in *Highly Efficient OLEDs*, 2018, pp. 543–572.
22 S. Kunić and Z. Šego, *OLED Technology and Displays*, 2012.
23 Y. Takahashi, Y. Furuki, S. Yoshida, T. Otani, M. Muto, Y. Suga and Y. Ito, A new achromatic quarter-wave film using liquid-crystal materials for anti-reflection of OLEDs, *SID Digest*, 2014, **45**, 381–384.
24 M. Y. Wong and E. Zysman-Colman, Purely Organic Thermally Activated Delayed Fluorescence Materials for Organic Light-Emitting Diodes, *Adv. Mater.*, 2017, **29**, 1605444.
25 G. Hong, X. Gan, C. Leonhardt, Z. Zhang, J. Seibert, J. M. Busch and S. Bräse, A Brief History of OLEDs—Emitter Development and Industry Milestones, *Adv. Mater.*, 2021, **33**, 2005630.
26 C. Hosokawa, K. Fukuoka, H. Kawamura, T. Sakai, M. Kubota, M. Funahashi, F. Moriwaki and H. Ikeda, 17.1: Invited Paper: Improvement of Lifetime in Organic Electroluminescence, *SID Digest*, 2004, **35**, 780–783.
27 T. Iwakuma, T. Aragane, Y. Hironaka, K. Fukuoka, H. Ikada, C. Hosokawa and T. Kusomoto, P-98: Red and White EL Materials Based on a New Fused Aromatic Ring, *SID Digest*, 2002, **33**, 598–601.
28 M. Kawamura, Y. Kawamura, Y. Mizuki, M. Funahashi, H. Kuma and C. Hosokawa, in *48th Annual SID Symposium, Seminar, and Exhibition 2010, Display Week 2010*, 2010, vol. 1, pp. 560–563.
29 D. H. Ahn, J. H. Jeong, J. Song, J. Y. Lee and J. H. Kwon, Highly Efficient Deep Blue Fluorescent Organic Light-Emitting Diodes Boosted by Thermally Activated Delayed Fluorescence Sensitization, *ACS Appl. Mater. Interfaces*, 2018, **10**, 10246–10253.
30 H. Uoyama, K. Goushi, K. Shizu, H. Nomura and C. Adachi, Highly efficient organic light-emitting diodes from delayed fluorescence, *Nature*, 2012, **492**, 234–238.
31 H. Nakanotani, T. Higuchi, T. Furukawa, K. Masui, K. Morimoto, M. Numata, H. Tanaka, Y. Sagara, T. Yasuda and C. Adachi, High-efficiency organic light-emitting diodes with fluorescent emitters, *Nat. Commun.*, 2014, **5**, 4016.
32 J. Yan, D. Y. Zhou, L. S. Liao, M. Kuhn, X. Zhou, S. M. Yiu and Y. Chi, Electroluminescence and hyperphosphorescence from stable blue Ir(III) carbene complexes with suppressed efficiency roll-off, *Nat. Commun.*, 2023, **14**, 1–8.
33 T. Hatakeyama, K. Shiren, K. Nakajima, S. Nomura, S. Nakatsuka, K. Kinoshita, J. Ni, Y. Ono and T. Ikuta, Ultrapure Blue Thermally Activated Delayed Fluorescence Molecules: Efficient HOMO-LUMO Separation by the Multiple Resonance Effect, *Adv. Mater.*, 2016, **28**, 2777–2781.
34 K. R. Naveen, P. Palanisamy, M. Y. Chae and J. H. Kwon, Multiresonant TADF materials: triggering the reverse

intersystem crossing to alleviate the efficiency roll-off in OLEDs, *Chem. Commun.*, 2023, **59**, 3685–3702.

35 J.-H. Lee, C.-H. Chen, P.-H. Lee, H.-Y. Lin, M. Leung, T.-L. Chiu and C.-F. Lin, Blue organic light-emitting diodes: current status, challenges, and future outlook, *J. Mater. Chem. C*, 2019, **7**, 5874–5888.

36 C. Bizzarri, E. Spuling, D. M. Knoll, D. Volz and S. Bräse, Sustainable metal complexes for organic light-emitting diodes (OLEDs), *Coord. Chem. Rev.*, 2018, **373**, 49–82.

37 T.-Y. Li, S.-J. Zheng, P. I. Djurovich and M. E. Thompson, Two-Coordinate Thermally Activated Delayed Fluorescence Coinage Metal Complexes: Molecular Design, Photophysical Characters, and Device Application, *Chem. Rev.*, 2024, **124**, 4332–4392.

38 M. A. Baldo, S. Lamansky, P. E. Burrows, M. E. Thompson and S. R. Forrest, Very high-efficiency green organic light-emitting devices based on electrophosphorescence, *Appl. Phys. Lett.*, 1999, **75**, 4–6.

39 S. Lamansky, P. Djurovich, D. Murphy, F. Abdel-Razzaq, H. E. Lee, C. Adachi, P. E. Burrows, S. R. Forrest and M. E. Thompson, Highly phosphorescent bis-cyclometalated iridium complexes: Synthesis, photophysical characterization, and use in organic light emitting diodes, *J. Am. Chem. Soc.*, 2001, **123**, 4304–4312.

40 K. H. Kim, C. K. Moon, J. H. Lee, S. Y. Kim and J. J. Kim, Highly efficient organic light-emitting diodes with phosphorescent emitters having high quantum yield and horizontal orientation of transition dipole moments, *Adv. Mater.*, 2014, **26**, 3844–3847.

41 M. Cocchi, J. Kalinowski, D. Virgili and J. A. G. Williams, Excimer-based red/near-infrared organic light-emitting diodes with very high quantum efficiency, *Appl. Phys. Lett.*, 2008, **92**, 113302.

42 T. Fleetham, G. Li and J. Li, Efficient Red-Emitting Platinum Complex with Long Operational Stability, *ACS Appl. Mater. Interfaces*, 2015, **7**, 16240–16246.

43 K. Tuong Ly, R. W. Chen-Cheng, H. W. Lin, Y. J. Shiau, S. H. Liu, P. T. Chou, C. S. Tsao, Y. C. Huang and Y. Chi, Near-infrared organic light-emitting diodes with very high external quantum efficiency and radiance, *Nat. Photonics*, 2017, **11**, 63–68.

44 M.-C. Tang, A. K.-W. Chan, M.-Y. Chan and V. W.-W. Yam, Platinum and Gold Complexes for OLEDs, *Top. Curr. Chem.*, 2016, **374**, 46.

45 W.-P. To, D. Zhou, G. S. M. Tong, G. Cheng, C. Yang and C.-M. Che, Highly Luminescent Pincer Gold(III) Aryl Emitters: Thermally Activated Delayed Fluorescence and Solution-Processed OLEDs, *Angew. Chem.*, 2017, **129**, 14224–14229.

46 R. Czerwieniec and H. Yersin, Diversity of copper(I) complexes showing thermally activated delayed fluorescence: Basic photophysical analysis, *Inorg. Chem.*, 2015, **54**, 4322–4327.

47 D. Di, A. S. Romanov, L. Yang, J. M. Richter, J. P. H. Rivett, S. Jones, T. H. Thomas, M. A. Jalebi, R. H. Friend, M. Linnolahti, M. Bochmann and D. Credgington, High-performance light-emitting diodes based on carbene-metal-amides, *Science*, 2017, **356**, 159–163.

48 A. S. Romanov, S. T. E. Jones, L. Yang, P. J. Conaghan, D. Di, M. Linnolahti, D. Credgington and M. Bochmann, Mononuclear Silver Complexes for Efficient Solution and Vacuum-Processed OLEDs, *Adv. Opt. Mater.*, 2018, **6**, 1801347.

49 H. Cho, A. S. Romanov, M. Bochmann, N. C. Greenham and D. Credgington, Matrix–Free Hyperfluorescent Organic Light–Emitting Diodes Based on Carbene–Metal–Amides, *Adv. Opt. Mater.*, 2021, **9**, 2001965.

50 Y. Zhang, T. S. Lee, J. M. Favale, D. C. Leary, J. L. Petersen, G. D. Scholes, F. N. Castellano and C. Milsmann, Delayed fluorescence from a zirconium(IV) photosensitizer with ligand-to-metal charge-transfer excited states, *Nat. Chem.*, 2020, **12**, 345–352.

51 J. Yang, N. Li, J. Li, X. Song, M.-D. Li, J. Zhang and K. Li, A thermally activated delayed fluorescent platinum(II) complex for red organic light emitting diodes with high efficiencies and small roll-off, *J. Mater. Chem. A*, 2024, **12**, 18977–18985.

52 J.-G. Yang, X. Feng, N. Li, J. Li, X.-F. Song, M.-D. Li, G. Cui, J. Zhang, C. Jiang, C. Yang and K. Li, Highly efficient and stable thermally activated delayed fluorescent palladium(II) complexes for organic light-emitting diodes, *Sci. Adv.*, 2023, **9**, eadh0198.

53 L. C.-C. Lee and K. K.-W. Lo, Shining New Light on Biological Systems: Luminescent Transition Metal Complexes for Bioimaging and Biosensing Applications, *Chem. Rev.*, 2024, **124**, 8825–9014.

54 F. Ni, Z. Zhu, X. Tong, M. Xie, Q. Zhao, C. Zhong, Y. Zou and C. Yang, Organic emitter integrating aggregation-induced delayed fluorescence and room-temperature phosphorescence characteristics, and its application in time-resolved luminescence imaging, *Chem. Sci.*, 2018, **9**, 6150–6155.

55 J. Zhang, F. Fang, B. Liu, J.-H. Tan, W.-C. Chen, Z. Zhu, Y. Yuan, Y. Wan, X. Cui, S. Li, Q.-X. Tong, J. Zhao, X.-M. Meng and C.-S. Lee, Intrinsically Cancer-Mitochondria-Targeted Thermally Activated Delayed Fluorescence Nanoparticles for Two-Photon-Activated Fluorescence Imaging and Photodynamic Therapy, *ACS Appl. Mater. Interfaces*, 2019, **11**, 41051–41061.

56 Z. Li, J. Lu and X. Li, Recent Progress in Thermally Activated Delayed Fluorescence Photosensitizers for Photodynamic Therapy, *Chem. – Eur. J.*, 2024, **30**, e202401001.

57 J. Zhang, J. Ma, S. Zhang, X. Lou, Y. Ding, Y. Li, M. Xu, X. Xie, X. Jiao, X. Dou, X. Wang and B. Tang, Exploration of Thermally Activated Delayed Fluorescence (TADF)-Based Photoredox Catalyst To Establish the Mechanisms of Action for Photodynamic Therapy, *ACS Nano*, 2023, **17**, 23430–23441.

58 S. Lv, Y. Miao, D. Zheng, X. Li, D. Liu and F. Song, Self-Assembled Platinum Supramolecular Metallacycles Based on a Novel TADF Photosensitizer for Efficient Cancer Photochemotherapy, *Mol. Pharm.*, 2021, **18**, 1229–1237.

59 Y. Fang, Y. Xue and D. Chao, Organic Thermally Activated Delayed Fluorescence (TADF) Compound as The Photosensitizer in CO_2 Photoreduction: Taking 4CzIPN as An Example, *Asian J. Org. Chem.*, 2025, **14**, e202500256.
60 F. Droghetti, A. Mantovani and M. Natali, Light–Driven CO_2 Reduction Catalysis with Organic Thermally Activated Delayed Fluorescence (TADF) Sensitizers, *ChemCatChem*, 2025, **17**, e202500247.
61 M. A. Bryden and E. Zysman-Colman, Organic thermally activated delayed fluorescence (TADF) compounds used in photocatalysis, *Chem. Soc. Rev.*, 2021, **50**, 7587–7680.
62 F. Ni, J. Zhang, Y. Zhou and L. Qiu, Recent progress in stereoselective transformations enabled by thermally activated delayed fluorescence photocatalysts, *Chem. Catal.*, 2024, **4**, 100915.
63 B. Michelet, C. Deldaele, S. Kajouj, C. Moucheron and G. Evano, A General Copper Catalyst for Photoredox Transformations of Organic Halides, *Org. Lett.*, 2017, **19**, 3576–3579.
64 V. Ferraro, C. Bizzarri and S. Bräse, Thermally Activated Delayed Fluorescence (TADF) Materials Based on Earth–Abundant Transition Metal Complexes: Synthesis, Design and Applications, *Adv. Sci.*, 2024, **11**, 2404866.
65 M. Bouzrati-Zerelli, N. Guillaume, F. Goubard, T.-T. Bui, S. Villotte, C. Dietlin, F. Morlet-Savary, D. Gigmes, J. P. Fouassier, F. Dumur and J. Lalevée, A novel class of photoinitiators with a thermally activated delayed fluorescence (TADF) property, *New J. Chem.*, 2018, **42**, 8261–8270.
66 C. L. Linfoot, M. J. Leitl, P. Richardson, A. F. Rausch, O. Chepelin, F. J. White, H. Yersin and N. Robertson, Thermally Activated Delayed Fluorescence (TADF) and Enhancing Photoluminescence Quantum Yields of [Cu I (diimine)(diphosphine)] + Complexes—Photophysical, Structural, and Computational Studies, *Inorg. Chem.*, 2014, **53**, 10854–10861.
67 L. E. Burmeister, L. J. Groth, P. R. Meinhold, J. P. Zurwellen, D. Bockfeld, R. Frank, M. Karnahl, M. Tamm and S. Tschierlei, Photoactive Neutral Three-Coordinate Cu(I) Complexes of Anionic N-Heterocyclic Carbenes, *JACS Au*, 2025, **5**, 2792–2801.
68 M. Knorn, T. Rawner, R. Czerwieniec and O. Reiser, [Copper(phenanthroline)(bisisonitrile)]$^+$-Complexes for the Visible-Light-Mediated Atom Transfer Radical Addition and Allylation Reactions, *ACS Catal.*, 2015, **5**, 5186–5193.
69 D. Yu, W.-P. To, G. S. M. Tong, L.-L. Wu, K.-T. Chan, L. Du, D. L. Phillips, Y. Liu and C.-M. Che, Luminescent tungsten(VI) complexes as photocatalysts for light-driven C–C and C–B bond formation reactions, *Chem. Sci.*, 2020, **11**, 6370–6382.
70 Z. Wu, Y. Liu, C. Zou and W. Guo, Thermally activated delayed fluorescence materials for CO_2 reduction, *Next Energy*, 2023, **1**, 100041.
71 B. Bie, Z. Jiang, J. Zhang, H. Deng and C. Yang, Long excited state lifetime of thermally activated delayed fluorescent photosensitizer integrated into Metal-organic framework enables efficient CO_2 photoreduction, *Chem. Eng. J.*, 2022, **431**, 133897.
72 S. E. Zieger, A. Steinegger, I. Klimant and S. M. Borisov, TADF-Emitting Zn(II)-Benzoporphyrin: An Indicator for Simultaneous Sensing of Oxygen and Temperature, *ACS Sens.*, 2020, **5**, 1020–1027.
73 G. Schwendt and S. M. Borisov, Achieving simultaneous sensing of oxygen and temperature with metalloporphyrins featuring efficient thermally activated delayed fluorescence and phosphorescence, *Sens. Actuators, B*, 2023, **393**, 134236.
74 A. Steinegger and S. M. Borisov, Zn(II) Schiff Bases: Bright TADF Emitters for Self-referenced Decay Time-Based Optical Temperature Sensing, *ACS Omega*, 2020, **5**, 7729–7737.
75 P. Li, Z. Zhou, Y. S. Zhao and Y. Yan, Recent advances in luminescent metal-organic frameworks and their photonic applications, *Chem. Commun.*, 2021, **57**, 13678–13691.
76 P. Li, Z. Zhou, Y. S. Zhao and Y. Yan, Recent advances in luminescent metal-organic frameworks and their photonic applications, *Chem. Commun.*, 2021, **57**, 13678–13691.
77 W. P. Lustig, S. Mukherjee, N. D. Rudd, A. V. Desai, J. Li and S. K. Ghosh, Metal–organic frameworks: functional luminescent and photonic materials for sensing applications, *Chem. Soc. Rev.*, 2017, **46**, 3242–3285.
78 Y. Cui, J. Zhang, H. He and G. Qian, Photonic functional metal–organic frameworks, *Chem. Soc. Rev.*, 2018, **47**, 5740–5785.
79 L. E. Kreno, K. Leong, O. K. Farha, M. Allendorf, R. P. Van Duyne and J. T. Hupp, Metal–Organic Framework Materials as Chemical Sensors, *Chem. Rev.*, 2012, **112**, 1105–1125.
80 H.-Y. Li, S.-N. Zhao, S.-Q. Zang and J. Li, Functional metal–organic frameworks as effective sensors of gases and volatile compounds, *Chem. Soc. Rev.*, 2020, **49**, 6364–6401.
81 H. Yuan, N. Li, W. Fan, H. Cai and D. Zhao, Metal–Organic Framework Based Gas Sensors, *Adv. Sci.*, 2022, **9**, 2104374.
82 C. Zhu, J. Hou, X. Wang, S. Wang, H. Xu, J. Hu, L. Jing and S. Wang, Optimizing ligand-to-metal charge transfer in metal–organic frameworks to enhance photocatalytic performance, *Chem. Eng. J.*, 2024, **499**, 156527.
83 C. Han and X. Liu, Emission Library and Applications of 2,1,3-Benzothiadiazole and Its Derivative–Based Luminescent Metal–Organic Frameworks, *Angew. Chem., Int. Ed.*, 2025, **64**, e202416286.
84 E. Özcan, Z. Mermer and Y. Zorlu, Metal-organic frameworks as photocatalysts in energetic and environmental applications, *Turk. J. Chem.*, 2023, **47**, 1018–1052.
85 T. J. Penfold, On Predicting the Excited-State Properties of Thermally Activated Delayed Fluorescence Emitters, *J. Phys. Chem. C*, 2015, **119**, 13535–13544.
86 P. K. Chow, C. Ma, W. P. To, G. S. M. Tong, S. L. Lai, S. C. F. Kui, W. M. Kwok and C. M. Che, Strongly phos-

phorescent palladium(II) complexes of tetradentate ligands with mixed oxygen, carbon, and nitrogen donor atoms: Photophysics, photochemistry, and applications, *Angew. Chem., Int. Ed.*, 2013, **52**, 11775–11779.

87 L. F. Gildea and J. A. G. Williams, in *Organic Light-Emitting Diodes (OLEDs)*, Elsevier, 2013, vol. 62, pp. 77–113.

88 P. Pander, R. Daniels, A. V. Zaytsev, A. Horn, A. Sil, T. J. Penfold, J. A. G. Williams, V. N. Kozhevnikov and F. B. Dias, Exceptionally fast radiative decay of a dinuclear platinum complex through thermally activated delayed fluorescence, *Chem. Sci.*, 2021, **12**, 6172–6180.

89 P. Pander, A. V. Zaytsev, A. Sil, J. A. G. Williams, P.-H. Lanoe, V. N. Kozhevnikov and F. B. Dias, The role of dinuclearity in promoting thermally activated delayed fluorescence (TADF) in cyclometallated, N^C^N-coordinated platinum(II) complexes, *J. Mater. Chem. C*, 2021, **9**, 10276–10287.

90 P. Pander, R. Motyka, P. Zassowski, M. K. Etherington, D. Varsano, T. J. da Silva, M. J. Caldas, P. Data and A. P. Monkman, Thermally Activated Delayed Fluorescence Mediated through the Upper Triplet State Manifold in Non-Charge-Transfer Star-Shaped Triphenylamine–Carbazole Molecules, *J. Phys. Chem. C*, 2018, **122**, 23934–23942.

91 M. Urban, P. H. Marek-Urban, K. Durka, S. Luliński, P. Pander and A. P. Monkman, TADF Invariant of Host Polarity and Ultralong Fluorescence Lifetimes in a Donor–Acceptor Emitter Featuring a Hybrid Sulfone–Triarylboron Acceptor, *Angew. Chem., Int. Ed.*, 2023, **62**, e202217530.

92 S. J. Strickler and R. A. Berg, Relationship between Absorption Intensity and Fluorescence Lifetime of Molecules, *J. Chem. Phys.*, 1962, **37**, 814–822.

93 P. Pander, A. V. Zaytsev, L. G. Franca, F. B. Dias and V. N. Kozhevnikov, Unusual Excimer/Dimer Behavior of a Highly Soluble C,N Platinum(II) Complex with a Spiro-Fluorene Motif, *Inorg. Chem.*, 2023, **62**, 18465–18473.

94 P. Pander, Y. M. Dikova, E. V. Puttock and J. A. G. Williams, Dinuclear platinum(II) complexes emitting through TADF: new ligand design to minimise aggregation and the S_1–T_1 energy gap, *Inorg. Chem. Front.*, 2024, **11**, 7545–7551.

95 Y. Tao, K. Yuan, T. Chen, P. Xu, H. Li, R. Chen, C. Zheng, L. Zhang and W. Huang, Thermally Activated Delayed Fluorescence Materials Towards the Breakthrough of Organoelectronics, *Adv. Mater.*, 2014, **26**, 7931–7958.

96 P. Pander, A. V. Zaytsev, A. Sil, J. A. G. Williams, V. N. Kozhevnikov and F. B. Dias, Enhancement of thermally activated delayed fluorescence properties by substitution of ancillary halogen in a multiple resonance-like diplatinum(II) complex, *J. Mater. Chem. C*, 2022, **10**, 4851–4860.

97 T. Hatakeyama, K. Shiren, K. Nakajima, S. Nomura, S. Nakatsuka, K. Kinoshita, J. Ni, Y. Ono and T. Ikuta, Ultrapure Blue Thermally Activated Delayed Fluorescence Molecules: Efficient HOMO-LUMO Separation by the Multiple Resonance Effect, *Adv. Mater.*, 2016, **28**, 2777–2781.

98 J. M. Ha, S. H. Hur, A. Pathak, J.-E. Jeong and H. Y. Woo, Recent advances in organic luminescent materials with narrowband emission, *NPG Asia Mater.*, 2021, **13**, 53.

99 X. F. Song, Z. W. Li, W. K. Chen, Y. J. Gao and G. Cui, Thermally Activated Delayed Fluorescence Mechanism of a Bicyclic "Carbene–Metal–Amide" Copper Compound: DFT/MRCI Studies and Roles of Excited-State Structure Relaxation, *Inorg. Chem.*, 2022, **61**, 7673–7681.

100 J. Gibson, A. P. Monkman and T. J. Penfold, The Importance of Vibronic Coupling for Efficient Reverse Intersystem Crossing in Thermally Activated Delayed Fluorescence Molecules, *ChemPhysChem*, 2016, **17**, 2956–2961.

101 L. de Thieulloy, L. E. de Sousa and P. de Silva, TADF Mechanism in a Carbene-Copper Emitter: Insights from the Nuclear Ensemble Simulations, *J. Phys. Chem. C*, 2024, **128**, 14887–14896.

102 N. Le Phuoc, A. Kumar, A. Baidak, A. S. Romanov and M. Linnolahti, Design Rules and Experimental Validation of Carbene–Metal–Amide Luminophores: Systematic Modification of the Amide Ligand, *Inorg. Chem. Front.*, 2025, **12**, 7615–7627.

103 L.-Y. Peng, Z.-W. Li, G.-N. Pan, W.-K. Chen, Y.-J. Gao and G. Cui, Thermally activated delayed fluorescence of a Ir (iii) complex: absorption and emission properties, non-radiative rates, and mechanism, *Phys. Chem. Chem. Phys.*, 2023, **25**, 6454–6460.

104 M. Z. Shafikov, R. Martinscroft, C. Hodgson, A. Hayer, A. Auch and V. N. Kozhevnikov, Non-Stereogenic Dinuclear Ir(III) Complex with a Molecular Rack Design to Afford Efficient Thermally Enhanced Red Emission, *Inorg. Chem.*, 2021, **60**, 1780–1789.

105 X. F. Song, L. Y. Peng, W. K. Chen, Y. J. Gao, W. H. Fang and G. Cui, Thermally Activated Delayed Fluorescence of a Dinuclear Platinum(II) Compound: Mechanism and Roles of an Upper Triplet State, *Chem. – Eur. J.*, 2022, **28**, e202201782.

106 J. Gibson and T. J. Penfold, Nonadiabatic coupling reduces the activation energy in thermally activated delayed fluorescence, *Phys. Chem. Chem. Phys.*, 2017, **19**, 8428–8434.

107 F. Neese, The ORCA program system, *Wiley Interdiscip. Rev.: Comput. Mol. Sci.*, 2012, **2**, 73–78.

108 F. Neese, Software update: The ORCA program system—Version 5.0, *Wiley Interdiscip. Rev.: Comput. Mol. Sci.*, 2022, **12**, e1606.

109 F. Neese, Software update: the ORCA program system, version 4.0, *Wiley Interdiscip. Rev.: Comput. Mol. Sci.*, 2018, **8**, e1327.

110 M. Etinski, J. Tatchen and C. M. Marian, Time-dependent approaches for the calculation of intersystem crossing rates, *J. Chem. Phys.*, 2011, **134**, 154105.

111 M. Etinski, V. Rai-Constapel and C. M. Marian, Time-dependent approach to spin-vibronic coupling: Implementation and assessment, *J. Chem. Phys.*, 2014, **140**, 114104.

112 M. Etinski, J. Tatchen and C. M. Marian, Thermal and solvent effects on the triplet formation in cinnoline, *Phys. Chem. Chem. Phys.*, 2014, **16**, 4740.
113 E. Y.-T. Li, T.-Y. Jiang, Y. Chi and P.-T. Chou, Semi-quantitative assessment of the intersystem crossing rate: an extension of the El-Sayed rule to the emissive transition metal complexes, *Phys. Chem. Chem. Phys.*, 2014, **16**, 26184–26192.
114 K. Mori, T. P. M. Goumans, E. van Lenthe and F. Wang, Predicting phosphorescent lifetimes and zero-field splitting of organometallic complexes with time-dependent density functional theory including spin–orbit coupling, *Phys. Chem. Chem. Phys.*, 2014, **16**, 14523–14530.
115 K. Nozaki, Theoretical Studies on Photophysical Properties and Mechanism of Phosphorescence in [fac-Ir(2-phenylpyridine)$_3$], *J. Chin. Chem. Soc.*, 2006, **53**, 101–112.
116 H. Yersin, in *Top Curr Chem*, 2012, vol. 241, pp. 1–26.
117 B. de Souza, G. Farias, F. Neese and R. Izsák, Predicting Phosphorescence Rates of Light Organic Molecules Using Time-Dependent Density Functional Theory and the Path Integral Approach to Dynamics, *J. Chem. Theory Comput.*, 2019, **15**, 1896–1904.
118 P. Pander, A. V. Zaytsev, A. Sil, G. V. Baryshnikov, F. Siddique, J. A. G. Williams, F. B. Dias and V. N. Kozhevnikov, Thermally activated delayed fluorescence in a deep red dinuclear iridium(III) complex: a hidden mechanism for short luminescence lifetimes, *Chem. Sci.*, 2023, **14**, 13934–13943.
119 **https://www.faccts.de/docs/orca/5.0/tutorials/spec/SOC.html**.
120 P. Pander, D. Nastula, P. Marek-Urban, V. Kozhevnikov and J. A. G. Williams, Evidence for thermally activated delayed fluorescence in iridium(III) complexes, *Inorg. Chem. Front.*, 2026, DOI: **10.1039/d5qi01968k**.
121 R. K. Konidena and K. R. Naveen, Boron–Based Narrowband Multiresonance Delayed Fluorescent Emitters for Organic Light–Emitting Diodes, *Adv. Photonics Res.*, 2022, **3**, 2200201.
122 Y. Ma, C. M. Che, H. Y. Chao, X. Zhou, W. H. Chan and J. Shen, High luminescence gold(I) and copper(I) complexes with a triplet excited state for use in light-emitting diodes, *Adv. Mater.*, 1999, **11**, 852–857.
123 Y.-G. Ma, W.-H. Chan, X.-M. Zhoub and C.-M. Che, *Light-emitting diode device from a luminescent organocopper(I) compound*, 1999.
124 R. Czerwieniec, J. Yu and H. Yersin, Blue-light emission of Cu(I) complexes and singlet harvesting, *Inorg. Chem.*, 2011, **50**, 8293–8301.
125 R. Hamze, S. Shi, S. C. Kapper, D. S. M. Ravinson, L. Estergreen, M. C. Jung, A. C. Tadle, R. Haiges, P. I. Djurovich, J. L. Peltier, R. Jazzar, G. Bertrand, S. E. Bradforth and M. E. Thompson, 'Quick-Silver' from a Systematic Study of Highly Luminescent, Two-Coordinate, d^{10} Coinage Metal Complexes, *J. Am. Chem. Soc.*, 2019, **141**, 8616–8626.
126 R. Hamze, J. L. Peltier, D. Sylvinson, M. Jung, J. Cardenas, R. Haiges, M. Soleilhavoup, R. Jazzar, P. I. Djurovich, G. Bertrand and M. E. Thompson, *Eliminating nonradiative decay in Cu(I) emitters: >99% quantum efficiency and microsecond lifetime*, 2019, vol. 363.
127 R. Tang, S. Xu, T. L. Lam, G. Cheng, L. Du, Q. Wan, J. Yang, F. F. Hung, K. H. Low, D. L. Phillips and C. M. Che, Highly Robust CuI-TADF Emitters for Vacuum-Deposited OLEDs with Luminance up to 222 200 cd m^{-2} and Device Lifetimes (LT90) up to 1300 hours at an Initial Luminance of 1000 cd m^{-2}, *Angew. Chem., Int. Ed.*, 2022, **61**, e202203982.
128 A. Ruduss, B. Turovska, S. Belyakov, K. A. Stucere, A. Vembris and K. Traskovskis, Carbene–Metal Complexes As Molecular Scaffolds for Construction of through-Space Thermally Activated Delayed Fluorescence Emitters, *Inorg. Chem.*, 2022, **61**, 2174–2185.
129 A. M. T. Muthig, O. Mrózek, T. Ferschke, M. Rödel, B. Ewald, J. Kuhnt, C. Lenczyk, J. Pflaum and A. Steffen, Mechano-Stimulus and Environment-Dependent Circularly Polarized TADF in Chiral Copper(I) Complexes and Their Application in OLEDs, *J. Am. Chem. Soc.*, 2023, **145**, 4438–4449.
130 A. Y. Baranov, M. I. Rakhmanova, X. Hei, D. G. Samsonenko, D. V. Stass, I. Y. Bagryanskaya, M. R. Ryzhikov, V. P. Fedin, J. Li and A. V. Artem'ev, A new subclass of copper(I) hybrid emitters showing TADF with near-unity quantum yields and a strong solvatochromic effect, *Chem. Commun.*, 2023, **59**, 2923–2926.
131 Y. L. Liu, R. Zhu, L. Liu, X. X. Zhong, F. B. Li, G. Zhou and H. M. Qin, High-performance TADF-OLEDs utilizing copper(I) halide complexes containing unsymmetrically substituted thiophenyl triphosphine ligands, *Inorg. Chem. Front.*, 2025, **12**, 1139–1155.
132 S. Yuan, G. Zhang, F. Chen, J. Chen, Y. Zhang, Y. Di, Y. Chen, Y. Zhu, M. Lin and H. Chen, Thermally Activated Delayed Fluorescent Ag(I) Complexes for Highly Efficient Scintillation and High-Resolution X-Ray Imaging, *Adv. Funct. Mater.*, 2024, **34**, 2400436.
133 M. Osawa, M. Hashimoto, I. Kawata and M. Hoshino, Photoluminescence properties of TADF-emitting three-coordinate silver(I) halide complexes with diphosphine ligands: A comparison study with copper(I) complexes, *Dalton Trans.*, 2017, **46**, 12446–12455.
134 C. Yang, O. Elbjeirami, C. S. P. Gamage, H. V. R. Dias and M. A. Omary, Luminescence enhancement and tuning via multiple cooperative supramolecular interactions in an ion-paired multinuclear complex, *Chem. Commun.*, 2011, **47**, 7434–7436.
135 M. Dosen, Y. Kawada, S. Shibata, K. Tsuge, Y. Sasaki, A. Kobayashi, M. Kato, S. Ishizaka and N. Kitamura, Control of Emissive Excited States of Silver(I) Halogenido Coordination Polymers by a Solid Solution Approach, *Inorg. Chem.*, 2019, **58**, 8419–8431.
136 D. H. Wang, Y. Zhang, Y. T. Wang, H. Y. Feng, Y. Chen and D. Z. Zhao, Silver(I) Complexes of Diphenylpyridines: Crystal Structures, Luminescence Studies, Theoretical

Insights, and Biological Activities, *ChemPlusChem*, 2017, **82**, 323–332.

137 M. Z. Shafikov, A. F. Suleymanova, R. Czerwieniec and H. Yersin, Design Strategy for Ag(I)-Based Thermally Activated Delayed Fluorescence Reaching an Efficiency Breakthrough, *Chem. Mater.*, 2017, **29**, 1708–1715.

138 A. Kobayashi and M. Kato, Stimuli-responsive Luminescent Copper(I) Complexes for Intelligent Emissive Devices, *Chem. Lett.*, 2017, **46**, 154–162.

139 E. Cariati, E. Lucenti, C. Botta, U. Giovanella, D. Marinotto and S. Righetto, Cu(I) hybrid inorganic–organic materials with intriguing stimuli responsive and optoelectronic properties, *Coord. Chem. Rev.*, 2016, **306**, 566–614.

140 E. Fresta, J. M. Carbonell-Vilar, J. Yu, D. Armentano, J. Cano, M. Viciano-Chumillas and R. D. Costa, Deciphering the Electroluminescence Behavior of Silver (I)–Complexes in Light–Emitting Electrochemical Cells: Limitations and Solutions toward Highly Stable Devices, *Adv. Funct. Mater.*, 2019, **29**, 1901797.

141 A. S. Romanov, S. T. E. Jones, L. Yang, P. J. Conaghan, D. Di, M. Linnolahti, D. Credgington and M. Bochmann, Mononuclear Silver Complexes for Efficient Solution and Vacuum-Processed OLEDs, *Adv. Opt. Mater.*, 2018, **6**, 1801347.

142 R. Hamze, S. Shi, S. C. Kapper, D. S. M. Ravinson, L. Estergreen, M. C. Jung, A. C. Tadle, R. Haiges, P. I. Djurovich, J. L. Peltier, R. Jazzar, G. Bertrand, S. E. Bradforth and M. E. Thompson, 'Quick-Silver' from a Systematic Study of Highly Luminescent, Two-Coordinate, d^{10} Coinage Metal Complexes, *J. Am. Chem. Soc.*, 2019, **141**, 8616–8626.

143 J. H. Jia, D. Liang, R. Yu, X. L. Chen, L. Meng, J. F. Chang, J. Z. Liao, M. Yang, X. N. Li and C. Z. Lu, Coordination-Induced Thermally Activated Delayed Fluorescence: From Non-TADF Donor-Acceptor-Type Ligand to TADF-Active Ag-Based Complexes, *Chem. Mater.*, 2020, **32**, 620–629.

144 W. P. To, G. Cheng, G. S. M. Tong, D. Zhou and C. M. Che, Recent Advances in Metal-TADF Emitters and Their Application in Organic Light-Emitting Diodes, *Front. Chem.*, 2020, **8**, 653.

145 Z. Han, X. Dong and S. Zang, Crystalline Metal–Organic Materials with Thermally Activated Delayed Fluorescence, *Adv. Opt. Mater.*, 2021, **9**, 2100081.

146 K. Li, Y. Chen, J. Wang and C. Yang, Diverse emission properties of transition metal complexes beyond exclusive single phosphorescence and their wide applications, *Coord. Chem. Rev.*, 2021, **433**, 213755.

147 D. Zhou, G. S. M. Tong, G. Cheng, Y. K. Tang, W. Liu, D. Ma, L. Du, J. R. Chen and C. M. Che, Stable Tetradentate Gold(III)-TADF Emitters with Close to Unity Quantum Yield and Radiative Decay Rate Constant of up to 2×10^6 s^{-1}: High-Efficiency Green OLEDs with Operational Lifetime (LT90) Longer than 1800 h at 1000 cd m^{-2}, *Adv. Mater.*, 2022, **34**, 2206598.

148 X. Feng, J. G. Yang, J. Miao, C. Zhong, X. Yin, N. Li, C. Wu, Q. Zhang, Y. Chen, K. Li and C. Yang, Au···H–C Interactions Support a Robust Thermally Activated Delayed Fluorescence (TADF) Gold(I) Complex for OLEDs with Little Efficiency Roll-Off and Good Stability, *Angew. Chem., Int. Ed.*, 2022, **61**, e202209451.

149 F. H. Yu, X. F. Song, G. H. Liu, X. Chang, K. Li, Y. Wang, G. Cui and Y. Chen, Highly Efficient Au(I) Alkynyl Emitters: Thermally Activated Delayed Fluorescence and Solution-Processed OLEDs, *Chem. – Eur. J.*, 2022, **28**, e202202439.

150 P. J. Conaghan, S. M. Menke, A. S. Romanov, S. T. E. Jones, A. J. Pearson, E. W. Evans, M. Bochmann, N. C. Greenham and D. Credgington, Efficient Vacuum-Processed Light-Emitting Diodes Based on Carbene–Metal–Amides, *Adv. Mater.*, 2018, **30**, 1802285.

151 M. Gernert, L. Balles-Wolf, F. Kerner, U. Müller, A. Schmiedel, M. Holzapfel, C. M. Marian, J. Pflaum, C. Lambert and A. Steffen, Cyclic (Amino)(aryl)carbenes Enter the Field of Chromophore Ligands: Expanded πsystem Leads to Unusually Deep Red Emitting CuICompounds, *J. Am. Chem. Soc.*, 2020, **142**, 8897–8909.

152 J. G. Yang, X. F. Song, J. Wang, K. Li, X. Chang, L. Y. Tan, C. X. Liu, F. H. Yu, G. Cui, G. Cheng, W. P. To, C. Yang, C. M. Che and Y. Chen, Highly Efficient Thermally Activated Delayed Fluorescence from Pyrazine-Fused Carbene Au(I) Emitters, *Chem. – Eur. J.*, 2021, **27**, 17834–17842.

153 P. J. Conaghan, C. S. B. Matthews, F. Chotard, S. T. E. Jones, N. C. Greenham, M. Bochmann, D. Credgington and A. S. Romanov, Highly efficient blue organic light-emitting diodes based on carbene-metal-amides, *Nat. Commun.*, 2020, **11**(1), 1758.

154 J. Wang, N. Li, C. Zhong, J. Miao, Z. Huang, M. Yu, Y. X. Hu, S. Luo, Y. Zou, K. Li and C. Yang, Metal-Perturbed Multiresonance TADF Emitter Enables High-Efficiency and Ultralow Efficiency Roll-Off Nonsensitized OLEDs with Pure Green Gamut, *Adv. Mater.*, 2023, **35**, 2208378.

155 S. M. Suresh, D. Hall, D. Beljonne, Y. Olivier and E. Zysman-Colman, Multiresonant Thermally Activated Delayed Fluorescence Emitters Based on Heteroatom–Doped Nanographenes: Recent Advances and Prospects for Organic Light–Emitting Diodes, *Adv. Funct. Mater.*, 2020, **30**, 1908677.

156 K. Stavrou, A. Danos, T. Hama, T. Hatakeyama and A. Monkman, Hot Vibrational States in a High-Performance Multiple Resonance Emitter and the Effect of Excimer Quenching on Organic Light-Emitting Diodes, *ACS Appl. Mater. Interfaces*, 2021, **13**, 8643–8655.

157 R. Tang, S. Xu, L. Du, F. F. Hung, T. L. Lam, G. Cheng, K. H. Low, Q. Wan, S. Wu, Y. Chen and C. M. Che, Au(I)-TADF Emitters for High Efficiency Full-Color Vacuum-Deposited OLEDs and TADF-Sensitized Fluorescent OLEDs with Ultrahigh Brightness and Prolonged Operational Lifetime, *Adv. Opt. Mater.*, 2023, **11**, 2300950.

158 S. J. Zheng, J. Ma, J. Su, P. I. Djurovich, M. E. Thompson and T. Y. Li, Simultaneous Thermally Stimulated Delayed Phosphorescence (TSDP) and Thermally Activated Delayed Fluorescence (TADF) in a Two-Coordinated Au(I)

Bimetallic Complex Featuring a Tandem Carbene Structure, *J. Am. Chem. Soc.*, 2024, **146**(28), 19042–19049.

159 C. Riley, W. Jones, N. Le Phuoc, M. Linnolahti and A. S. Romanov, Cyclic(amino)(barrelene)carbene metal amide complexes: Synthesis and thermally activated delayed fluorescence, *Org. Electron.*, 2025, **137**, 107156.

160 T.-Y. Li, J. Schaab, P. I. Djurovich and M. E. Thompson, Toward rational design of TADF two-coordinate coinage metal complexes: understanding the relationship between natural transition orbital overlap and photophysical properties, *J. Mater. Chem. C*, 2022, **10**, 4674–4683.

161 D. Zhou, W. P. To, G. S. M. Tong, G. Cheng, L. Du, D. L. Phillips and C. M. Che, Tetradentate Gold(III) Complexes as Thermally Activated Delayed Fluorescence (TADF) Emitters: Microwave-Assisted Synthesis and High-Performance OLEDs with Long Operational Lifetime, *Angew. Chem., Int. Ed.*, 2020, **59**, 6375–6382.

162 W. To, D. Zhou, G. S. M. Tong, G. Cheng, C. Yang and C. Che, Highly Luminescent Pincer Gold(III) Aryl Emitters: Thermally Activated Delayed Fluorescence and Solution–Processed OLEDs, *Angew. Chem.*, 2017, **129**, 14224–14229.

163 V. K. M. Au, K. M. C. Wong, D. P. K. Tsang, M. Y. Chan, N. Zhu and V. W. W. Yam, High-efficiency green organic light-emitting devices utilizing phosphorescent bis-cyclometalated alkynylgold(III) complexes, *J. Am. Chem. Soc.*, 2010, **132**, 14273–14278.

164 M. C. Tang, D. P. K. Tsang, M. M. Y. Chan, K. M. C. Wong and V. W. W. Yam, Dendritic luminescent gold(III) complexes for highly efficient solution-processable organic light-emitting devices, *Angew. Chem., Int. Ed.*, 2013, **52**, 446–449.

165 B. Y. Wong, H. Wong, Y. Wong, M. Chan and V. W. Yam, Versatile Synthesis of Luminescent Tetradentate Cyclometalated Alkynylgold(III) Complexes and Their Application in Solution–Processable Organic Light–Emitting Devices, *Angew. Chem.*, 2017, **129**, 308–311.

166 M. C. Tang, C. H. Lee, S. L. Lai, M. Ng, M. Y. Chan and V. W. W. Yam, Versatile Design Strategy for Highly Luminescent Vacuum-Evaporable and Solution-Processable Tridentate Gold(III) Complexes with Monoaryl Auxiliary Ligands and Their Applications for Phosphorescent Organic Light Emitting Devices, *J. Am. Chem. Soc.*, 2017, **139**, 9341–9349.

167 D. Zhou, G. Cheng, G. S. M. Tong and C. M. Che, High Efficiency Sky-Blue Gold(III)-TADF Emitters, *Chem. – Eur. J.*, 2020, **26**, 15718–15726.

168 C. C. Au-Yeung, L. K. Li, M. C. Tang, S. L. Lai, W. L. Cheung, M. Ng, M. Y. Chan and V. W. W. Yam, Molecular design of efficient yellow-To red-emissive alkynylgold(III) complexes for the realization of thermally activated delayed fluorescence (TADF) and their applications in solution-processed organic light-emitting devices, *Chem. Sci.*, 2021, **12**, 9516–9527.

169 D. Zhou, G. S. M. Tong, G. Cheng, Y. K. Tang, W. Liu, D. Ma, L. Du, J. R. Chen and C. M. Che, Stable Tetradentate Gold(III)-TADF Emitters with Close to Unity Quantum Yield and Radiative Decay Rate Constant of up to 2×10^6 s^{-1}: High-Efficiency Green OLEDs with Operational Lifetime (LT90) Longer than 1800 h at 1000 cd m^{-2}, *Adv. Mater.*, 2022, **51**, 2206598.

170 W. K. Kwok, L. K. Li, S. L. Lai, M. Y. Leung, W. K. Tang, S. C. Cheng, M. C. Tang, W. L. Cheung, C. C. Ko, M. Y. Chan and V. W. W. Yam, Tetradentate C^C^N^N Ligand-Containing Gold(III) Complexes with Orange to Deep-Red Thermally Activated Delayed Fluorescence (TADF) and Their Application in Organic Light-Emitting Devices, *J. Am. Chem. Soc.*, 2023, **145**, 9584–9595.

171 M. C. Tang, L. K. Li, S. L. Lai, W. L. Cheung, M. Ng, C. Y. Wong, M. Y. Chan and V. W. W. Yam, Design Strategy Towards Horizontally Oriented Luminescent Tetradentate-Ligand-Containing Gold(III) Systems, *Angew. Chem., Int. Ed.*, 2020, **59**, 21023–21031.

172 G. Li, Q. Chen, J. Zheng, Q. Wang, F. Zhan, W. Lou, Y. F. Yang and Y. She, Metal-Assisted Delayed Fluorescent Pd(II) Complexes and Phosphorescent Pt(II) Complex Based on [1,2,4]Triazolo[4,3-A[pyridine-Containing Ligands: Synthesis, Characterization, Electrochemistry, Photophysical Studies, and Application, *Inorg. Chem.*, 2019, **58**, 14349–14360.

173 Z. Q. Zhu, T. Fleetham, E. Turner and J. Li, Harvesting all electrogenerated excitons through metal assisted delayed fluorescent materials, *Adv. Mater.*, 2015, **27**, 2533–2537.

174 M. K. Sit, G. S. M. Tong, T. L. Lam, G. Cheng, F. F. Hung, K. M. So, L. Du, K. O. Choy, K. H. Low and C. M. Che, Strongly Luminescent Tetradentate Palladium(II)-TADF Emitters. Blue TADF And TADF-Sensitized OLEDs with External Quantum Efficiencies Over 23%, *Adv. Opt. Mater.*, 2024, **12**, 2302308.

175 J. Zhang, X. F. Song, Y. Xu, J. G. Yang, Y. Zhang, J. Miao and K. Li, Pd(II)-TADF Emitters Featuring Multiple Intramolecular Noncovalent Interactions: Toward Organic Light-Emitting Diodes with EQEs up to 31.5% and Operational Half-Lifetimes Exceeding 1600 h at 3000 cd m^{-2}, *Adv. Funct. Mater.*, 2024, **34**, 2404148.

176 A. Upadhyay, A. Nepalia, A. Bera, D. K. Saini and A. R. Chakravarty, A Platinum(II) Boron-dipyrromethene Complex for Cellular Imaging and Mitochondria-targeted Photodynamic Therapy in Red Light, *Chem. – Asian J.*, 2023, **18**, e202300667.

177 S. W. Botchway, M. Charnley, J. W. Haycock, A. W. Parker, D. L. Rochester, J. A. Weinstein and J. A. G. Williams, Time-resolved and two-photon emission imaging microscopy of live cells with inert platinum complexes, *Proc. Natl. Acad. Sci. U. S. A.*, 2008, **105**, 16071–16076.

178 M. Yoshida, K. Saito, H. Matsukawa, S. Yanagida, M. Ebina, Y. Maegawa, S. Inagaki, A. Kobayashi and M. Kato, Immobilization of luminescent Platinum(II) complexes on periodic mesoporous organosilica and their water reduction photocatalysis, *J. Photochem. Photobiol., A*, 2018, **358**, 334–344.

179 P. K. Chow, C. Ma, W. P. To, G. S. M. Tong, S. L. Lai, S. C. F. Kui, W. M. Kwok and C. M. Che, Strongly phosphorescent palladium(II) complexes of tetradentate

ligands with mixed oxygen, carbon, and nitrogen donor atoms: Photophysics, photochemistry, and applications, *Angew. Chem., Int. Ed.*, 2013, **52**, 11775–11779.

180 D. Gómez de Segura, A. Corral-Zorzano, E. Alcolea, M. T. Moreno and E. Lalinde, Phenylbenzothiazole-Based Platinum(II) and Diplatinum(II) and (III) Complexes with Pyrazolate Groups: Optical Properties and Photocatalysis, *Inorg. Chem.*, 2024, **63**, 1589–1606.

181 G. Cheng, P. K. Chow, S. C. F. Kui, C. C. Kwok and C. M. Che, High-efficiency polymer light-emitting devices with robust phosphorescent platinum(II) emitters containing tetradentate dianionic O^N^C^N ligands, *Adv. Mater.*, 2013, **25**, 6765–6770.

182 Y. C. Wei, S. F. Wang, Y. Hu, L. S. Liao, D. G. Chen, K. H. Chang, C. W. Wang, S. H. Liu, W. H. Chan, J. L. Liao, W. Y. Hung, T. H. Wang, P. T. Chen, H. F. Hsu, Y. Chi and P. T. Chou, Overcoming the energy gap law in near-infrared OLEDs by exciton–vibration decoupling, *Nat. Photonics*, 2020, **14**, 570–577.

183 S. Luo, X. F. Song, Y. Y. Jing, X. Wan, J. Zhang and K. Li, Photoluminescence of a Platinum(II) Complex Containing Multiresonance B-N Motif in the Cyclometalated Ligand, *Organometallics*, 2023, **42**, 3323–3327.

184 T. Fleetham, G. Li and J. Li, Phosphorescent Pt(II) and Pd (II) Complexes for Efficient, High–Color–Quality, and Stable OLEDs, *Adv. Mater.*, 2017, **29**, 1601861.

185 Z. Abedin-Siddique, T. Ohno, K. Nozaki and T. Tsubomura, Intense Fluorescence of Metal-to-Ligand Charge Transfer in $[Pt(0)(binap)_2]$ [binap = 2,2′-Bis(diphenylphosphino)-1,1′-binaphthyl], *Inorg. Chem.*, 2004, **43**, 663–673.

186 P. Pander, R. Daniels, A. V. Zaytsev, A. Horn, A. Sil, T. J. Penfold, J. A. G. Williams, V. N. Kozhevnikov and F. B. Dias, Exceptionally fast radiative decay of a dinuclear platinum complex through thermally activated delayed fluorescence, *Chem. Sci.*, 2021, **12**, 6172–6180.

187 P. Pander, A. V. Zaytsev, A. Sil, J. A. G. Williams, P. H. Lanoe, V. N. Kozhevnikov and F. B. Dias, The role of dinuclearity in promoting thermally activated delayed fluorescence (TADF) in cyclometallated, NCN-coordinated platinum(II) complexes, *J. Mater. Chem. C*, 2021, **9**, 10276–10287.

188 P. Pander, A. V. Zaytsev, A. Sil, J. A. G. Williams, V. N. Kozhevnikov and F. B. Dias, Enhancement of thermally activated delayed fluorescence properties by substitution of ancillary halogen in a multiple resonance-like diplatinum(II) complex, *J. Mater. Chem. C*, 2022, **10**, 4851–4860.

189 J. G. Yang, N. Li, J. Li, X. F. Song, M. De Li, J. Zhang and K. Li, A thermally activated delayed fluorescent platinum (II) complex for red organic light emitting diodes with high efficiencies and small roll-off, *J. Mater. Chem. A*, 2024, **12**, 18977–18985.

190 P. Pander, Y. M. Dikova, E. V. Puttock and J. A. G. Williams, Dinuclear platinum(II) complexes emitting through TADF: new ligand design to minimise aggregation and the S_1–T_1 energy gap, *Inorg. Chem. Front.*, 2024, **11**, 7545–7551.

191 A. Russegger, S. M. Fischer, A. C. Debruyne, H. Wiltsche, A. D. Boese, R. I. Dmitriev and S. M. Borisov, Tunable Self-Referenced Molecular Thermometers via Manipulation of Dual Emission in Platinum(II) Pyridinedipyrrolide Complexes, *ACS Appl. Mater. Interfaces*, 2024, **16**, 11930–11943.

192 A. Russegger, A. C. Debruyne, D. C. Berrio, S. Fuchs, J. Marzi, K. Schenke-Layland, R. I. Dmitriev and S. M. Borisov, Bright and Photostable TADF-Emitting Zirconium(IV) Pyridinedipyrrolide Complexes: Efficient Dyes for Decay Time-Based Temperature Sensing and Imaging, *Adv. Opt. Mater.*, 2023, **11**, 2202720.

193 Y. Zhang, D. C. Leary, A. M. Belldina, J. L. Petersen and C. Milsmann, Effects of Ligand Substitution on the Optical and Electrochemical Properties of (Pyridinedipyrrolide)zirconium Photosensitizers, *Inorg. Chem.*, 2020, **59**, 14716–14730.

194 Y. Zhang, T. S. Lee, J. M. Favale, D. C. Leary, J. L. Petersen, G. D. Scholes, F. N. Castellano and C. Milsmann, Delayed fluorescence from a zirconium(IV) photosensitizer with ligand-to-metal charge-transfer excited states, *Nat. Chem.*, 2020, **12**, 345–352.

195 Y. Zhang, J. L. Petersen and C. Milsmann, A Luminescent Zirconium(IV) Complex as a Molecular Photosensitizer for Visible Light Photoredox Catalysis, *J. Am. Chem. Soc.*, 2016, **138**, 13115–13118.

196 N. Komine, R. W. Buell, C. H. Chen, A. K. Hui, M. Pink and K. G. Caulton, Probing the steric and electronic characteristics of a new bis-pyrrolide pincer ligand, *Inorg. Chem.*, 2014, **53**, 1361–1369.

197 W. L. Jia, Q. De Liu, R. Wang and S. Wang, Novel phosphorescent cyclometalated organotin(IV) and organolead(IV) complexes of 2,6-bis(2′-indolyl)pyridine and 2,6-bis[2′-(7-azaindolyl)]pyridine, *Organometallics*, 2003, **22**, 4070–4078.

198 Q. Liu, L. Thorne, I. Kozin, D. Song, C. Seward, M. D'Iorio, Y. Tao and S. Wang, New red-orange phosphorescent/electroluminescent cycloplatinated complexes of 2,6-bis(2′-indolyl)pyridine, *J. Chem. Soc., Dalton Trans.*, 2002, 3234–3240.

199 A. F. Rausch, H. H. H. Homeier and H. Yersin, Organometallic Pt(II) and Ir(III) triplet emitters for OLED applications and the role of spin-orbit coupling: A study based on high-resolution optical spectroscopy, *Top. Organomet. Chem.*, 2010, **29**, 193–235.

200 G. Baryshnikov, B. Minaev and H. Ågren, Theory and Calculation of the Phosphorescence Phenomenon, *Chem. Rev.*, 2017, **117**, 6500–6537.

201 L. Wang, Z. Gao, C. Liu, Y. Chen, W. Tao and L. Lu, Synthesis and properties of fluorinated cyclometalated Ir (III) complexes, *Tetrahedron*, 2020, **76**, 131390.

202 Y. C. Zhu, L. Zhou, H. Y. Li, Q. L. Xu, M. Y. Teng, Y. X. Zheng, J. L. Zuo, H. J. Zhang and X. Z. You, Highly efficient green and blue-green phosphorescent oleds based on iridium complexes with the tetraphenylimidodiphosphinate ligand, *Adv. Mater.*, 2011, **23**, 4041–4046.

203 T.-Y. Li, J. Wu, Z.-G. Wu, Y.-X. Zheng, J.-L. Zuo and Y. Pan, Rational design of phosphorescent iridium(III) complexes for emission color tunability and their applications in OLEDs, *Coord. Chem. Rev.*, 2018, **374**, 55–92.

204 S. Lee and W.-S. Han, Cyclometalated Ir(iii) complexes towards blue-emissive dopant for organic light-emitting diodes: fundamentals of photophysics and designing strategies, *Inorg. Chem. Front.*, 2020, **7**, 2396–2422.

205 K. S. Yook and J. Y. Lee, Organic Materials for Deep Blue Phosphorescent Organic Light–Emitting Diodes, *Adv. Mater.*, 2012, **24**, 3169–3190.

206 Y. Im, S. Y. Byun, J. H. Kim, D. R. Lee, C. S. Oh, K. S. Yook and J. Y. Lee, Recent Progress in High-Efficiency Blue-Light-Emitting Materials for Organic Light-Emitting Diodes, *Adv. Funct. Mater.*, 2017, **27**, 1603007.

207 C. Murawski, K. Leo and M. C. Gather, Efficiency roll-off in organic light-emitting diodes, *Adv. Mater.*, 2013, **25**, 6801–6827.

208 W. Song and J. Y. Lee, Degradation Mechanism and Lifetime Improvement Strategy for Blue Phosphorescent Organic Light–Emitting Diodes, *Adv. Opt. Mater.*, 2017, **5**, 1600901.

209 P. Pander, A. V. Zaytsev, A. Sil, G. V. Baryshnikov, F. Siddique, J. A. G. Williams, F. B. Dias and V. N. Kozhevnikov, Thermally activated delayed fluorescence in a deep red dinuclear iridium(III) complex: a hidden mechanism for short luminescence lifetimes, *Chem. Sci.*, 2023, **14**, 13934–13943.

210 M. Z. Shafikov, R. Martinscroft, C. Hodgson, A. Hayer, A. Auch and V. N. Kozhevnikov, Non-Stereogenic Dinuclear Ir(III) Complex with a Molecular Rack Design to Afford Efficient Thermally Enhanced Red Emission, *Inorg. Chem.*, 2021, **60**, 1780–1789.

211 L. Y. Peng, Z. W. Li, G. N. Pan, W. K. Chen, Y. J. Gao and G. Cui, Thermally activated delayed fluorescence of a Ir (iii) complex: absorption and emission properties, non-radiative rates, and mechanism, *Phys. Chem. Chem. Phys.*, 2023, **25**, 6454–6460.

212 R. E. Daniels, S. Culham, M. Hunter, M. C. Durrant, M. R. Probert, W. Clegg, J. A. G. Williams and V. N. Kozhevnikov, When two are better than one: bright phosphorescence from non-stereogenic dinuclear iridium (III) complexes, *Dalton Trans.*, 2016, **45**, 6949–6962.

213 D. M. Arias-Rotondo and J. K. McCusker, The photophysics of photoredox catalysis: a roadmap for catalyst design, *Chem. Soc. Rev.*, 2016, **45**, 5803–5820.

214 Y. Zhang, J. L. Petersen and C. Milsmann, A Luminescent Zirconium(IV) Complex as a Molecular Photosensitizer for Visible Light Photoredox Catalysis, *J. Am. Chem. Soc.*, 2016, **138**, 13115–13118.

215 P. Chábera, Y. Liu, O. Prakash, E. Thyrhaug, A. El Nahhas, A. Honarfar, S. Essén, L. A. Fredin, T. C. B. Harlang, K. S. Kjær, K. Handrup, F. Ericson, H. Tatsuno, K. Morgan, J. Schnadt, L. Häggström, T. Ericsson, A. Sobkowiak, S. Lidin, P. Huang, S. Styring, J. Uhlig, J. Bendix, R. Lomoth, V. Sundström, P. Persson and K. Wärnmark, A low-spin Fe(III) complex with 100 ps ligand-to-metal charge transfer photoluminescence, *Nature*, 2017, **543**, 695–699.

216 K. S. Kjær, N. Kaul, O. Prakash, P. Chábera, N. W. Rosemann, A. Honarfar, O. Gordivska, L. A. Fredin, K.-E. Bergquist, L. Häggström, T. Ericsson, L. Lindh, A. Yartsev, S. Styring, P. Huang, J. Uhlig, J. Bendix, D. Strand, V. Sundström, P. Persson, R. Lomoth and K. Wärnmark, Luminescence and reactivity of a charge-transfer excited iron complex with nanosecond lifetime, *Science*, 2019, **363**, 249–253.

217 Y. Zhang, D. C. Leary, A. M. Belldina, J. L. Petersen and C. Milsmann, Effects of Ligand Substitution on the Optical and Electrochemical Properties of (Pyridinedipyrrolide)zirconium Photosensitizers, *Inorg. Chem.*, 2020, **59**, 14716–14730.

218 F. Zhang, Y. Zhou, Z. Chen, M. Wang, Z. Ma, X. Chen, M. Jia, D. Wu, J. Xiao, X. Li, Y. Zhang, Z. Shi and C. Shan, Thermally Activated Delayed Fluorescence Zirconium-Based Perovskites for Large-Area and Ultraflexible X-ray Scintillator Screens, *Adv. Mater.*, 2022, **34**, 2204801.

219 A. Steinegger and S. M. Borisov, Zn(II) Schiff Bases: Bright TADF Emitters for Self-referenced Decay Time-Based Optical Temperature Sensing, *ACS Omega*, 2020, **5**, 7729–7737.

220 A. Russegger, L. Eiber, A. Steinegger and S. M. Borisov, Zinc Donor–Acceptor Schiff Base Complexes as Thermally Activated Delayed Fluorescence Emitters, *Chemosensors*, 2022, **10**(3), 91.

221 K. Zhang, X. Meng and L. He, Cationic Zinc(II) Complexes with Carbazole-Type Counter-Anions: Intracomplex Donor/Acceptor Pairs Affording Exciplexes with Thermally Activated Delayed Fluorescence, *Inorg. Chem.*, 2023, **62**(5), 2135–2145.

222 H. Deng, T. Wang, Y. Chen, K. Dou, X. Liu, C. Zhao, H. Zhan, C. Yang, C. Qin and Y. Cheng, Enhanced Thermally Activated Delayed Fluorescence by Sole Coordination: From an Organic Molecule to Its Zinc Complex, *J. Phys. Chem. Lett.*, 2024, **15**, 7003–7010.

223 T.-C. Lee, J. Hung, Y. Chi, Y. Cheng, G. Lee, P. Chou, C. Chen, C. Chang and C. Wu, Rational Design of Charge-Neutral, Near-Infrared-Emitting Osmium(II) Complexes and OLED Fabrication, *Adv. Funct. Mater.*, 2009, **19**, 2639–2647.

224 X. Peng, C. Yeh, S. F. Wang, J. Yan, S. Gan, S. Su, X. Zhou, Y. Zhang and Y. Chi, Near–Infrared OLEDs Based on Functional Pyrazinyl Azolate Os(II) Phosphors and Deuteration, *Adv. Opt. Mater.*, 2022, **2201291**, 2201291.

225 Y. Yuan, J. Liao, S. Ni, A. K.-Y. Jen, C. Lee and Y. Chi, Boosting Efficiency of Near–Infrared Organic Light–Emitting Diodes with Os(II)–Based Pyrazinyl Azolate Emitters, *Adv. Funct. Mater.*, 2020, **30**, 1–8.

226 Z. Zhu, S. Wang, L. Fu, J. Tan, C. Cao, Y. Yuan, S. Yiu, Y. Zhang, Y. Chi and C. Lee, Efficient Pyrazolo[5,4-f]quinoxaline Functionalized Os(II) Based Emitter with an Electroluminescence Peak Maximum at 811 nm, *Chem. – Eur. J.*, 2022, **28**, e202103202.

